



Norwegian University of
Science and Technology

Thermoelectric Properties of Non- Aqueous Electrochemical Cells

Local Reversible Heat Effects Relevant for
Lithium Ion Batteries

Astrid Fagertun Gunnarshaug

Chemistry

Submission date: May 2018

Supervisor: Signe Kjelstrup, IKJ

Norwegian University of Science and Technology
Department of Chemistry

Abstract

The aim of this thesis was to investigate the thermoelectric properties and local reversible heat effects of cells relevant to lithium-ion batteries. The theory of non-equilibrium thermodynamics and experimental measurements of the thermoelectric power of these cells were used to study the system. The Seebeck coefficients, Peltier heats and transported entropies of Li^+ in the cells have been estimated. The three different thermoelectric cells studied consisted of lithium cobalt oxide (LiCoO_2), graphite (C_6) and lithium iron phosphate (LiFePO_4) electrodes and separators wetted with the same ternary electrolyte with lithium hexafluorophosphate (LiPF_6), ethylene carbonate and diethyl carbonate.

The time-evolution of the thermoelectric potential measured indicated that two thermal diffusion phenomena of different time scales were present during the measurements for the LiCoO_2 and LiFePO_4 cells. These Soret effects in the electrolyte were found to contribute significantly to the electric potential. For LiCoO_2 , the Peltier heat at the electrode was estimated to be 84 ± 9 kJ/mol initially, -45 ± 6 kJ/mol at an intermediate state and 51 ± 6 kJ/mol at stationary state. For LiFePO_4 , the Peltier heat at the electrode was estimated to be 35 ± 9 kJ/mol initially, 26 ± 6 kJ/mol at an intermediate state and 127 ± 12 kJ/mol at stationary state. These values indicate large and time-dependent local reversible heat effects in Li-ion batteries during charging and discharging. These local heat effects are currently not included in thermal description of lithium-ion battery cells given in the literature.

The transported entropy of Li^+ in the LiCoO_2 cell was found to be 200 ± 20 J/K mol, while in the LiFePO_4 cell it was estimated to be 460 ± 60 J/K mol. The discrepancy in $S_{\text{Li}^+}^*$ could indicate that the transported entropy depends on the electrode material in the thermoelectric cell.

No consistent behaviour was observed for the C_6 cells, probably due to irreversible changes inside the cells during the measurements. The large changes and uncertainties in the Seebeck coefficient and bias potential over time can indicate that structural changes occurred in the cell during and between the measurement.

Sammendrag

Målet med dette masterprosjektet var å undersøke de termoelektriske egenskapene og lokale reversible varmeeffekter i celler relevante til litium-ione batterier. Irreversibel termodynamikk og eksperimentelle målinger av den termoelektriske effekten av disse cellene ble brukt for å studere systemet. Seebeck koeffisientene, Peltier varmen og de transporterte entropiene av Li^+ i cellene har blitt estimert. De tre forskjellige termoelektriske cellene bestod av litium koboltoksid (LiCoO_2), grafitt (C_6) og litium jernfosfat (LiFePO_4) elektroder og separasjoner fuktet med den samme ternære elektrolytten med litiumheksafluorofosfat (LiPF_6), etylenkarbonat og dietylkarbonat.

Tidsutviklingen av den termoelektriske potensialet målt indikerte at to termiske diffusjonsfenomen med forskjellig tidsskala var tilstede under målingene for LiCoO_2 og LiFePO_4 cellene. Soret effektene i elektrolytten bidrog signifikant til det elektriske potensialet. For LiCoO_2 ble Peltier varmen ved elektroden estimert til 84 ± 9 kJ/mol ved initiell tilstand, -45 ± 6 kJ/mol ved intermediat tilstand og 51 ± 6 ved stasjonær tilstand. For LiFePO_4 ble Peltier varmen ved elektroden estimert til 35 ± 9 kJ/mol ved initiell tilstand, 26 ± 6 kJ/mol ved intermediat tilstand og 127 ± 12 ved stasjonær tilstand. Disse verdiene indikerer store og tidsavhengige lokale reversible varmeeffekter i Li-ione batterier under ladning og utladning. Disse lokale varmeeffektene er på det nåværende tidspunktet ikke inkludert i beskrivelser av temperaturen av litium-ione batterier gitt i litteraturen.

Den transporterte entropien av Li^+ ble estimert til 200 ± 20 for LiCoO_2 , mens for LiFePO_4 ble den estimert til 460 ± 60 J/K mol. Forskjellen i verdiene for $S_{\text{Li}^+}^*$ kan indikere at den transporterte entropien er avhengig av elektrodematerialet i den termoelektriske cellen.

Ingen konsistent oppførsel ble observert for C_6 cellene, antakelig på grunn av irreversible endringer i cellene under målingene. Store endringer og usikkerheter i Seebeck koeffisienten og bias potensialet over tid kan indikere at strukturelle endringer foregikk inne i cellen under og mellom målingene.

Acknowledgements

I would like to thank professor Signe Kjelstrup for being an incredible supervisor and role model throughout the work on my master's thesis.

Secondly I would also like to thank Frank Richter, for including me in his experimental work, for his guidance in the making of pouch cells, with the initial experimental setup and help with interpretation of data. The first thermoelectric power measurements were made in cooperation with Richter, and the pouch cells used in the experiments were made by him. I would also like to thank Odne Burheim and PoreLab, for helpful guidance, advice and many meaningful discussions. I would like to acknowledge the Research Council of Norway (RCN) for funding the thesis through project no. 228739, "Life and Safety for Li-ion batteries in Maritime conditions (SafeLiLife)".

A great thank you to Kim R. Kristiansen for the valuable discussions, help with Matlab coding and statistics, experimental set-up and laboratory electronics. I would also like to thank him for feedback from reading this thesis, and him and Solrun Lid listening to my presentation and as well as being great friends throughout the thesis work. I am also grateful to Andreas Brusvik, for taking the great challenge of simulating the electrolyte in his project work.

Contents

Abstract

Sammendrag

Acknowledgements

1	Introduction	1
1.1	Project Background	1
1.2	Motivation	1
1.3	Structure of the Electrolyte Solution	4
1.4	The Transported Entropy of Lithium-Ions	5
1.5	Problem Definition	6
1.6	Outline of the Thesis	6
2	Description of the System	7
2.1	Description of the Thermoelectric Cells	7
2.2	Description of Li-ion Cells	8
3	Theory	11
3.1	Temperature and Potential Profiles of the System	11
3.1.1	The Electrolyte	12
3.1.2	The Anode and Cathode Bulk Phases	17
3.1.3	The Electrode Surfaces	18
3.2	The Soret Effect	20
3.3	The Seebeck Coefficient	21
3.3.1	The Electrolyte	21
3.3.2	The Electrode Bulk Phases	22
3.3.3	The Electrode Surfaces	23
3.3.4	The Total Seebeck Coefficient of the System	24
3.3.5	The Time-Evolution of the Thermoelectric Potential	25
3.4	Peltier Heat	26
3.4.1	Total Reversible Heat Effect in a Lithium Ion Battery Cell	27

4	Experimental	29
4.1	Pouch Cells	29
4.2	Temperature Calibration	30
4.3	Thermoelectric Potential Measurements	33
5	Results and Discussion	35
5.1	Thermoelectric Potential of LiCoO ₂ Pouch Cells	37
5.1.1	Diffusion Coefficients and Heats of Transfer	41
5.2	Thermoelectric Potential of C ₆ Pouch Cells	46
5.3	Thermoelectric Potential of LiFePO ₄ Pouch Cells	54
5.3.1	Diffusion Coefficients and Heats of Transfer	58
5.4	Peltier Heats from Literature Data	62
5.5	Further Work	68
6	Conclusion	71
	References	79
7	List of Symbols and Abbreviations	81
A	Statistics	i
B	Thermal Profile from Fourier’s Law	iii
C	Thermoelectric Potential Data	vii
C.1	LiCoO ₂ Measurements	viii
C.2	C ₆ Measurements	xiii
C.3	LiFePO ₄ Measurements	xxiii
D	Time Evolution of Multi-Component Diffusion	xxix
E	Entropy of Intercalation	xxxiii
E.1	Li _x CoO ₂ electrode	xxxvi
E.2	Methodology	xxxvii
E.3	Results and Discussion	xxxvii
E.4	Matlab Codes Lattice Model Calculations	xliii

Chapter 1

Introduction

1.1 Project Background

The work in this master thesis was done in collaboration with Frank Richter and was funded through the Research Council of Norway (RCN) project no. 228739, through the project "Life and Safety for Li-ion batteries in Maritime conditions (SafeLiLife)". The purpose of the thesis was to contribute to the work for Richter's doctoral thesis. The pouch cells investigated were assembled by Richter. The results from the LiCoO_2 measurements have been reported by Richter *et al.* during the course of this master's thesis [1], but with different assumptions for the flux equations used in the theory.

1.2 Motivation

Since the first lithium ion battery was assembled in 1985, it has revolutionized wireless electronics and energy storage technology [2]. A lithium ion battery cell is composed of a positive electrode and negative electrode, electrolyte, separator and current collectors contained in a cell housing [3]. The purpose of the separator is to keep the two electrodes apart to avoid internal short circuiting.

Thermoelectric or thermogalvanic cells are galvanic cells with a non-uniform temperature [4]. Such cells can also be used for energy harvesting. The Seebeck coefficients of aqueous thermoelectric cells, defined as the potential of an electrochemical cell per degree temperature difference at stationary state, are typically in the range 1 mV/K [5]. In comparison, thermoelectric semiconductors typically have Seebeck coefficients up to a few hundred μV [5]. Thermogalvanic cells with organic electrolytes have been shown to have high Seebeck coefficients, and Bonetti *et al.* reported Seebeck coefficients in the range 2.8-7 mV/K for thermogalvanic cells with organic nitrate and bromide salts [6]. These values are amongst the highest reported.

Heat effects inside the battery are important in battery technology as ageing of

lithium battery cells is temperature dependent [7]. In addition there is the possibility that the electrolyte salt may precipitate at low temperatures and thus damage the battery [8]. An accurate description of the thermal profile of the cell is therefore needed and information about local heat sources is important. During charging and discharging both irreversible and reversible heat effects occur inside the battery. The irreversible heat effects include contributions from the overpotential and the ohmic resistance, and increases the temperature of the battery [9]. The reversible heat effects are a result of the entropy change due to the electrode reactions. The reversible heat effect will be of opposite sign, but the same magnitude during charging and discharging [9, 10]. Though Viswanathan *et al.* have studied the entropy change in battery cells by calculating the entropy change of one electrode through the use of lithium metal as a counter electrode [9], little has been done in terms of the single electrode thermal signature and local reversible heat production through these cells. If total entropy change within a lithium-ion battery cell during discharging or charging is positive, this gives internal heating inside the cell. If it is negative it gives an internal cooling inside the cell.

Transport in a system indicates non-equilibrium conditions, and can be studied using non-equilibrium thermodynamics. Non-equilibrium thermodynamics is also a suitable theory to use when studying interfaces [11]. Thermoelectric cells are cells to which a temperature gradient is applied and a potential is generated as a response [12]. The thermal force induces transport inside the cell. In thermoelectric cells it is important to know the thermal and potential profile throughout the cell, including the interfaces, to give an accurate description of the system. The interfaces of the system will typically be the surfaces of the electrodes. In this thesis, the reversible heat effects in thermoelectric cells with Li-ion battery electrolyte and electrodes will be studied by the use of non-equilibrium thermodynamics. The same theory has been used to study the thermal profile in fuel cells [11, 13, 14].

The temperature and potential profile of Li-ion thermoelectric cells will be derived to explore the possibility of using these cell materials as thermoelectric cells and the importance of reversible heat effects in Li-ion batteries. A temperature gradient will be applied to the cells, inducing transport in the system. Temperature gradients can also give rise to thermal diffusion (the Soret effect [15]) and a thermoelectric potential (the Seebeck effect [13]). Non-equilibrium thermodynamics or irreversible thermodynamics will therefore be suitable to apply when treating the transport processes in the systems in this thesis.

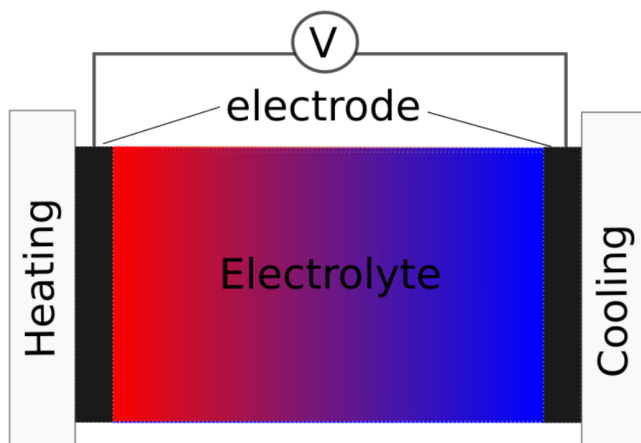


Figure 1.1: An illustration of the thermoelectric effect in an electrochemical cell.

The Seebeck coefficient of the cells will be derived from the potential and temperature profiles of the system and obtained from potential measurements on the thermoelectric cells. The initial thermoelectric potential of Li_xTiS_2 symmetric cells has been reported by Kuzminskii *et al.* and Hudak *et al.* for various electrolytes [5, 16]. Hudak and Amatucci also reported the initial thermoelectric potential of $\text{Li}_x\text{V}_2\text{O}_5$. In these studies, no stationary state was reached. Only an initial value that was reported, not the stationary state Seebeck coefficient. The application of thermoelectric cells will typically be at steady state conditions. A system exposed to a temperature gradient will eventually reach a stationary state or Soret equilibrium. This was not been investigated due to a large drift in bias potential observed by Hudak *et al.* [16]. A similar experiment was performed by Black *et al.* using lithium electrodes for assembled batteries with two different electrodes with a 1M LiClO_4 and 1:1 EC/DEC electrolyte [17]. A Seebeck coefficient was also reported by Kobayashi *et al.* for LiCoO_2 , $\text{Na}_{0.99}\text{CoO}_2$, $\text{Na}_{0.52}\text{MnO}_2$ and $\text{Na}_{0.51}\text{Mn}_{0.5}\text{Fe}_{0.5}\text{O}_2$ thermoelectric cells [18]. However, no mention of thermoelectric effects in the electrolyte was made and no evidence of a stationary state was given. From the Seebeck coefficient, the transported entropy of the reversible ion in the solution and Peltier heat can be found [11, 19]. From the difference between the initial thermoelectric potential and the thermoelectric potential at Soret equilibrium, information of the Soret effect may be obtained.

1.3 Structure of the Electrolyte Solution

Ethylene carbonate (EC) has a higher dipole moment than diethyl carbonate (DEC). Li^+ and PF_6^- are charged ions and EC will bind more strongly to them than DEC. EC molecules will therefore surround the Li^+ ions and hence a solvation layer of ethylene carbonate around the ions will form in the solution. Jeong *et al.* found that on average 3.1 EC and 1.1 DEC molecules surround Li^+ in an electrolyte with 50:50 volume percent of EC and DEC and 1M LiClO_4 [20]. This solvation layer will give some local order to the composition of the solution. The structure of the electrolyte solution at different EC/DEC compositions has been studied by Andreas Bursvik during the project work prior to his master's thesis [21]. The composition will affect the system through properties such as mobility of lithium ions in the system, the conductivity and the viscosity of the electrolyte [22]. This local ordering is often ignored in literature to simplify the transport equations when treating Li-battery systems. However, it can be of great importance to understand the processes happening if diffusion would occur as a response to the thermal driving force.

Since both EC and DEC are big, bulky molecules, they are likely to diffuse slowly. This can be seen from the Einstein-Smoluchowski equation for the diffusion coefficient [23]:

$$D = \frac{k_B T}{\xi} \quad (1.1)$$

where k_B is the Boltzmann constant, T is the temperature and ξ is the friction coefficient. The friction coefficient is dependent on the shape of the particle, in particular the dimensions of the particle, such as the radius if the particle is spherical or shaped like a disc. For a big, bulky molecule, ξ will be a large number, so the diffusion coefficient will also be small and the molecule will diffuse slowly. How fast the ions diffuse will depend on the electrolyte structure. If the ions bind strongly to the solvent molecules, they will effectively have a larger diameter and the diffusion process will be slow. This will likely also be the case with thermal diffusion. In thermal diffusion it is usually the lighter component that diffuse towards the hot side of the cell and the heavier component to the cold side. The lighter components of the electrolyte is Li^+ and EC, while DEC and PF_6^- are the heaviest components. The solvation layer and charge-charge interactions complicates this and simulations of the electrolyte is therefore needed to confirm the sign of the concentration gradients that may build up within the electrolyte when the system is exposed to a temperature gradient.

1.4 The Transported Entropy of Lithium-Ions

The transported entropy of charge carriers in the system will largely determine the conversion between thermal and electric energy [13]. It is a property related to the heat transport in the cell and electric energy conversion [24, 25]. The expressions for the Seebeck coefficient and the Peltier heat will contain both thermodynamic and transported entropies. The convention is that transported entropies are positive when heat is transported in the direction of the positive electric current [13]. As Li^+ is the charge carriers of the system it follows that the transported entropy of Li^+ must be positive if heat is transported along with the ions.

In literature, the transported entropy of ions, in particular small cations, have been related to the hydration shells surrounding the ion in aqueous solution [26]. Thus the values of transported entropies reported are typically for salts in aqueous solution. Values in molten salts have also been reported [24]. The electrolyte structure will therefore be important to understand the transported entropy in Li-ion cells. These electrolytes are, as already described, not aqueous solutions and the solvation is thus not comparable. The high Seebeck effects reported for non-aqueous solutions by Bonetti *et al.* [6] and high initial thermal potential reported by Kuzminskii *et al.* [5] can suggest (several orders of magnitude) higher values for transported entropy of ions in non-aqueous electrolytes. The highest reported Seebeck coefficient (7.16 mV/K) by Bonetti *et al.* will, according to the theory used in the article, give an Eastman entropy for tetrabutylammonium of 1380 J/K mol! The Eastman entropy is the difference between the transported and thermodynamic entropy of an ion [25]. By comparison the same ion in water will, using the same theory and a reported Seebeck coefficient of 371 $\mu\text{V}/\text{K}$, have an Eastman entropy of around 70 J/K mol [6].

Though literature frequently reports the transported entropy of an ion in different electrolytes and electrolyte concentrations, nothing has been reported on thermoelectric cells with the same electrolyte, but different electrodes. The transported entropy of the ion involved in the electrode reaction has been found to be constant over different electrolytes and it is believed to be a property associated with the electrode surface [13]. At the electrode surface the charge carrier changes from the one inside the electrode to the ion in the electrolyte, and it is expected that this transition will be important for the value of the transported entropy. Since the heat production and heat consumption locally in a cell is determined by the electrode surface, it can be reasonable to expect a large dependence on the electrode surface.

1.5 Problem Definition

The aim of this thesis is to investigate the local reversible heat effects around electrodes used in lithium-ion batteries and the possibility to use these materials as thermoelectric cells. This will be done by measuring the thermoelectric potential of three different thermoelectric cells with lithium cobalt oxide (LiCoO_2), graphite (C_6) or lithium iron phosphate (LiFePO_4) electrodes and separators wetted with the same ternary electrolyte with lithium hexafluorophosphate (LiPF_6), ethylene carbonate and diethyl carbonate. The systems will be analyzed using the theory of non-equilibrium thermodynamics. The aim of these measurements is to investigate the thermoelectric properties of the cells by calculating the Seebeck coefficient, the Peltier heat associated with the electrodes and the transported entropy of lithium ions in the individual cells. The contribution from the Soret effect of these cells will be studied by continuing the experiment until a steady state is reached. The results reported on the thermoelectric potential of Li_xTiS_2 cells by Hudak *et al.* and Kuzminskii *et al.* and Li cells by Black *et al.* will also be analyzed using the same theory.

Though the transported entropy of ions is related to the Peltier heat and heat of transfer of a cell, both of which are clearly associated with the interface of an electrode, no reports on this surface dependence exist in literature. Traditionally, transported entropies of ions are measured by using the same electrodes and varying the electrolyte. In this project, the same electrolyte will be used with different electrodes. Another aim of this thesis will therefore be to contribute to a better understanding on the concept of the transported entropy of ions.

1.6 Outline of the Thesis

The thesis is divided into four main parts. A description of the system to be investigated is given in Chapter 2. This is followed by the derivation of the thermal and potential profiles, and the Seebeck coefficient and Peltier heat in Chapter 3. Experimental and equipment descriptions are given in Chapter 4. The results are then given and their meaning and importance are discussed in Chapter 5.

Chapter 2

Description of the System

The thermoelectric potential of thermoelectric Li-ion cells will be described using non-equilibrium thermodynamics. A general description of the lithium battery cells and electrodes is given, in addition to a description of the thermoelectric cells investigated in this thesis.

2.1 Description of the Thermoelectric Cells

A thermoelectric cell is a non-isothermal cell [25], typically containing two electrodes of the same material. At equilibrium conditions, the ideal thermoelectric cell will have no potential. In practice, because the two electrodes will never be identical, a small bias potential is observed. When acted upon by a driving force, such as a temperature gradient, the cell would no longer be at equilibrium. The temperature gradient between the two electrodes will then serve as a driving force for the transport in the system and a gradient in the electrochemical potential of the cell will be a result of this [12]. A gradient in the electrochemical potential is proportional to the electric field over a cell [27]. If thermal diffusion is present, particles will then start to move from the side with the highest electrochemical potential to reequalise the electrochemical potentials of the system. The fluxes induced in this system can be used relate the driving forces in this system, which will consist of a thermal gradient, a potential gradient and a gradient in chemical potential, using non-equilibrium thermodynamics.

The system can be divided into five parts; three bulk phases and two interfaces, as shown in figure 2.1. The bulk phases consists of the anode, cathode and electrolyte, while the interfaces will be the electrode surfaces. To find the temperature and potential profiles of the system, the measurable heat, mass and current fluxes of the system must be determined.

The thickness of the interfaces between the electrodes and the electrolyte, δ , will be assumed to be 0. This is not true, as such interfaces will give a double layer of ions of non-zero dimension. These layers are typically in the order of 1-10 nm

[28], decreasing in thickness with increasing concentration. The thickness of the electrolyte is, however, in the order of a few mm. Hence it is a reasonable approximation given the dimensions of the cell.

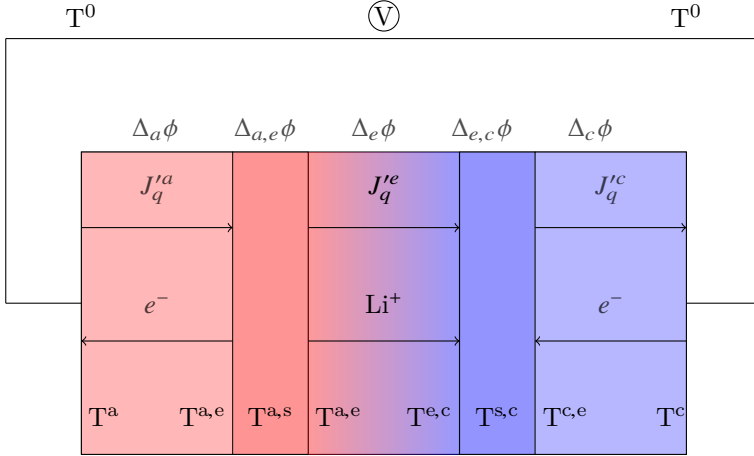


Figure 2.1: Measurable heat fluxes and temperatures at steady state in the five parts of the cell.

The cell reaction will only be treated at the interface between the electrode and the electrolyte and not in the electrode bulk phase. This can be done because the lithium at the bulk of the electrode and the surface must have equal chemical potential in order for the electrode to be in equilibrium with its interface [23]. The electrode will be assumed to be thermostatted, and thus the bulk phase and its interface should be at equilibrium with each other. Initially, mass fluxes of the components of the electrolyte will be present. At steady state, only the flux of Li^+ present in the electrolyte as it is the charge carrier for the current flux.

2.2 Description of Li-ion Cells

The Li-ion thermoelectric cells which will be studied in this thesis are composed of a separator wetted with an electrolyte consisting of $LiPF_6$, ethylene carbonate (EC) and diethyl carbonate (DEC) sandwiched between two identical electrodes connected to current collectors. The current collectors are metallic conductors on the back of the electrodes which are connected to the outer circuit. It will therefore be treated as a part of the outer circuit. Lithium cobalt oxide, graphite and lithium iron phosphate electrodes will be investigated in this thesis.

In the literature the convention is to describe the electrodes as Li_xCoO_2 , Li_xFePO_4 and Li_xC_6 , where x indicates the lithiated state of the electrode. x typically has values between 0 and 1 for the electrodes studied in this thesis. If $x=1$ in Li_xCoO_2 , there will be one Li per unit of CoO_2 . In a Li-ion battery, Li_xCoO_2 and Li_xFePO_4 electrodes are cathodes while Li_xC_6 is used as the anode [2]. Li_xCoO_2 , Li_xTiS_2 and

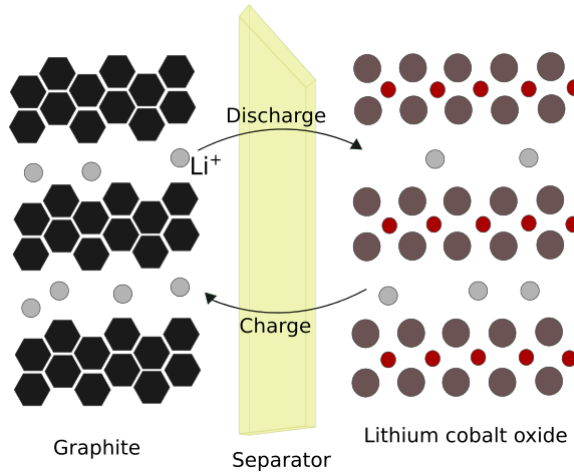


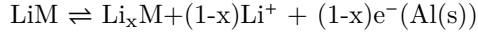
Figure 2.2: Example of assembled Li-ion battery set-up with intercalation electrodes Li_xC_6 and Li_xCoO_2 .

Li_xC_6 electrodes consist of two-dimensional layers of CoO_2 , TiS_2 and C_6 units held together in a three-dimensional structure through Van der Waals forces [29]. Li^+ reacts at the electrode and enters the electrode through an intercalation between the CoO_2 layers [2]. The same process also happens at the titanium disulfide and graphite electrode. Li_xFePO_4 have a crystal structure of FePO_4 units which creates one dimensional channels into which Li^+ is inserted [2]. The electrode material is in the literature referred to as the host lattice [30]. Since Li^+ is intercalated into the host and is mostly considered to be in its ionic form inside the host structure, it can be argued that it is more accurate to consider this intercalation as a solvation process of Li within the electrodes [31]. Henceforth Li in the electrode will be written as $\text{Li}(x,s)$, where s indicates that it is solvated between the layers of the electrode.

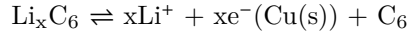
Around the graphite electrodes in lithium-ion batteries a solid electrolyte interphase (SEI) is formed and grows as the battery is charged and discharged [32]. The SEI layer is not present when the electrode is in pristine condition. This layer consists of inorganic and organic decomposition products of the electrolyte, and

serves as a passivating layer to prevent the electrolyte from further decomposition and co-intercalation of electrolyte (here EC/DEC) into the electrode [33]. Lithium ions are able to pass through the SEI layer.

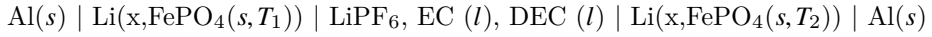
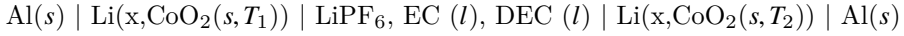
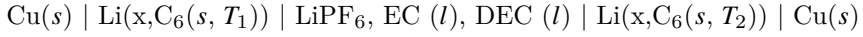
The electrode reaction for LiCoO_2 , LiFePO_4 and LiTiS_2 can be written as:



Where $\text{M}=\text{CoO}_2$, FePO_4 or LiTiS_2 . Electrode reaction for C_6 :



In the thermoelectric cells one electrode is kept at a higher temperature than the other. The electrodes are thermostatted, so that the temperature gradient is present primarily in the electrolyte/separator.



Chapter 3

Theory

The definitions used in this thesis follow the definitions given in the book by Kjelstrup and Bedeaux [13]. This chapter will include a derivation of the temperature, chemical potential and potential profiles of the system from the flux equations using non-equilibrium thermodynamics. A derivation of the Seebeck coefficient and Peltier heat of the system using the potential profile found follows.

3.1 Temperature and Potential Profiles of the System

For heterogeneous systems where surfaces need to be considered, the surface frame of reference is the natural choice which gives a simple and realistic description of the surface. It will therefore be used at the start of the derivation. The fluxes in this system will be treated as normal to the electrode surfaces. The surface frame of reference is thus equivalent to the laboratory frame of reference in this case.

There are a total of three components in the electrolyte; LiPF_6 , EC and DEC. Initially the system will have a uniform concentration of the components over the separator matrix. However, due to the presence of multiple components, the temperature gradient in the system might induce a gradient in the concentration of the three components relative to the separator matrix and the electrodes and therefore a gradient in the chemical potential. At $t \approx 0$ the chemical potential gradients will not be present. They will build up over time, reaching a steady value at $t \rightarrow \infty$. At stationary state, the potential will be the result of a balance between the two driving forces; the thermal gradient and the induced chemical potential gradient.

There are five driving forces in the system; $\frac{d(1/T)}{dx}$, $-\frac{1}{T} \frac{d\phi}{dx}$, $-\frac{1}{T} \frac{d\mu_{1,T}}{dx}$, $-\frac{1}{T} \frac{d\mu_{2,T}}{dx}$ and $-\frac{1}{T} \frac{d\mu_{3,T}}{dx}$. LiPF_6 will be denoted as component 1 and ethylene carbonate and diethyl carbonate component 2 and 3 respectively.

3.1.1 The Electrolyte

The entropy production of the bulk phase of the electrolyte is:

$$\sigma = J'_q \frac{\partial}{\partial x} \left(\frac{1}{T} \right) - \sum_i J_i \frac{1}{T} \left(\frac{\partial \mu_{i,T}}{\partial x} \right) - j \frac{1}{T} \left(\frac{\partial \phi}{\partial x} \right) \quad (3.1)$$

Where σ is the entropy production, J'_q is the heat flux, J_i is the mass flux of component i , j is the current density, T is the temperature, μ_i is the chemical potential of component i and ϕ is the potential. The fluxes, when the electrode surfaces are used as a frame of reference, are given by the following equations:

$$\begin{aligned} J'_q = L_{qq} \left(\frac{\partial}{\partial x} \frac{1}{T} \right) + L_{q1} \left(-\frac{1}{T} \frac{\partial \mu_{1,T}}{\partial x} \right) + L_{q2} \left(-\frac{1}{T} \frac{\partial \mu_{2,T}}{\partial x} \right) \\ + L_{q3} \left(-\frac{1}{T} \frac{\partial \mu_{3,T}}{\partial x} \right) + L_{q\phi} \left(-\frac{1}{T} \frac{\partial \phi}{\partial x} \right) \end{aligned} \quad (3.2)$$

$$\begin{aligned} J_1 = L_{1q} \left(\frac{\partial}{\partial x} \frac{1}{T} \right) + L_{11} \left(-\frac{1}{T} \frac{\partial \mu_{1,T}}{\partial x} \right) + L_{12} \left(-\frac{1}{T} \frac{\partial \mu_{2,T}}{\partial x} \right) \\ + L_{13} \left(-\frac{1}{T} \frac{\partial \mu_{3,T}}{\partial x} \right) + L_{1\phi} \left(-\frac{1}{T} \frac{\partial \phi}{\partial x} \right) \end{aligned} \quad (3.3)$$

$$\begin{aligned} J_2 = L_{2q} \left(\frac{\partial}{\partial x} \frac{1}{T} \right) + L_{21} \left(-\frac{1}{T} \frac{\partial \mu_{1,T}}{\partial x} \right) + L_{22} \left(-\frac{1}{T} \frac{\partial \mu_{2,T}}{\partial x} \right) \\ + L_{23} \left(-\frac{1}{T} \frac{\partial \mu_{3,T}}{\partial x} \right) + L_{2\phi} \left(-\frac{1}{T} \frac{\partial \phi}{\partial x} \right) \end{aligned} \quad (3.4)$$

$$\begin{aligned} J_3 = L_{3q} \left(\frac{\partial}{\partial x} \frac{1}{T} \right) + L_{31} \left(-\frac{1}{T} \frac{\partial \mu_{1,T}}{\partial x} \right) + L_{32} \left(-\frac{1}{T} \frac{\partial \mu_{2,T}}{\partial x} \right) \\ + L_{33} \left(-\frac{1}{T} \frac{\partial \mu_{3,T}}{\partial x} \right) + L_{3\phi} \left(-\frac{1}{T} \frac{\partial \phi}{\partial x} \right) \end{aligned} \quad (3.5)$$

$$\begin{aligned} j = L_{\phi q} \left(\frac{\partial}{\partial x} \frac{1}{T} \right) + L_{\phi 1} \left(-\frac{1}{T} \frac{\partial \mu_{1,T}}{\partial x} \right) + L_{\phi 2} \left(-\frac{1}{T} \frac{\partial \mu_{2,T}}{\partial x} \right) \\ + L_{\phi 3} \left(-\frac{1}{T} \frac{\partial \mu_{3,T}}{\partial x} \right) + L_{\phi\phi} \left(-\frac{1}{T} \frac{\partial \phi}{\partial x} \right) \end{aligned} \quad (3.6)$$

Since there are five forces, but only four are linearly independent, this system has linear dependency. The Onsager relation is unimpaired by this linear dependency which comes from the Gibbs-Duhem equation [12]. This dependency will be dealt with later in the derivation. The coupling coefficients, L_{ij} are related through the Onsager relation ($L_{ij} = L_{ji}$) since the system is not influenced by an external magnetic field [12]. Here the phenomenological coefficient L_{qq} is characteristic of the heat conductivity of the system. L_{iq} is related to thermal diffusion, the coupling coefficients between mass fluxes to interdiffusion. The flux equations for

this system can be rearranged by eliminating the electric potential gradient in the system from the mass and measurable heat fluxes.

$$\frac{\partial \phi}{\partial x} = \frac{T}{L_{\phi\phi}} \left(-j + L_{q\phi} \left(\frac{\partial}{\partial x} \frac{1}{T} \right) - L_{1\phi} \left(\frac{1}{T} \frac{\partial \mu_{1,T}}{\partial x} \right) - L_{2\phi} \left(\frac{1}{T} \frac{\partial \mu_{2,T}}{\partial x} \right) - L_{3\phi} \left(\frac{1}{T} \frac{\partial \mu_{3,T}}{\partial x} \right) \right) \quad (3.7)$$

A new coefficient, l_{ij} , the conductivity coefficient, can then be introduced to simplify these equations.

$$l_{ij} = L_{ij} - \frac{L_{i\phi} L_{\phi j}}{L_{\phi\phi}} \quad (3.8)$$

It follows from the Onsager relation that $l_{ij} = l_{ji}$. The following approximation will be made: $l_{12} = l_{21} = l_{13} = l_{31} = l_{23} = l_{32} \approx 0$. This means that the diffusive interaction coefficients, i.e. the influence on the diffusion of one component by the two other components in the electrolyte, are neglected. J'_q , J_1 , J_2 and J_3 can be now rewritten to the equations below:

$$J'_q = l_{qq} \left(\frac{\partial}{\partial x} \frac{1}{T} \right) - l_{q1} \left(\frac{1}{T} \frac{\partial \mu_{1,T}}{\partial x} \right) - l_{q2} \left(\frac{1}{T} \frac{\partial \mu_{2,T}}{\partial x} \right) - l_{q3} \left(\frac{1}{T} \frac{\partial \mu_{3,T}}{\partial x} \right) + \frac{L_{\phi q}}{L_{\phi\phi}} j \quad (3.9)$$

$$J_1 = l_{1q} \left(\frac{\partial}{\partial x} \frac{1}{T} \right) - l_{11} \left(\frac{1}{T} \frac{\partial \mu_{1,T}}{\partial x} \right) + \frac{L_{\phi 1}}{L_{\phi\phi}} j \quad (3.10)$$

$$J_2 = l_{2q} \left(\frac{\partial}{\partial x} \frac{1}{T} \right) - l_{22} \left(\frac{1}{T} \frac{\partial \mu_{2,T}}{\partial x} \right) + \frac{L_{\phi 2}}{L_{\phi\phi}} j \quad (3.11)$$

$$J_3 = l_{3q} \left(\frac{\partial}{\partial x} \frac{1}{T} \right) - l_{33} \left(\frac{1}{T} \frac{\partial \mu_{3,T}}{\partial x} \right) + \frac{L_{\phi 3}}{L_{\phi\phi}} j \quad (3.12)$$

J_1 in the equations above will be the flux of LiPF₆ in the electrolyte, J_2 is the flux of EC and J_3 the flux of DEC.

The following parameters can now be introduced:

$$\pi = \left(\frac{J'_q}{j/F} \right)_{dT=0} \quad (3.13)$$

$$t_i = \left(\frac{J_i}{j/F} \right)_{d\mu_T=0, dT=0} = F \frac{L_{i\phi}}{L_{\phi\phi}} \quad (3.14)$$

$$q_i^* = \left(\frac{J'_q - \sum_{j \neq i} q_j^* J_j}{J_i} \right)_{j=0, dT=0} = \frac{l_{qi}}{l_{ii}} \quad (3.15)$$

$$\kappa = \left(-\frac{J'_q}{\frac{\partial T}{\partial x}} \right)_{j=0} = \frac{l_{qq}}{T^2} \quad (3.16)$$

$$r = \frac{T}{L_{\phi\phi}} \quad (3.17)$$

where π is the Peltier coefficient, t_i is the transference coefficient of component i , q^* is the measurable heat of transfer, κ is the thermal conductivity and r is the electric resistivity at a stationary state. The Peltier coefficient is in this case the heat transferred reversibly with the current in the electrolyte. When no thermal diffusion is occurring, it is related to the transported entropy of the charge carrier, S^* , which in this case will be lithium ions. When thermal diffusion processes take place in the electrolyte, concentration gradients will build up. These concentration gradients will also induce reversible heat effects due to entropy changes. This must therefore also be included in the final expression for the Peltier coefficient.

The transport numbers of the ions in the salt is given by the expression for the transference coefficient, with the ion fluxes instead of the neutral component flux. Since Li^+ ions are the only ions involved in the electrode reaction, the flux of Li^+ is given by:

$$J_{\text{Li}^+} = \frac{L_{\phi 1}}{L_{\phi \phi}} j + J_1 = j/F + J_1 \quad (3.18)$$

That is, it is the sum of the flux of the ions as a response to the other driving forces (i.e. with the neutral salt flux J_1) and the flux of ions due to the electrode reaction. At stationary state, only the flux Li^+ ions is different from 0. At open circuit, $j \approx 0$ and the flux of Li^+ effectively be equal to the flux of component 1. PF_6^- does not react and hence the net flux of the ion follows the flux of the neutral component LiPF_6 .

$$J_{\text{PF}_6^-} = J_1 \quad (3.19)$$

The following is then obtained for the transference coefficient of component 1:

$$t_1 = -t_{\text{PF}_6^-} = -1 + t_{\text{Li}^+} \quad (3.20)$$

At stationary state $J_1 = J_2 = J_3 = 0$. The only charge carrier at stationary state will therefore be Li^+ . The temperature gradient can now be expressed, using the parameters introduced above:

$$\frac{\partial T}{\partial x} = -\frac{1}{\kappa} \left(J'_q + \frac{l_{1q}}{T} \frac{\partial \mu_{1,T}}{\partial x} + \frac{l_{2q}}{T} \frac{\partial \mu_{2,T}}{\partial x} + \frac{l_{3q}}{T} \frac{\partial \mu_{3,T}}{\partial x} + rj \right) \quad (3.21)$$

This shows that the temperature profile will not be fully established before stationary state is reached. $\partial T/\partial x$ will therefore be time-dependent. $\Delta T/\Delta x$ will however be known and controlled. The chemical potential can, using the definitions above, be expressed as:

$$\left(\frac{\partial \mu_{i,T}}{\partial x} \right) = -\frac{TJ_i}{l_{ii}} - \frac{q_i^*}{T} \frac{\partial T}{\partial x} + \frac{T}{l_{ii}} \frac{t_i}{F} j \quad (3.22)$$

The stationary state chemical potential at open circuit conditions can then be identified as:

$$\left(\frac{\partial\mu_{i,T}}{\partial x}\right)_{J_i=0,j=0} = -\frac{q_i^*}{T} \frac{\partial T}{\partial x} \quad (3.23)$$

q^* is defined from both J'_q and J_i , both of which are dependent on $\Delta\phi$. However, since these terms will have the same dependence on $\Delta\phi$ this dependence will cancel. Therefore the gradient in chemical potential at stationary state will only be dependent on the temperature gradient which will be controlled during measurements. The thermal driving force is then the driving force that gives rise to a gradient in chemical potential and hence the concentration gradient in the system. If such a concentration gradient is induced in the system, it would indicate a Soret effect. At open circuit conditions, the temperature gradient can be rewritten to:

$$\begin{aligned} \frac{\partial T}{\partial x} &= -\frac{1}{\kappa} \left(J'_q + \frac{l_{1q}}{T} \left(-\frac{T}{l_{11}} J_1 - \frac{q_1^*}{T} \frac{\partial T}{\partial x} \right) \right. \\ &\quad \left. + \frac{l_{2q}}{T} \left(-\frac{T}{l_{22}} J_2 - \frac{q_2^*}{T} \frac{\partial T}{\partial x} \right) + \frac{l_{3q}}{T} \left(-\frac{T}{l_{33}} J_3 - \frac{q_3^*}{T} \frac{\partial T}{\partial x} \right) \right) \\ \left(\kappa - \frac{l_{1q}}{T^2} q_1^* - \frac{l_{2q}}{T^2} q_2^* - \frac{l_{3q}}{T^2} q_3^* \right) \frac{\partial T}{\partial x} &= - \left(J'_q - q_1^* J_1 - q_2^* J_2 - q_3^* J_3 \right) \\ \frac{\partial T}{\partial x} &= -\frac{1}{\lambda} \left(J'_q - q_1^* J_1 - q_2^* J_2 - q_3^* J_3 \right) \end{aligned} \quad (3.24)$$

where λ is the stationary state thermal conductivity. By putting the parameters 3.13 and 3.14 into equation 3.7, the potential can be expressed as:

$$\frac{\partial\phi}{\partial x} = -\frac{\pi}{TF} \frac{\partial T}{\partial x} - \frac{t_1}{F} \frac{\partial\mu_{1,T}}{\partial x} - \frac{t_2}{F} \frac{\partial\mu_{2,T}}{\partial x} - \frac{t_3}{F} \frac{\partial\mu_{3,T}}{\partial x} - rj \quad (3.25)$$

At steady state this expression becomes:

$$\frac{\partial\phi}{\partial x} = -\frac{\pi}{TF} \frac{\partial T}{\partial x} - \frac{t_1}{TF} q_1^* \frac{\partial T}{\partial x} - \frac{t_2}{TF} q_2^* \frac{\partial T}{\partial x} - \frac{t_3}{TF} q_3^* \frac{\partial T}{\partial x} - rj \quad (3.26)$$

This equation can be simplified and the linear dependence of the flux equations removed by using Gibbs-Duhem's equation:

$$\sum_i x_i d\mu_{i,T} = 0 \quad (3.27)$$

where x_i is the mole fraction of component i in the electrolyte, to give:

$$\frac{\partial\phi}{\partial x} = -\frac{\pi}{TF} \frac{\partial T}{\partial x} - \frac{1}{F} \left(t_1 - \frac{x_1}{x_3} t_3 \right) \frac{\partial\mu_{1,T}}{\partial x} - \frac{1}{F} \left(t_2 - \frac{x_2}{x_3} t_3 \right) \frac{\partial\mu_{2,T}}{\partial x} - rj \quad (3.28)$$

This is equivalent to changing the frame of reference to the third component. This must be done in order to interpret the experimental results, since only two diffusion

phenomena will be observable due to the linear dependence. The change in the frame of reference will not affect the stationary state, since at this state $J_1 = J_2 = J_3 = 0$. The measurable heat flux, electric current flux and temperature gradient are also invariant to the choice of frame of reference [13]. From Gibbs-Duhem's equation and equation 3.23 the following relationship can be found between the heats of transfer:

$$-q_3^* = \frac{x_1}{x_3} q_1^* + \frac{x_2}{x_3} q_2^* \quad (3.29)$$

The chemical potential of the species in the electrolyte is given by

$$\mu_i = \begin{cases} \mu_i^0 + RT \ln a_i = \mu_i^0 + RT \ln(\gamma_i x_i) & \text{for EC, DEC} \\ \mu_i^0 + RT \ln a_i = \mu_i^0 + 2RT \ln(\gamma_i x_i) & \text{for LiPF}_6 \end{cases} \quad (3.30)$$

where a_i is the activity coefficient of component i , γ_i is the activity coefficient and x_i is the mole fraction of i in the electrolyte. As a salt is dissolved into its respective ions, the expression must be adapted for LiPF₆. Thereby $\frac{\partial \mu_{i,T}}{\partial x}$ can be rewritten to:

$$\frac{\partial \mu_{i,T}}{\partial x} = \frac{\partial \mu_{i,T}}{\partial x_i} \frac{\partial x_i}{\partial x} = \begin{cases} \left(\frac{RT}{x_i} \frac{\partial x_i}{\partial x} \left(1 + \frac{\partial \ln \gamma_i}{\partial \ln x_i} \right) \right) & \text{for EC, DEC} \\ \left(\frac{2RT}{x_i} \frac{\partial x_i}{\partial x} \left(1 + \frac{\partial \ln \gamma_i}{\partial \ln x_i} \right) \right) & \text{for LiPF}_6 \end{cases} \quad (3.31)$$

Which gives the following expression for the gradient in the composition at stationary state when using equation 3.23:

$$\frac{\partial x_i}{\partial x} = \begin{cases} -\frac{q_i^* x_i}{RT^2} \frac{\partial T}{\partial x} \left(1 + \frac{\partial \ln \gamma_i}{\partial \ln x_i} \right) \approx -\frac{q_i^* x_i}{RT^2} \frac{\partial T}{\partial x} & \text{for EC, DEC} \\ -\frac{q_i^* x_i}{2RT^2} \frac{\partial T}{\partial x} \left(1 + \frac{\partial \ln \gamma_i}{\partial \ln x_i} \right) \approx -\frac{q_i^* x_i}{2RT^2} \frac{\partial T}{\partial x} & \text{for LiPF}_6 \end{cases} \quad (3.32)$$

The last approximation holds at low concentrations of LiPF₆. A further simplification can be made for the potential gradient by inserting this into equation 3.28.

$$\frac{\partial \phi}{\partial x} = -\frac{\pi^{el}}{TF} \frac{\partial T}{\partial x} - \frac{2RT}{F} \left(\frac{1}{x_1} t_1 - \frac{1}{x_3} t_3 \right) \frac{\partial x_1}{\partial x} - \frac{RT}{F} \left(\frac{1}{x_2} t_2 - \frac{1}{x_3} t_3 \right) \frac{\partial x_2}{\partial x} - rj \quad (3.33)$$

The Peltier coefficient of the electrolyte must now be identified. $S_{Li^+}^*$ is the transported entropy of Li⁺, defined here as Peltier coefficient of the electrolyte in the absence of contribution from chemical potential gradients of neutral components:

$$\pi_{d\mu_{T,1}=d\mu_{T,2}=d\mu_{T,3}=0}^{el} = F \frac{L_{q\phi}}{L_{\phi\phi}} = TS_{Li^+}^* \quad (3.34)$$

It is interpreted as the heat carried by the charge carrier Li⁺ at stationary state. Outside of the stationary state mass fluxes will be present and affect the Peltier

coefficient through heats of transfer. At the initial state there is no chemical potential gradient. The Peltier coefficient of the electrolyte at can now be identified as:

$$\pi^{el} = TS_{\text{Li}^+}^* + \left(t_1 - \frac{x_1}{x_3}t_3\right)q_1^* + \left(t_2 - \frac{x_2}{x_3}t_3\right)q_2^* \quad (3.35)$$

Thereby, expressions for the temperature, concentration and potential gradients has been derived for the bulk phases. The contribution to the initial potential can also be expressed using the heats of transfer:

$$\begin{aligned} \frac{\partial\phi^{el}}{\partial x} = -\frac{\pi^{el}}{TF} \left(\frac{\partial T^e}{\partial x}\right) = -\frac{S_{\text{Li}^+}^*}{F} \left(\frac{\partial T^{el}}{\partial x}\right)_{J_1=J_2=J_3=0} - \frac{1}{F} \left(t_1 - \frac{x_1}{x_3}t_3\right) \frac{q_1^*}{T} \left(\frac{\partial T^{el}}{\partial x}\right)_{J_1=J_2=J_3=0} \\ - \frac{1}{F} \left(t_2 - \frac{x_2}{x_3}t_3\right) \frac{q_2^*}{T} \left(\frac{\partial T^{el}}{\partial x}\right)_{J_1=J_2=J_3=0} \end{aligned} \quad (3.36)$$

At steady state the concentration gradient and hence the chemical potential gradient will be fully developed and contribute to the potential. The chemical potential gradient will not be present at $t=0$. Using equation 3.23 and 3.35 this will then give another expression for the final potential gradient at open circuit conditions:

$$\begin{aligned} \frac{\partial\phi^{el}}{\partial x} = \frac{1}{TF} \left(-\pi^{el} - \left(t_1 - \frac{x_1}{x_3}t_3\right)q_1^* - \left(t_2 - \frac{x_2}{x_3}t_3\right)q_2^*\right) \left(\frac{\partial T^{el}}{\partial x}\right) \\ = -\frac{S_{\text{Li}^+}^*}{F} \left(\frac{\partial T^{el}}{\partial x}\right) \end{aligned} \quad (3.37)$$

Transported entropies are temperature dependent values [25]. The values at the cold and hot side of the cell will therefore be different. This change leads to a heat effect within the electrolyte called the Thomson heat and the variation in the transported entropy with temperature at constant pressure is given by the Thomson coefficient:

$$\left(\frac{\partial S_i^*}{\partial \ln T}\right)_p = \tau_i \quad (3.38)$$

When small temperature gradients are used, this temperature dependence is normally negligible. The middle temperature of the temperature gradient will be kept constant for the system. τ_{Li^+} typically is in the same order of magnitude as entropy terms and is in addition divided by a temperature term in the contribution to the potential. Because small temperature gradients will be used in the experiment, it will be assumed to have a small contribution and will be neglected.

3.1.2 The Anode and Cathode Bulk Phases

The electrode bulk phases are considered to be homogeneous systems and thus there is no gradient in chemical potential. Since the electrodes studied here are

either fully lithiated or no lithium is present, diffusion within the electrode will be neglected. Hence, it can be treated in a simpler way, by removing the terms containing the chemical potential gradient. The flux equations can then be described as:

$$J_q = L_{qq} \left(\frac{\partial}{\partial x} \frac{1}{T} \right) + L_{q\phi} \left(-\frac{1}{T} \frac{\partial \phi}{\partial x} \right) \quad (3.39)$$

$$j = L_{\phi q} \left(\frac{\partial}{\partial x} \frac{1}{T} \right) + L_{\phi\phi} \left(-\frac{1}{T} \frac{\partial \phi}{\partial x} \right) \quad (3.40)$$

The Peltier coefficient for the electrodes is:

$$\pi = TS_e^* \quad (3.41)$$

Where S_e^* is the transported entropy of the charge carrier of the electrode. However, it is not certain whether the Li-ions react at the surface and then diffuse or react within the pores of the electrodes. In the first case, the electrons will be the charge carriers and $S_e^* = S_e^*$. In the latter case, the lithium ions will be the charge carriers and $S_e^* = S_{\text{Li}^+,e}^*$, that is the transported entropy of lithium ions within the electrodes. Another complication is the charge on the intercalated Li. Silbernagel *et al.* found that Li is partially ionized inside Li_xTiS_2 electrodes [34]. The lithium atom/ions left are highly mobile. Lithium in Li_xMO_2 is also mobile. This means that there are most likely two charge carriers inside the electrodes, and S_e^* must be a combination of the two. The expressions for the temperature and potential gradient for the anode will then be:

$$\frac{\partial T^a}{\partial x} = -\frac{1}{\lambda} \left(J_q^a - \frac{\pi^a}{F} j \right) \quad (3.42)$$

$$\frac{\partial \phi}{\partial x} = -\frac{\pi^a}{TF} \frac{\partial T}{\partial x} - rj \quad (3.43)$$

and the equivalent expression also applies for the cathode.

3.1.3 The Electrode Surfaces

At the electrode surfaces a distinction must be made between the flow in and out of the electrode. The lithium ions move from the anode to the cathode. The anode surface will therefore have a flow in to the surface from the anode bulk phase and a flow out from the surface to the electrolyte. The cathode surface will have a flow in to the surface from the electrolyte and out of the surface to the cathode bulk phase. The entropy production thus becomes:

$$\sigma^s = J_q^i \Delta_{i,s} \left(\frac{1}{T} \right) + J_q^o \Delta_{s,o} \left(\frac{1}{T} \right) - j \frac{1}{T^s} \left(\Delta_{i,o} \phi + \frac{\Delta_n G^s}{F} \right) \quad (3.44)$$

Here, the rate of the reaction r is expressed in terms of the current density by $r = j/F$. Hence the entropy production from the potential and the Gibbs energy of the reaction will both be a product of the current density. The forces at the electrode surface can be expressed in terms of the corresponding resistivities:

$$\Delta_{i,s} \frac{1}{T} = r_{ii}^{s,i} J_q^{i} + r_{io}^{s,i} J_q^{o} + r_{i\phi}^{s,i} j \quad (3.45)$$

$$\Delta_{s,o} \frac{1}{T} = r_{oi}^{s,o} J_q^{i} + r_{oo}^{s,o} J_q^{o} + r_{o\phi}^{s,o} j \quad (3.46)$$

$$-\frac{1}{T^s} \left(\Delta_{i,o} \phi + \frac{\Delta_n G^s}{F} \right) = r_{\phi i}^{s,i} J_q^{i} + r_{\phi o}^{s,o} J_q^{o} + r_{\phi\phi}^{s,i} j \quad (3.47)$$

It is assumed that $r_{io}^s = r_{oi}^s = 0$. This means that coupling of the heat fluxes across the surface is neglected.

$$\pi^{i,s} = F \left(\frac{J_q^i}{j} \right)_{\Delta_{i,s} T=0} = F \frac{r_{i\phi}^s}{r_{ii}^s} \quad (3.48)$$

$$\pi^{s,o} = F \left(\frac{J_q^o}{j} \right)_{\Delta_{s,o} T=0} = F \frac{r_{o\phi}^s}{r_{oo}^s} \quad (3.49)$$

$$\lambda^{i,s} = \frac{1}{r_{ii}^s T_{i,o}^2} \quad (3.50)$$

$$\lambda^{s,o} = \frac{1}{r_{oo}^s T_{o,i}^2} \quad (3.51)$$

$$r^s = T^s \left(r_{\phi\phi}^s - \frac{r_{q\phi}^s r_{\phi q}^s}{r_{qq}^s} - \frac{r_{q\phi}^s r_{\phi q}^s}{r_{qq}^s} \right) \quad (3.52)$$

The expressions above can now be introduced to give the following expressions for the forces:

$$\Delta_{i,s} T = -\frac{1}{\lambda^{i,s}} \left(J_q^i - \frac{\pi^i}{F} j \right) \quad (3.53)$$

$$\Delta_{s,o} T = -\frac{1}{\lambda^{s,o}} \left(J_q^o - \frac{\pi^o}{F} j \right) \quad (3.54)$$

The electric potential can now be expressed similarly as before, as the potential also will have a contribution from the reaction happening at the electrode surface, the Peltier coefficient and the resistance across the surface.

$$\left(\Delta_{i,o} \phi + \frac{\Delta_n G^s}{F} \right) = \frac{\pi^i}{T^{i,o} F} \Delta_{i,s} T + \frac{\pi^o}{T^{o,i} F} \Delta_{s,o} T - r^s j \quad (3.55)$$

However, since these are surface parameters and the electrodes are thermostatted, it can be noted that $T_s = T_{i,o} = T_{o,i}$.

3.2 The Soret Effect

The thermal gradient will work as a driving force for the Soret effect and establish concentration gradients within the electrolyte. The Soret coefficient is defined in one direction for one component as [13]:

$$s_{T,i} = - \left(\frac{\left(\frac{\partial c_i}{\partial x} \right)}{c_i \left(\frac{\partial T}{\partial x} \right)} \right)_{J_i=0} = \frac{D'_i}{D_i} = \frac{q_i^*}{c_i T} \left(\frac{\partial \mu_{T,i}}{\partial c_i} \right)^{-1} \quad (3.56)$$

Where D'_i is the thermal diffusion coefficient for component i and D_i is the interdiffusion coefficient for component i . The expression for $\frac{\partial x_i}{\partial x}$ has already been found in equation 3.32, so the Soret coefficient can be rewritten as:

$$s_{T,i} = - \left(\frac{\left(\frac{\partial c_i}{\partial x} \right)}{c_i \left(\frac{\partial T}{\partial x} \right)} \right)_{J_i=0} = - \left(\frac{\left(\frac{\partial \left(\frac{c_i}{c_{tot}} \right)}{\partial x} \right)}{\frac{c_i}{c_{tot}} \left(\frac{\partial T}{\partial x} \right)} \right)_{J_i=0} = - \left(\frac{\left(\frac{\partial x_i}{\partial x} \right)}{x_i \left(\frac{\partial T}{\partial x} \right)} \right)_{J_i=0} \quad (3.57)$$

The results from equation 3.32 can be used to describe the gradients in the composition of the electrolyte.

$$\frac{\partial x_i}{\partial x} \approx \begin{cases} -\frac{q_i^* x_i}{RT^2} \frac{\partial T}{\partial x} & \text{for EC/DEC} \\ -\frac{q_i^* x_i}{2RT^2} \frac{\partial T}{\partial x} & \text{for LiPF}_6 \end{cases} \quad (3.58)$$

By inserting this into the equation above, the Soret coefficient can be determined to be:

$$s_{T,i} \approx \begin{cases} - \left(\frac{\left(\frac{-q_i^* x_i}{RT^2} \left(\frac{\partial T}{\partial x} \right) \right)}{x_i \left(\frac{\partial T}{\partial x} \right)} \right)_{J_i=0} = \frac{q_i^*}{RT^2} & \text{for EC/DEC} \\ - \left(\frac{\left(\frac{-q_i^* x_i}{2RT^2} \left(\frac{\partial T}{\partial x} \right) \right)}{x_i \left(\frac{\partial T}{\partial x} \right)} \right)_{J_i=0} = \frac{q_i^*}{2RT^2} & \text{for LiPF}_6 \end{cases} \quad (3.59)$$

The Soret coefficients can be related in similarly as the heats of transfer through Equation 3.29:

$$-s_{T,3} \left(1 + \frac{\partial \ln \gamma_3}{\partial \ln x_3} \right) = 2 \frac{x_1}{x_3} s_{T,1} \left(1 + \frac{\partial \ln \gamma_1}{\partial \ln x_1} \right) + \frac{x_2}{x_3} s_{T,2} \left(1 + \frac{\partial \ln \gamma_2}{\partial \ln x_2} \right) \quad (3.60)$$

If the logarithm of activity coefficients is approximately constant with the logarithm of the molar fraction of a components, this relation is simplified to:

$$-s_{T,3} \approx 2 \frac{x_1}{x_3} s_{T,1} + \frac{x_2}{x_3} s_{T,2} \quad (3.61)$$

3.3 The Seebeck Coefficient

The Seebeck coefficient is defined as the potential over the temperature gradient and can be divided into three contributions for the system:

$$\eta_s = \left[\frac{\Delta\phi}{\Delta T} \right]_{j=0} = \left(\frac{\Delta_a\phi + \Delta_c\phi}{\Delta T} + \frac{\Delta_{a,e}\phi + \Delta_{e,c}\phi}{\Delta T} + \frac{\Delta_e\phi}{\Delta T} \right)_{j=0} \quad (3.62)$$

Where $\Delta_a\phi$ is the potential gradient over the anode, $\Delta_c\phi$ is the potential gradient over the cathode, $\Delta_{e,a}\phi$ and $\Delta_{e,c}\phi$ is the potential gradient between the anode surface and the electrolyte and the cathode surface and the electrolyte respectively and $\Delta_e\phi$ is the potential difference over the electrolyte. ΔT is the temperature gradient between the two electrode surfaces, i.e. $T^{e,c} - T^{a,e}$. These potentials can be related to the expressions found in the previous section. Then $\Delta_a\phi$, $\Delta_c\phi$ and $\Delta_e\phi$ can be expressed by the expressions found for the potential in the bulk phase. $\Delta_{a,e}\phi$ and $\Delta_{e,c}\phi$ can be expressed by using the potential at the electrode surfaces and the equivalent expression for the cathode. Because the electrodes are thermostatted, the electrode temperatures are related by $T^{a,e} = T^{a,s} = T^{e,a}$ and $T^{e,c} = T^{s,c} = T^{c,e}$.

The notation used in the previous section can be rewritten to fit the two electrode surfaces in question by introducing the following notation for the anode:

$$\begin{aligned} i &= a, e \\ i, o &= o, i = a, s \\ o &= e, a \\ \Delta_{i,s} &= a, s - a, e \\ \Delta_{s,o} &= e, a - a, s \end{aligned}$$

3.3.1 The Electrolyte

At $t = 0$ and open circuit conditions, the following expression can be found for the electrolyte potential:

$$\Delta\phi_{j=0} = -\frac{L_{\phi q}}{L_{\phi\phi}} \frac{1}{T} \Delta T + \frac{1}{F} \left(t_1 - \frac{x_1}{x_3} t_3 \right) \Delta\mu_{1,T} + \frac{1}{F} \left(t_2 - \frac{x_2}{x_3} t_3 \right) \Delta\mu_{2,T} \quad (3.63)$$

The Peltier coefficient of the electrolyte is

$$\pi^e = TS_{\text{Li}^+}^* + \left(t_1 - \frac{x_1}{x_3} t_3 \right) q_1^* + \left(t_2 - \frac{x_2}{x_3} t_3 \right) q_2^* \quad (3.64)$$

Alternatively it can be expressed using the Soret coefficient (see Eq. 3.59):

$$\pi^e \approx TS_{\text{Li}^+}^* + 2 \left(t_1 - \frac{x_1}{x_3} t_3 \right) RT^2 s_{T,1} + \left(t_2 - \frac{x_2}{x_3} t_3 \right) RT^2 s_{T,2} \quad (3.65)$$

At any time the contribution to the electric potential from the electrolyte will be:

$$\begin{aligned} \Delta_e \phi &= \frac{1}{F} \left(-S_{\text{Li}^+}^* (T^{e,c} - T^{e,a}) \right) - \frac{1}{TF} \left(t_1 - \frac{x_1}{x_3} t_3 \right) q_1^* (T^{e,c} - T^{e,a}) \\ &\quad - \frac{1}{TF} \left(t_1 - \frac{x_1}{x_3} t_3 \right) q_2^* (T^{e,c} - T^{e,a}) + \frac{1}{F} \left(t_1 - \frac{x_1}{x_3} t_3 \right) \Delta \mu_{1,T} \\ &\quad + \frac{1}{F} \left(t_2 - \frac{x_2}{x_3} t_3 \right) \Delta \mu_{2,T} \end{aligned} \quad (3.66)$$

Then the contribution from the electrolyte to the thermoelectric potential initially will be:

$$\begin{aligned} \left(\frac{\Delta_e \phi}{\Delta T} \right)_{j=0, t=0} &= -\frac{1}{F} S_{\text{Li}^+}^* - \frac{1}{TF} \left(t_1 - \frac{x_1}{x_3} t_3 \right) q_1^* + \frac{1}{TF} \left(t_2 - \frac{x_2}{x_3} t_3 \right) q_2^* \\ &\approx -\frac{1}{F} S_{\text{Li}^+}^* - \frac{2RT}{F} \left(t_1 - \frac{x_1}{x_3} t_3 \right) s_{T,1} + \frac{RT}{F} \left(t_2 - \frac{x_2}{x_3} t_3 \right) s_{T,2} \end{aligned} \quad (3.67)$$

The stationary state contribution to the Seebeck coefficient will be:

$$\left(\frac{\Delta_e \phi}{\Delta T} \right)_{j=0, d\mu=0} = -\frac{1}{F} S_{\text{Li}^+}^* \quad (3.68)$$

3.3.2 The Electrode Bulk Phases

The following expression has been found for the change in the electric potential through the electrode bulk phase for the anode:

$$\frac{\partial}{\partial x} \phi^a = -\frac{\pi^a}{TF} \frac{\partial T}{\partial x} - r^a j \quad (3.69)$$

An equivalent expression can also be used for the cathode. On integrated form and by putting $j = 0$, the expression for the potential in the anode and the cathode becomes:

$$\Delta_a \phi + \Delta_c \phi = \frac{1}{F} \left(S^{*,a} (T^{a,0} - T^{a,e}) + S^{*,c} (T^{c,e} - T^{c,0}) \right) \quad (3.70)$$

From before it has been seen that the transported entropy of the charge carrier in both electrodes is S_e^* . The temperature dependence of the transported entropy of the charge carrier in electrode is assumed negligible. $T^{a,0} = T^{c,0} = T^0$ can then be inserted into the equation to give the following:

$$\Delta_a \phi + \Delta_c \phi = \frac{1}{F} (S_e^*) (T^{c,e} - T^{a,e}) \quad (3.71)$$

The contribution from the electrode bulk phases to the Seebeck coefficient:

$$\left(\frac{\Delta_a \phi + \Delta_c \phi}{\Delta T} \right)_{j=0} = \frac{1}{F} S_e^* \quad (3.72)$$

3.3.3 The Electrode Surfaces

The partial entropy can be expressed by the following Maxwell relation:

$$S_j = \left(\frac{S}{N_j} \right)_{p,T,N_{i \neq j}} = - \left(\frac{\partial \mu_j}{\partial T} \right)_{p,N} \quad (3.73)$$

From before it has been found that at equilibrium, the entropy production is 0 and hence the expression for the potential drop over the electrode can be expressed as:

$$\left(\Delta_{i,o} \phi + \frac{\Delta_n G^s}{F} \right) = \frac{\pi^i}{T^{i,o} F} \Delta_{i,s} T + \frac{\pi^o}{T^{o,i} F} \Delta_{s,o} T - \frac{1}{F} \Delta_{i,s} \mu_{Li^+,T} - \frac{1}{F} \Delta_{s,o} \mu_{Li^+,T} - r^s j \quad (3.74)$$

And the equivalent notation for the cathode. The anode surface potential with $j = 0$ can then be expressed as:

$$\Delta_{a,e} \phi = \frac{\pi^{a,e}}{T^{a,e} F} (T^{a,e} - T^{a,s}) + \frac{\pi^{e,a}}{T^{e,a} F} (T^{a,s} - T^{e,a}) - \frac{\Delta_n G^{a,s}}{F} \quad (3.75)$$

Because of the thermostatted electrodes, all terms except the last will disappear. Hence the anode surface potential can be expressed by:

$$\Delta_{a,e} \phi = - \frac{\Delta_n G^{a,s}}{F} \quad (3.76)$$

Which is in agreement with Nernst equation. Similarly the cathode potential can be expressed as:

$$\Delta_{e,c} \phi = - \frac{\Delta_n G^{s,c}}{F} \quad (3.77)$$

Since $\Delta_n G^{a,s}$ has contributions from neutral surface components [35], the contribution to the anode potential is:

$$\frac{\Delta_n G^{a,s}}{F} = \frac{1}{F} \left(- \mu_{Li(x,s)} (T^{a,e}) \right) \quad (3.78)$$

And similarly for the cathode:

$$\frac{\Delta_n G^{s,c}}{F} = \frac{1}{F} \left(\mu_{Li(x,s)} (T^{c,e}) \right) \quad (3.79)$$

Where $\mu_{Li(x,s)}$ is the chemical potential of Li in the electrode. By using equation 3.73, these equations can be rewritten to:

$$\Delta_{a,e} \phi = - \frac{1}{F} (S_{Li(x,s)} T^{a,e}) \quad (3.80)$$

$$\Delta_{e,c}\phi = \frac{1}{F} (S_{\text{Li}(x,s)} T^{c,e}) \quad (3.81)$$

The contribution from the electrode surfaces to the Seebeck coefficient can therefore be expressed as:

$$\left(\frac{\Delta_{a,e}\phi + \Delta_{e,c}\phi}{\Delta T} \right)_{j=0} = \frac{1}{F} S_{\text{Li}(x,s)} \quad (3.82)$$

3.3.4 The Total Seebeck Coefficient of the System

The Seebeck coefficient can now be found by adding the individual contributions to the thermoelectric potential that has been found. The thermoelectric potential is then at stationary state:

$$\eta_{s,\infty} = \left[\frac{\Delta\phi}{\Delta T} \right]_{j=0,t=\infty} = \frac{1}{F} (S_e^* - S_{\text{Li}^+}^* + S_{\text{Li}(x,s)}) \quad (3.83)$$

At $t \approx 0$ it is:

$$\begin{aligned} \eta_{s,0} &= \left[\frac{\Delta\phi}{\Delta T} \right]_{j=0,t=0} \\ &= \frac{1}{F} \left(S_e^* - S_{\text{Li}^+}^* - \frac{1}{T} \left(t_1 - \frac{x_1}{x_3} t_3 \right) q_1^* - \frac{1}{T} \left(t_2 - \frac{x_2}{x_3} t_3 \right) q_2^* + S_{\text{Li}(x,s)} \right) \end{aligned} \quad (3.84)$$

This shows that the Seebeck coefficient will be dependent on the Soret effect in the cell. Since both q_1^* and q_2^* affect the thermoelectric potential, this means that there might be two Soret equilibrium that have to be established before the system reaches a stationary state. When $t = 0$, the heat of transfer terms will make a large contribution to the Seebeck coefficient, but as $t \rightarrow \infty$ and the system approaches a stationary state it will give a smaller contribution to the coefficient [25]. If both the initial and steady state Seebeck coefficient is known, this can be used to find the measurable heat of transfer as a function of the temperature:

$$\frac{1}{TF} \left(t_1 - \frac{x_1}{x_3} t_3 \right) q_1^* + \frac{1}{TF} \left(t_2 - \frac{x_2}{x_3} t_3 \right) q_2^* = -((\eta_s)_{t \rightarrow \infty} - (\eta_s)_{t=0}) \quad (3.85)$$

From this it can be seen that the Seebeck coefficient is dependent on the material of the electrode, the solvent of the electrolyte and the ion of the electrolyte.

As q^* is related to the chemical potential gradient, and the chemical potential gradients may have opposite signs, it is likely that the measurable heat of transfer for the salt and at least one of the solvent molecules is of opposite sign.

$S_{\text{Li}(x,s)}$, the entropy is the entropy of Li in the two-dimensional layer, will not

be equal to the standard entropy of lithium. An estimate of the value of $S_{\text{Li}(x,s)}$ will be the standard entropy and an additional intercalation contribution. With different x , $S_{\text{Li}(x,s)}$ will have a different value. The intercalation contribution is discussed and a model developed and compared to a model used in literature in Appendix E. The contribution can however be shown to be small.

3.3.5 The Time-Evolution of the Thermoelectric Potential

The change in composition with time as a result of the Soret effect has been derived by de Groot for solutions at infinite dilution and uniform density, and extended by Bierlein to include thermal expansion [15, 36]. From this, the time dependence of the thermoelectric potential of binary solutions has been derived by Agar et al. and Tyrrell [19, 37]:

$$\epsilon_t = \begin{cases} \epsilon_\infty - \frac{8(\epsilon_\infty - \epsilon_0)}{\pi^2} \exp\left(-\frac{t}{\theta}\right) & t > \theta/3 \\ \epsilon_0 + 4\pi \left(\frac{\theta t}{\pi^3}\right)^{1/2} (\epsilon_\infty - \epsilon_0) \left(1 - 2\sqrt{\pi} i \operatorname{erfc} \left[\frac{\pi}{2} \sqrt{t/\theta}\right]\right) & t < \theta/3 \end{cases} \quad (3.86)$$

Here ϵ_t is the thermoelectric potential at time t and θ is the time constant given by:

$$\theta = \frac{h^2}{D\pi^2} \quad (3.87)$$

Here h is the distance between the electrodes, i.e. the diffusion path length, and D is the diffusion coefficient. $i \operatorname{erfc}$ is here the integral complementary error function defined as:

$$i \operatorname{erfc} x = \frac{1}{\sqrt{\pi}} \exp(-x^2) - x \operatorname{erfc} x \quad (3.88)$$

By fitting an exponential equation to a plot of the thermoelectric potential over time, the diffusion constant of the components of the system can be determined.

The electrolyte used in the cells in this thesis is not binary, but ternary. Therefore the expression given by Tyrrell is not valid. However, when coupling between mass fluxes is assumed negligible, that is $l_{ij} \approx 0$ which is an assumption used for the derivation in this thesis, the time development of the composition of the components are independent. If the two diffusion phenomena do not overlap to a significant degree, i.e. occur on different time-scales, the expression by Tyrrell could be implemented twice to describe the evolution of the electric potential of a ternary electrolyte with time.

3.4 Peltier Heat

The Peltier heat is defined for interfaces or junctions [13]. It is the heat that is transferred reversibly when current passes through the electrodes to the electrolyte. The Peltier heat over the temperature is the entropy transferred across the interface. It is the difference in the Peltier coefficient of the two sides of the interface and the heat from the electrode reaction. The Peltier heat at one electrode and the surrounding electrolyte can be defined from experimental measurements of $\Delta\phi/\Delta T$ at initial time and stationary state to be [25]:

$$\begin{aligned} \pi &= \pi^{\text{electrolyte}} - \pi^{\text{electrodes}} - TS_{\text{Li}(x,s)} = -F \left(\frac{\Delta\phi}{\Delta T} \right) T \\ &= \begin{cases} T \left(-S_e^* + S_{\text{Li}^+}^* - S_{\text{Li}(x,s)} \right) + \left(t_1 - \frac{x_1}{x_3} t_3 \right) q_1^* + \left(t_2 - \frac{x_2}{x_3} t_3 \right) q_2^* & \text{at } t \approx 0 \\ T \left(-S_e^* + S_{\text{Li}^+}^* - S_{\text{Li}(x,s)} \right) & \text{at } t \rightarrow \infty \end{cases} \end{aligned} \quad (3.89)$$

Faraday's constant is included to give the correct units. When charge is passed through a cell, the Peltier heat of the anode is positive, i.e. heat is absorbed, and the Peltier heat of the cathode is negative, leading to local cooling at the anode and heating at the cathode. For lithium ion batteries, LiCoO_2 will be the anode during charging and thus local cooling will occur during charging and heating during discharging [9]. C_6 will be the anode during discharging and thus local heating will occur during charging and heating during discharging. The opposite is true during discharging. It can clearly be seen that the composition of the electrolyte must affect the Peltier heat of the electrode-electrolyte surface. The correct description of the Peltier heat of these cells is then the Peltier heat at the electrode and its surrounding electrolyte.

This expression at stationary state is consistent with the expression for the Peltier coefficient at the double layer of one electrode of a lithium-ion battery given by Latz *et al.* [38]. The only discrepancy comes from the definition of the Peltier coefficient they used, which was $\pi = T\eta_s$. Latz *et al.* did not include any contribution from the Soret effect in the Peltier coefficient, but included it as a separate heat effect. By including the temperature dependence of the chemical potential of Li-metal neglected by Latz *et al.*, the expression found can be written using the definition of the Peltier heat and the notation used in this thesis as:

$$\pi = -TF (\eta_s^s - \eta_s^e) + T \frac{\partial ((\mu_s - \mu_e)/z_+)}{\partial T} \quad (3.90)$$

where η_s^s and η_s^e is the contribution to the Seebeck coefficient from the electrode and electrolyte respectively, and $\frac{\partial(\mu_s - \mu_e)}{\partial T}$ is the temperature derivative of the chemical potential of the active particle in the electrode and electrolyte. The difference $\mu_s - \mu_e$ is related to the electric potential change over the surface at one electrode. The temperature derivative of this is $-S_{\text{Li}(x,s)}$ (see chapter 3.3.3). This is the entropy of the active particle in the intercalation process of the electrode, which is Li. z_+ is the charge number of the ion involved, which for lithium is 1. The terms can be interpreted as S_e^*/F , $S_{\text{Li}^+}^*/F$ and $-S_{\text{Li}(x,s)}$ respectively.

3.4.1 Total Reversible Heat Effect in a Lithium Ion Battery Cell

The total reversible heat effect is the sum of the local heat effects, i.e. the single electrode Peltier heats, occurring at the cathode and anode.

$$Q^{\text{rev}} = \frac{j}{F} (\pi^a - \pi^c) = jT \left(\left(-\frac{\Delta\phi}{\Delta T} \right)^a - \left(-\frac{\Delta\phi}{\Delta T} \right)^c \right) \quad (3.91)$$

It is thus a sum related to the thermoelectric potential of two thermoelectric cells related to only the anode and only the cathode with the same electrolyte. At initial state:

$$\begin{aligned} \pi^a - \pi^c = & T \left(S_e^{*,c} - S_{\text{Li}^+}^{*,c} + S_{\text{Li}(x,s)}^c \right) - \left(t_1 - \frac{x_1}{x_3} t_3 \right) q_1^{*,c} \\ & - \left(t_2 - \frac{x_2}{x_3} t_3 \right) q_2^{*,c} - T \left(S_e^{*,a} - S_{\text{Li}^+}^{*,a} + S_{\text{Li}(x,s)}^a \right) \\ & - \left(t_1 - \frac{x_1}{x_3} t_3 \right) q_1^{*,a} - \left(t_2 - \frac{x_2}{x_3} t_3 \right) q_2^{*,a} \end{aligned} \quad (3.92)$$

where the superscripts a and c again relates to the values for the anode and cathode respectively. However, since this is inside one cell, the electrolyte is the same. It will now be assumed that $q_i^{*,a} = q_i^{*,c}$, since these are properties related to transport of components in the electrolyte. This simplifies the expression to:

$$\begin{aligned} \pi^a - \pi^c = & T \left(S_e^{*,c} - S_{\text{Li}^+}^{*,c} + S_{\text{Li}(x,s)}^c \right) - T \left(S_e^{*,a} - S_{\text{Li}^+}^{*,a} + S_{\text{Li}(x,s)}^a \right) \\ = & FT(\eta_s^c - \eta_s^a) \end{aligned} \quad (3.93)$$

This then means that the total heat effect in the cell is a constant value while the Seebeck coefficient of each half-cell is constant. By measuring the Peltier heat at the individual electrodes, both the local and total heat effects in a Li-ion battery can be found. In literature, the convention is to express the total reversible heat effects in a battery as [9]:

$$Q^{\text{rev}} = T\Delta S \frac{j}{nF} \quad (3.94)$$

where n is the number of electrons in the electrode reaction (here $n=1$) and ΔS is the entropy change related to the reaction of one Li^+ at the anode and the cathode:

$$\Delta S = \frac{nF\Delta\phi}{\Delta T} \quad (3.95)$$

This Viswanathan *et al.* stated that since one reaction occurs at the anode and one at the cathode, the total entropy can be divided into a contribution from the anode and the cathode [9]:

$$\Delta S = \Delta S^c + \Delta S^a = F \left(\frac{\Delta\phi}{\Delta T} \right)^c - F \left(\frac{\Delta\phi}{\Delta T} \right)^a = \frac{\pi^a}{T} - \frac{\pi^c}{T} \quad (3.96)$$

This is consistent with the theory developed by Newman, which related the sum of the Peltier heats, and thus the Seebeck coefficient, of the electrodes to the entropy change of the cell [39]. Newman did not include the transported entropy of the charge carrier in the electrodes or in the electrolyte, rather expressing the Seebeck coefficient using only partial molar entropies. This treatment does not include the contribution from the transported entropy, which differs for the different electrodes and electrode surfaces. However, it is known through the Nernst equation that

$$\frac{\partial\Delta\phi}{\partial T} = -\frac{1}{F} \frac{\partial\Delta G}{\partial T} = \frac{1}{F} \Delta S \quad (3.97)$$

The same relation holds for the theory used in this thesis when cells with identical charge carriers in the electrodes are considered and the assumption is made that the transported entropy of the ion is the same for both electrodes, which was shown by Førland *et al.* [25]. This relation must also hold here, as the equation above is valid for electrochemical cells. If the transported entropy for the two electrode charge carriers and the ion is the same for the two electrodes, only the entropy change from the reaction is left. This would then mean that the total reversible heat effect is independent on the electrolyte, while the local reversible heat effect is not. It is unlikely that the transported entropy of the charge carrier is equal for the two electrodes, so in general $S_e^{*,c} \neq S_e^{*,a}$. However, if the external circuit is also considered these differences will cancel. This will also be true for the transported entropy of lithium. It can therefore be concluded that the same result is obtained by adding the Peltier heat of two half cells and by measuring the entropy change over a battery cell.

Chapter 4

Experimental

The experimental part is divided into three parts; the assembling of thermoelectric pouch cells, the temperature calibration of the measurements and the thermoelectric potential measurements. The thermoelectric potential measurements involves the measurement on LiCoO_2 cells, C_6 cells and LiFePO_4 cells.

4.1 Pouch Cells

The pouch cells were made by Frank Richter. The pouch cell housing consisted of a laminate of 12 μm polyester polyethylene terephthalate (PET), 9 μm aluminium and 100 μm polyethylene (PE). This laminate was cut so that it had 4 cm height and 4 cm width. The laminate melts under the application of heat, which was used to seal the cell. A current collector, for LiCoO_2 and LiFePO_4 aluminium and copper for C_6 , was connected to the cell through a contact sealed to the laminate. Because of the size of the current collector, a thermal bonding film was added to seal the side. This thermal bonding film was from 3M with the article number TBF615. A tape from 3M with article number SC-100-10 was used to keep this film in place. The cell was then sealed on the side with the current collectors in the cell by applying heat to melt the thermal bonding film. The electrodes (LiCoO_2 HS-LIB-P-Co-001, C_6 HS-LIB-N-Gr-001 and LiFePO_4 HS-LIB-P-LFP-001 from Hohsen) and a stack of 4 separators made of Whatman Glass Microfibre Filters GF/D (no 1823070, pore diameter of 2.7 μm) were then placed inside the pouch. The electrodes were placed so that they are in contact with one current collector and the current collectors did not have any physical contact (no internal short circuiting). Another side was sealed by applying heat to the thermal bonding film on the edge. The electrolyte used was LP40 electrolyte from BASF consisting of a 1M solution of LiPF_6 and a 50:50 mixture of EC/DEC by weight. The concentrations of the components of the electrolyte was 0.528 mol/kg, 5.223 mol/kg and 3.893 mol/kg for LiPF_6 , EC and DEC respectively. The molar ratios was then $x_1=0.0547$, $x_2=0.5416$ and $x_3=0.4037$. The electrolyte was then added drop-wise to the separator stack inside a glove-box. The pouch was then vacuumized before the finale side was sealed by applying heat. The assembling of the individual components of the pouch cells is

illustrated in Figure 4.1.

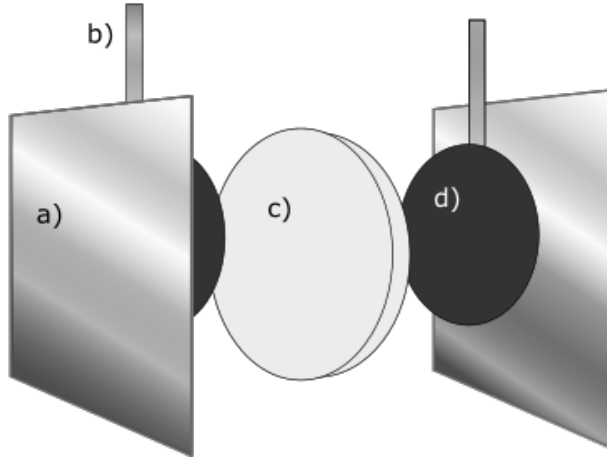


Figure 4.1: Illustration of the individual components of a pouch cell. a) The outer walls made of aluminum film with a thermal bonding film, b) the current collector made of aluminum (LiCoO_2 and LiFePO_4) or copper foil (C_6), c) the wetted separator, d) the electrodes of either LiCoO_2 , LiFePO_4 or C_6 . The electrolyte is added to one electrode, after which the separator is soaked with the electrolyte and the second electrode is added before the pouch cell is sealed.

4.2 Temperature Calibration

To determine the thermoelectric potential of a cell, the temperature gradient present inside the cell had to be estimated and measured. The thermal profile in the cell was calculated using thermal conductivity data and the cell dimensions (see Table B.1 in Appendix B). However, it is reasonable to assume that the deviation from the stationary state temperature profile is small. Due to the dimensions of the separator and electrodes, the assumption of thermostatted electrodes is reasonable and it can be assumed that the temperature gradient exist only over the separator (see the thermal conductivity data and thicknesses in table B.1 in Appendix B). The same assumption and similar choice of cell dimensions were used by Hudak *et al.* for studying thermoelectric properties of Li_xTiS_2 cells [16].

In the LiCoO_2 , LiFePO_4 and C_6 pouch cell, the temperature was measured on the outside of a copper plate. To measure the temperature gradient within the

cell, Richter made a LiCoO_2 cell with thermocouples inside the cell. The temperature gradient inside the cell was then calibrated against a measurement with a cell made with thermocouples between the electrodes and the separator. Omega Self-Adhesive K-type thermocouples with diameter of 12-20 μm were placed between the electrode and the separator on each side of the cell. The temperature gradient inside the cell was then measured for 5 different external temperature gradients. The experimental set-up for the temperature calibration is shown in Figure 4.2.

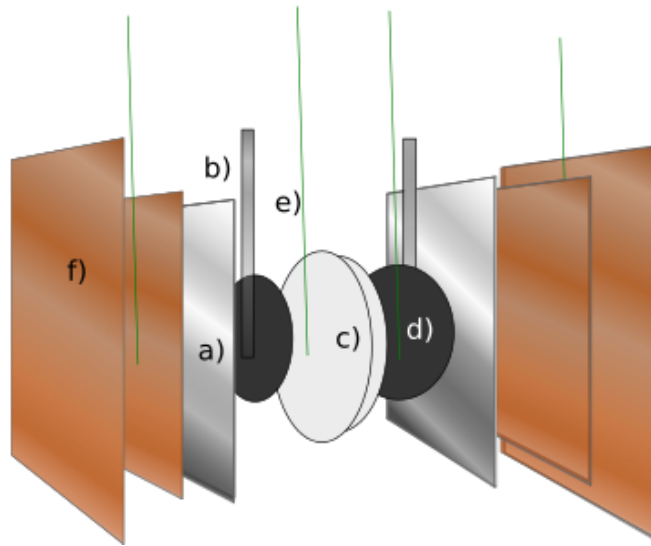


Figure 4.2: Illustration of the individual components of the temperature calibration. a) The outer walls made of aluminium film with a thermal bonding film, b) the current collector made of aluminum (LiCoO_2 and LiFePO_4) or copper foil (C_6), c) the wetted separator, d) the electrodes of either LiCoO_2 , LiFePO_4 or C_6 , e) thermocouples between the electrodes and separator and between the copper plates, f) copper plates used for thermostating the cell. The electrolyte is added to one electrode, after which the separator is soaked with the electrolyte and the second electrode is added before the pouch cell is sealed.

A deviation was observed between the temperature profile obtained using Fourier's law (see Figure B.1) and the temperature profile found experimentally shown in Figure 4.3. Since the cell is not completely flat, this deviation is believed to be the result of air trapped between the copper plates and the pouch cell. An air

gap between the copper plate and the pouch cell will have a high resistance. It is therefore likely that this is the primary source of temperature gradient loss. The resulting temperature gradient was 71 ± 1 % of the temperature gradient measured between the copper plates. The temperature gradient inside the cell is primarily in the electrolyte, supporting the assumption of thermostatted electrodes. Another source of heat loss or gain is the current collectors. Part of the Al or Cu current collectors are outside of the cell. The current collectors will therefore conduct heat to the cold part of the cell from the surroundings and heat will be lost to the surroundings from the hot part of the cell. This source of heat loss/gain is assumed to be minor. A source of error present in these calculations is that the conductivity of the wetted separator was measured without LiPF_6 present in the carbonate solution.

Since the calibration cell was only made using LiCoO_2 electrodes, it will be assumed in this thesis that it is valid also for the LiFePO_4 and C_6 cells. The cell dimensions are the same and the electrode thermal conductivity is high enough in comparison with the wetted separator that this is a reasonable assumption.

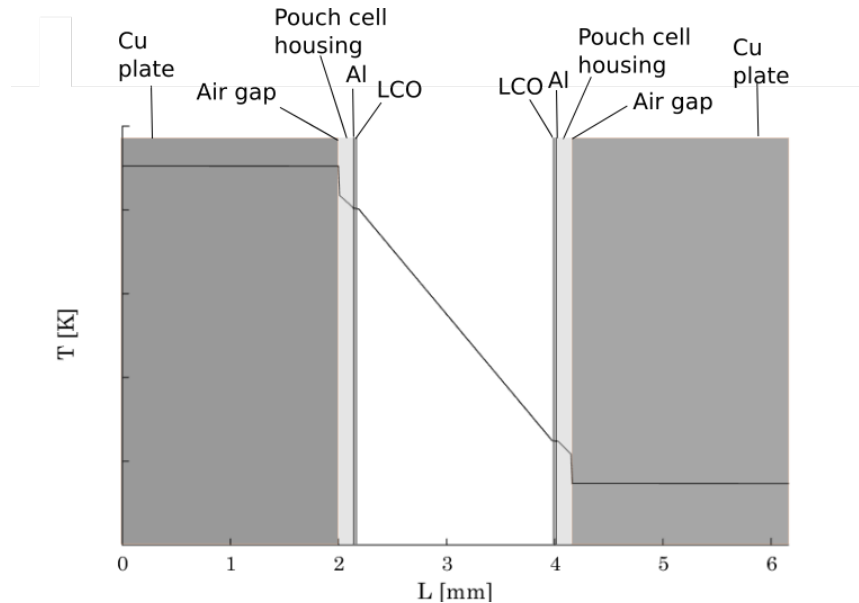


Figure 4.3: Shows the stationary state temperature profile calculated using Fourier's law and the thermal conductivity data for the pouch cell, see Table B.1 in Appendix B.

4.3 Thermoelectric Potential Measurements

The electric potential was recorded using an Agilent 34970A Data acquisition/Switch unit. The temperature gradient was established using two water baths set to different temperatures (thermostat Grant GD 120). The middle temperature was kept constant at 25°C throughout the experiments, and the water baths were set so that an external water bath temperature gradient of 5, 10 and 15°C was applied and in addition 12.5 and 20 °C for the LiFePO₄ cells. The water circulated in tubes through a frame holding the equipment together and the tubes were in contact with the frame exchanging heat with copper plates, one for the tube with cold water and one for the tube with hot water. The hot water flow was set on top of the cell to avoid convection. The copper plates were used as a heat conductor to apply the temperature gradient uniformly to the two sides of the pouch cell. Omega Self-Adhesive K-type thermocouples were placed between the copper plates and the pouch cell housing to measure the temperature gradient during the experiment. The electric potential and temperature was recorded until a stationary state was reached and until system had relaxed to the initial equilibrium state. A calibration curve and heat conduction measurements were used to determine the temperature gradient between the electrodes. An illustration of the experimental set up within the frame is shown in Figure 4.4.

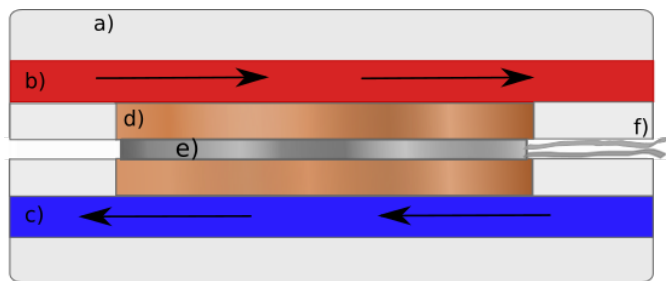


Figure 4.4: Illustration of the initial experimental setup; a) frame , b) hot water flow, c) cold water flow, d) heat conducting copper plates and thermocouples, e) pouch cell, f) current collectors of the pouch cell. The heat conducting copper plates transfers the heat from the water flowing in tubes inside the frame continuously to the pouch cell. The hot water flow is placed at the top of the frame to avoid errors due to convection and thereby an increased heat transfer from the hot electrode to the cold electrode.

The LiCoO₂ cells were short-circuited prior to the start of the first experiments. A

gradual change in the bias potential over the course of the measurements was in the case of the graphite cells very large. A smaller, though significant change in the bias potential was also observed for the LiFePO_4 cell. The graphite and LiFePO_4 cells were short-circuited at room temperature for 2-3 days prior to each of the measurements and allowed to reach an equilibrium state again before every measurement. Due to the change in bias potential, the graphite cells were turned around and the experiment repeated with the opposite order of temperature gradients.

Chapter 5

Results and Discussion

The electric potential before, during and after a temperature gradient was applied to LiCoO₂, LiFePO₄ and C₆ pouch cells has been measured for external temperature gradients of 5, 10 and 15K (and 12.5 and 20 K for the LiFePO₄ cell).

The LiCoO₂ cells investigated had already been used in previous measurements and so showed a very constant behaviour in the bias potential, though a small drift was observed. The C₆ cells were, however, unused and had large changes in the bias potential for each measurement. The LiFePO₆ cell was also unused, but had a smaller change in bias potential of around 2 mV per measurement. A similar drift was observed by Hudak et al. for Li_xTiS₂ symmetric cells [16]. The pristine condition of the C₆ and LiFePO₄ cells and used condition of the LiCoO₂ cells will be taken into consideration in the interpretation of the results.

The values of S_e^* for the electrodes have been reported in literature (including the current collectors) and are given in Table C.1. As mentioned in Section 3.3 the entropy of Li inside the electrode is not known. As a first approximation to get an estimate of $S_{Li^+}^*$, the standard entropy of Li in the solid crystal state will be used as an estimate for $S_{Li(x,s)}$. At 298 K, this value is 29 J K⁻¹ mol⁻¹. For LiCoO₂ and LiFePO₄, this estimate is reasonable, as the completely filled electrodes should have a very small contribution from the intercalation, as the logarithm of 1 is 0. A more complicated case occurs for the graphite cells. The graphite cells have no lithium inside the electrodes prior to the assembling and the lithiated state is therefore unknown. If there still is no lithium inside the electrode at the time of measurement, how can an estimate of the entropy be made for particles not present? It is also possible that some lithium may have diffused into the electrodes from the electrolyte. If this is the case it is not possible to know the lithiated state of the electrode at the time of the measurements.

Lundgren *et al.* measured the transport number of Li⁺ for the electrolyte used in this thesis to be 0.225 with the laboratory frame of reference at 25°C [40]. t_{Li^+} values of 0.17 and 0.23 were obtained at 10 and 40°C respectively. At 10°C, how-

ever, the solvent will be partially crystallized [40]. Since the temperature of the electrolyte will be in the range of 20-30 °C, a t_{Li^+} value of 0.225 will be assumed if applicable. This gives $t_1=0.775$. t_2 and t_3 have not been reported in literature.

Kandhasamy *et al.* measured Seebeck coefficients in salt melts inside a MgO matrix structure. Their results indicate that even though the pores in MgO are in the μm scale, it still affected the Seebeck coefficient [41]. The inert separator used inside the cells have pores of the same scale and it is likely that this will affect the measurements, possibly by increasing the time needed to reach stationary state. Though the separator is assumed to not affect the stationary state thermoelectric potential it is recommended that new cells are made with separators of different pore-sizes in future studies.

5.1 Thermoelectric Potential of LiCoO₂ Pouch Cells

A plot of the temperature difference inside the LiCoO₂ cells and the electric potential of the cell against time is shown in Figure 5.1 for the experiment with a water bath temperature difference of 10 K.

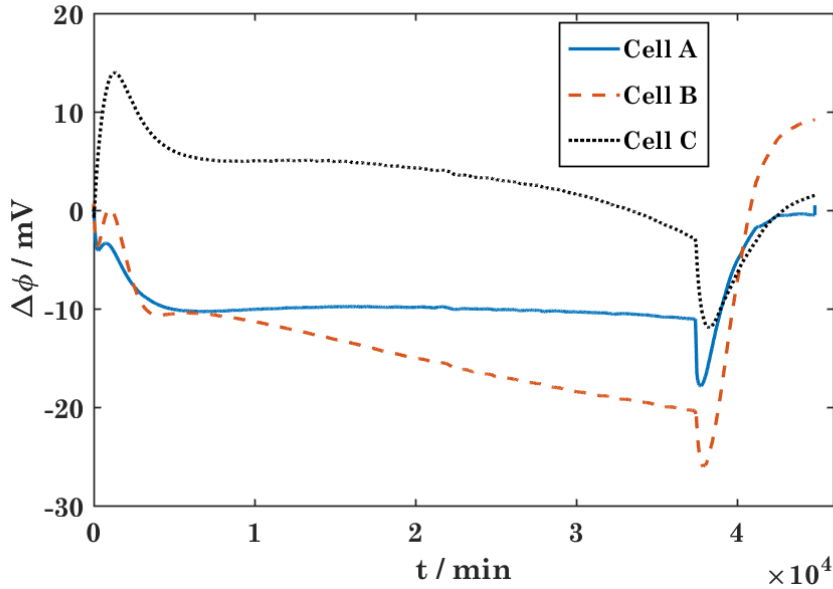


Figure 5.1: The electric potential of LiCoO₂ Cell A, Cell B and Cell C with a temperature difference of 5.7 K inside the cell.

A general trend, as shown in Figure 5.1, is repeated; a local minimum in the electric potential is reached initially. The electric potential then increases to a local maximum and before it decreases to a minimum plateau at stationary state. The initial minimum is reached on the time-scale of minutes (see Figure C.3).

The initial thermoelectric potential as given in Equation 3.84 in Section 3.3.4 will be estimated as the first minimum. It should be noted that at this point in time thermal diffusion processes are already contributing to the electric potential. The changes in the thermoelectric potential after this point are assumed to be the result of several thermal diffusion phenomena in the electrolyte. One diffusion process increases the electric potential, while the other decreases the electric potential. Thermal diffusion phenomena, though complicated in the transient time period, generally follow an exponential curve as the concentration gradient builds

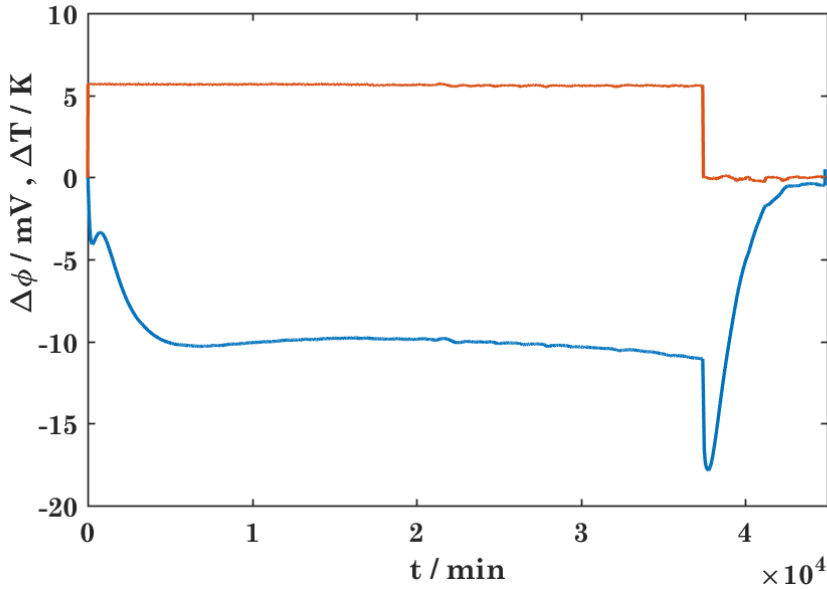


Figure 5.2: The internal temperature difference and electric potential of LiCoO₂ Cell A when the water bath temperature difference was set to 10 K.

up exponentially with time [12]. Since the temperature gradient was not established immediately, but took several minutes to develop, it is reasonable to assume that the onset of diffusion happens before the initial thermoelectric potential negative peak was established. That there is no common initial value of ϵ_t (see Figure 5.4) supports this. This means that the true initial thermoelectric potential is not observed in this experiment. Since there is an increase after the first minimum, the initial thermoelectric potential is most likely underestimated in the graphs. Repeating the experiments using a different heat source to establish the temperature gradient faster is therefore a way to improve the experimental results.

The relaxation process after the temperature gradient is reset to 0 involves a sharp decrease followed by a sharp increase in the electric potential. This indicates that in the relaxation process, all diffusion phenomena happens simultaneously while the thermoelectric potential also drops. This means that the difference between the stationary state value before the temperature gradient is turned off and the negative peak after the temperature gradient has been set to 0 should be close to $\Delta\phi_{\infty,1} - \Delta\phi_0$, where $\Delta\phi_{\infty,1}$ is the electric potential at the intermediate state. The negative peak can therefore be used to determine more accurately the initial electric

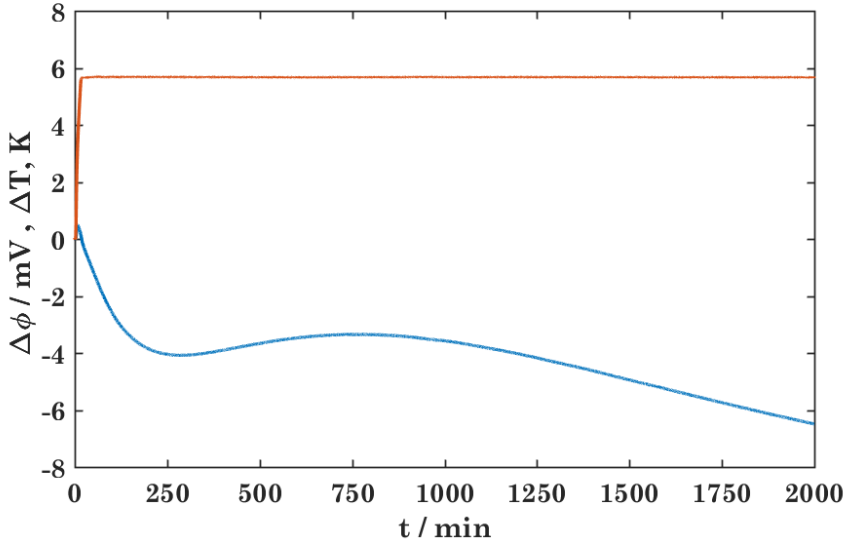


Figure 5.3: A zoom-in on the measurements at the initial time-period of the measurement on the LiCoO₂ Cell A when the water bath temperature difference was set to 10 K.

potential, and thus the initial thermoelectric potential. The difference between this negative peak and the bias potential when an equilibrium state has been reached will then be close to $\Delta\phi_{\infty,2} - \Delta\phi_{\infty,1}$, where $\Delta\phi_{\infty,2}$ is the final stationary state electric potential. This process will arise from interdiffusion. A diffusion process occurring because of a concentration gradient is generally more rapid than a thermal diffusion process. This should mean that the differences between the initial thermoelectric potential and the stationary states could be more accurately given by looking at the values from the relaxation curves.

The Peltier heats at initial, intermediate and steady state have been estimated from Equation 3.89. Using Equation 3.83, an estimate of $S_{\text{Li}^+}^*$ has been calculated from the steady state value. The results are given in Table 5.1. The stationary state thermoelectric potential does not converge towards a common value. This makes predicting $S_{\text{Li}^+}^*$ hard, as it is typically obtained from a linear plot of potential against the temperature gradient. The Seebeck coefficient is typically found by linear curve fitting of the results of $\Delta\phi$ against ΔT . Here, however, only two data points could be used for the curve fitting. It was thus not possible to use this method. A more uncertain method is to use the measured potential gradient

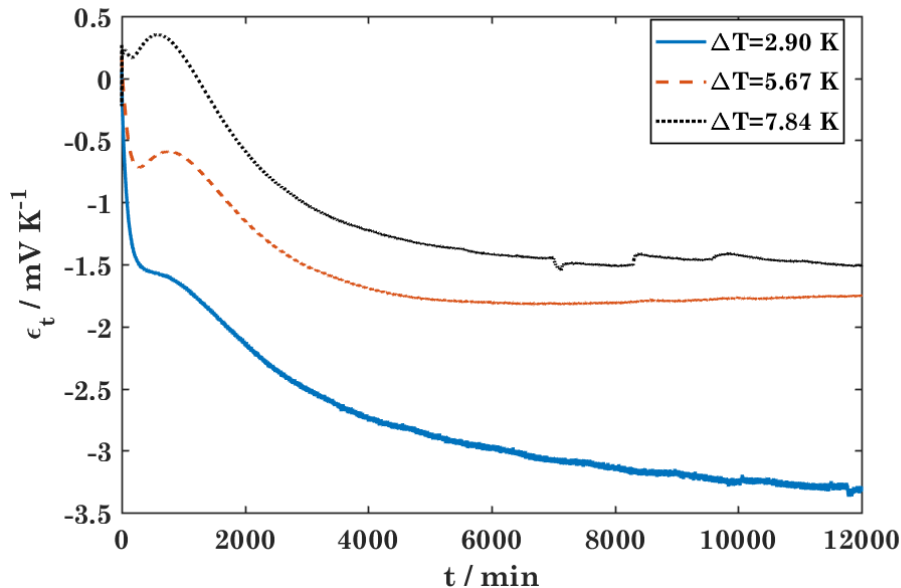


Figure 5.4: Plot of the electric potentials of the LiCoO_2 cell over the temperature differences within the cell (thermoelectric potential) for the 5, 10 and 15K external water bath temperature difference measurement.

and temperature gradient from each experiment directly to calculate the Seebeck coefficient as the stationary state thermoelectric potential measured. The thermoelectric potential at stationary state can then be used to calculate the transported entropy of Li^+ by using Equation 3.83. Repeating the experiment for cells of the same electrolyte would help determine η_s and $S_{\text{Li}^+}^*$ more accurately.

Viswanathan *et al.* reported the cell entropy of a $\text{Li}_x\text{CoO}_2/\text{Li}_x\text{C}_6$ cell with a 1M LiPF_6 EC/DMC (dimethyl carbonate) 1:1 electrolyte for various states of charge [9]. This is not the same electrolyte used in the cells investigated in this thesis and is also important to note that Viswanathan *et al.* do not specify whether the 1:1 ratio of EC/DMC is in weight, volume or mole percent. However, the entropy change over a battery cell should only be determined by the electrodes and be independent of the electrolyte. The numbers reported by Viswanathan *et al.* will therefore be used as estimates. At state of charge 0 for a lithium cobalt oxide and graphite cell ($x=1$ in Li_xCoO_2 and $x=0$ in Li_xC_6), the cell entropy change found by Viswanathan was -105 J/mol K . This gives a reversible heat effect of 31.3 kJ/mol . By using this total cell entropy the individual heat effects of graphite may be esti-

mated using Eq. 3.96 from the Peltier heat measured for LiCoO₂. The results are shown in Table 5.1.

Table 5.1: Seebeck coefficients and electrode Peltier heats of LiCoO₂ at uniform electrolyte and at Soret equilibrium and the estimated transported entropy of Li⁺. The errors are given to two standard deviations. The values of $S_{\text{Li}^+}^*$ are calculated using $S_e^* = 10 \text{ J K}^{-1} \text{ mol}^{-1}$ and $S_{\text{Li}(x,s)} = 29 \text{ J K}^{-1} \text{ mol}^{-1}$. The Peltier heat of C₆ is calculated from the entropy of the LiCoO₂/C₆ cell of -105 J/mol K (for x=1 in Li_xCoO₂ and x=0 in Li_xC₆) measured by Viswanathan *et al.* [9]. *Not included in the average value.

ΔT /K	ϵ_0 /mV K ⁻¹	$\epsilon_{\infty,1}$ /mV K ⁻¹	$\epsilon_{\infty,2}$ /mV K ⁻¹	$S_{\text{Li}^+}^*$ /J K ⁻¹ mol ⁻¹
2.90*	-3.5* ± 0.1	0.68* ± 0.05	-3.4* ± 0.05	294* ± 3
5.67	-2.5 ± 0.1	1.3 ± 0.1	-1.8 ± 0.1	214 ± 2
7.84	-3.1 ± 0.1	1.6 ± 0.1	-1.5 ± 0.1	181 ± 5
Average	-2.8 ± 0.3	1.5 ± 0.2	-1.7 ± 0.2	200 ± 20
Peltier heat at electrode				
LiCoO ₂ /kJ mol ⁻¹	84 ± 9	-45 ± 6	51 ± 6	
C ₆ /kJ mol ⁻¹	-53 ± 9	-76 ± 6	-20 ± 6	

The value of $200 \pm 20 \text{ J K}^{-1} \text{ mol}^{-1}$ for $S_{\text{Li}^+}^*$ for this electrolyte is a high value compared with values reported in literature for other thermoelectric cells. However, since the transported entropy is specific for the cell used this is not unexpected. The positive sign of the transported entropy indicates that heat is transported with Li⁺.

Few data points were obtained in the measurements on these cells. To check the reproducibility of the results, new cells should be made. New cells in pristine condition could ascertain whether ageing effects can have affected the measurements and results in these cells.

5.1.1 Diffusion Coefficients and Heats of Transfer

The second Soret effect will start as soon as the temperature gradient is set and decreases the electric potential. The first Soret effect increases the electric potential. It is likely that the measurable heat of transfers will both be slightly underestimated because of overlap of these opposing forces. Gunawan *et al.* pointed out that since the Soret effect usually is small and it can take days to reach Soret equilibrium, often only the initial thermoelectric potential or initial Seebeck coefficient is measured for thermocells [42]. However, as is evident from Figure 5.1-5.4, the

Soret effect is not small in the case of the LiCoO_2 cell.

The curves in Fig C.1-C.6 indicates that two diffusion phenomena of different time scales occurs during the measurement. As a first approximation, Tyrrell's model will be implemented twice to estimate the two diffusion constants for the two processes. At this time no model exists for the time evolution of a multi-component diffusion process with a thermal driving force (the development of such a model has been attempted in Appendix D). An assumption must have been made that the composition after the first diffusion process has happened is the starting point for the second diffusion process. By fitting exponential curves to the plot of the thermoelectric potential, the time constant of the diffusion process, and thus the interdiffusion coefficient, can be estimated. The two expressions found were:

$$\epsilon_t \approx 48.2 \cdot \exp(-0.003716 \cdot t) - 49.6 \cdot \exp(-0.003503 \cdot t) + 3.3 \cdot \exp(-0.0007792 \cdot t) - 1.8$$

and

$$\epsilon_t \approx 4.5 \cdot \exp(-0.00508 \cdot t) - 6.2 \cdot \exp(-0.003679 \cdot t) + 3.4 \cdot \exp(-0.0006462 \cdot t) - 1.5$$

for the plots of the thermoelectric potential with temperature gradients of 5.7 and 7.8 K respectively. In these equations, t is given in minutes. The last exponential term can here be identified as the exponential describing the last diffusion process. The fitted curves found had high R^2 values of 0.9997 and 0.9990 respectively. The fitted curve for the electric potential measurement at a temperature gradient of 5.7 is shown in Figure C.9.

As the experimental method underestimates ϵ_0 , last exponential term in the curves correspond reasonably well with Equation 3.86. These exponentials have therefore been used to calculate a characteristic time θ_2 value and therefore also the diffusion constant D_2 . The diffusion constant for the first diffusion process is more difficult to obtain due to the complexity of the curve in the transient state when t is small. The first diffusion process gives a decrease in the electric potential, the second terms in the equations above can be identified as the exponential curves associated with the first diffusion. The first term is associated with the initial thermoelectric potential.

The constant in front of the terms are not totally in agreement with Tyrrell's theory. That the theory does not fit perfectly with the experimental results is

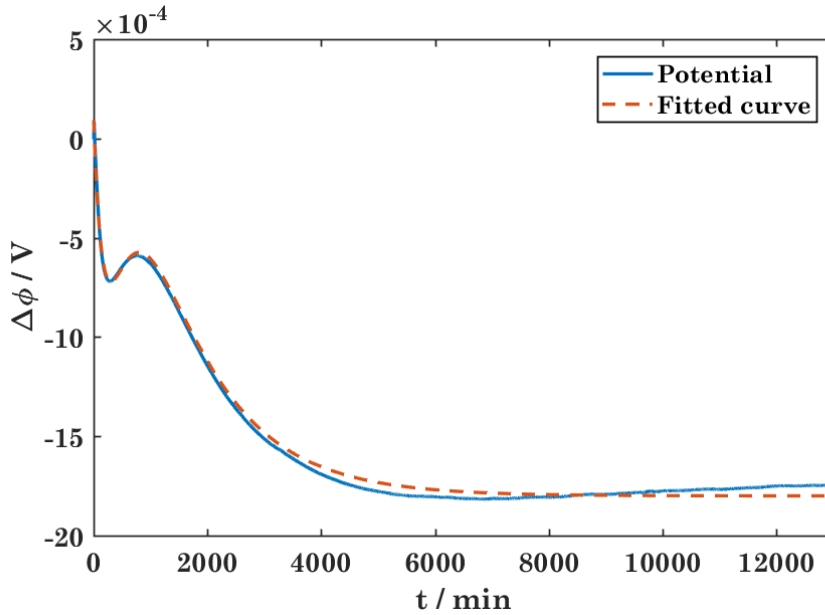


Figure 5.5: Shows the plot of the electric potential measurement at an internal temperature difference of 5.7 K and the fitted curve.

understandable since it is an approximation to use it for a ternary mixture. The initial thermoelectric potential will be underestimated by the onstart of the diffusion phenomena. The slowest diffusion process will begin before the first Soret equilibrium has been reached. It can also be assumed that the first Soret equilibrium will be perturbed slightly by the build up of a concentration gradient of another component. The two diffusion processes will therefore affect each other, and a complete agreement with Tyrrell's theory cannot be expected. The characteristic time of the diffusion process will therefore be obtained as an estimate from these terms.

As stated before the time scales of the two diffusion processes are very different. An estimate of $\left(t_1 - \frac{x_1}{x_3}t_3\right)q_1^*$ and $\left(t_2 - \frac{x_2}{x_3}t_3\right)q_2^*$ can be made by using Equation 3.85 and assuming that the intermediate state is the initial state of the second diffusion process.

$$\left(t_1 - \frac{x_1}{x_3}t_3\right)q_1^* = -TF(\epsilon_{\infty,1} - \epsilon_0) \quad (5.1)$$

$$\left(t_2 - \frac{x_2}{x_3}t_3\right)q_2^* = -TF(\epsilon_{\infty,2} - \epsilon_{\infty,1}) \quad (5.2)$$

The notation used here assumes that LiPF_6 is the faster diffusion process. Otherwise the notation for component 1 and 2 must be switched. This must be confirmed from simulations of the electrolyte. Since t_2 and t_3 are undetermined, isolated values for q_1^* , q_2^* and (through Equation 3.29) q_3^* cannot be estimated. The same data can be used to estimate $(t_2 - \frac{x_1}{x_3}t_3) s_{T,2}$ and $(t_2 - \frac{x_1}{x_3}t_3) s_{T,2}$ through Eq. 3.59. If the first process is associated with component 2, the Soret coefficients presented here must be adjusted for the factor 2 in Eq. 3.59.

Table 5.2: Heat of transfer and Soret coefficient data, characteristic times and corresponding diffusion coefficients obtained from the measurements of LiCoO_2 cells. The errors are given to two standard deviations.

ΔT / K	$(t_1 - \frac{x_1}{x_3}t_3) q_1^*$ / kJ mol ⁻¹	$(t_2 - \frac{x_2}{x_3}t_3) q_2^*$ / kJ mol ⁻¹	$(t_1 - \frac{x_1}{x_3}t_3) s_{T,1}$ / K ⁻¹	$(t_2 - \frac{x_1}{x_3}t_3) s_{T,2}$ / K ⁻¹
5.7	-34.4 ± 0.4	88.5 ± 0.3	-0.0233 ± 0.0003	0.120 ± 0.001
7.8	-43.0 ± 2.2	86.6 ± 1.2	-0.029 ± 0.002	0.117 ± 0.002
ΔT / K	θ_1 / min	θ_2 / min	D_1 / m ² s ⁻¹	D_2 / m ² s ⁻¹
5.7	290 ± 20	1283 ± 3	$2 \cdot 10^{-11} \pm 0.1 \cdot 10^{-11}$	$4.20 \cdot 10^{-12} \pm 0.01 \cdot 10^{-12}$
7.8	272 ± 15	1548 ± 4	$2 \cdot 10^{-11} \pm 0.1 \cdot 10^{-11}$	$3.48 \cdot 10^{-12} \pm 0.01 \cdot 10^{-12}$

The two estimates for the measurable heat of transfer values calculated has opposite signs. There can be two reasons for this. One possibility is that the "effective" transport number of the second component $(t_2 - \frac{x_2}{x_3}t_3)$ is negative (indicating transport in the opposite direction of the lithium ions). Investigating cells of different x_2 and x_3 values can be a possible method of determining this. The other possibility is that the heats of transfer have opposite sign due to an opposite sign in the chemical potential gradient.

The values for the diffusion coefficient for the second diffusion process, in the order of 10^{-12} m²/s, are significantly different from the self-diffusion coefficients for Li^+ , PF_6^- , EC and DEC reported by Hayamizy *et al.*, which are one order of magnitude higher [43]. The values for the first diffusion process have a higher uncertainty, which is not unexpected. Lundgren *et al.* measured a diffusion coefficient for LiPF_6 of $1.5 \cdot 10^{-10}$ m²/s for the same electrolyte that has been used here [40]. The electrolyte is held in an inert matrix by the porous separator. Could the separator material with 2.7 μm large pores be the reason for the discrepancy between these values? To establish the effect of the separator on the thermal diffusion process the experiment should be repeated using separators of different pore diameters.

Without results from simulations, it is difficult to be certain which diffusion process is associated with which components in the electrolyte solution. However, one possibility is to investigate a similar cell with an ion exchange membrane instead of a liquid electrolyte. Such a cell was built and tested as a battery by Liu *et al.* [44]. For an ideal system, the transport number of a cell with an ion exchange membrane Li^+ is 1. This means that there is no net flux of the salt in the electrolyte. At open circuit conditions, there would also be no flux of Li^+ ions. Since the ions would be associated with the fixed negative ions in the membrane, the charge-charge interaction would prevent any thermal diffusion of Li^+ inside the membrane when a temperature gradient is applied under open circuit conditions. Thus, the only flux possible, and only thermal diffusion phenomena of the system, is that of the non-aqueous liquid in the membrane, which can be chosen to be EC and DEC. This is a possible system to investigate in further studies to get a better understanding of the diffusion phenomena in the electrolyte.

5.2 Thermoelectric Potential of C₆ Pouch Cells

The graphite electrodes were in pristine condition during assembling and the cells were not used prior to the measurements. Originally the lithiated state was 0, meaning that there should be no lithium present inside the electrodes. This makes the entropy term difficult to interpret, as the logarithm of 0 is infinite. The contribution from the electrode surface has a greater uncertainty than in the LiCoO₂ case, as $S_{\text{Li}(x,s)}$ is undefined.

A change in the bias potential was observed during the experiment. To determine if this could affect the behaviour of the cells, the experiment was repeated with the gradient applied to the opposite side of the cell. From now on the first arrangement of the cell is referred to as arrangement 1, while the other is referred to as arrangement 2. The change in bias potential during the experiments decreased for cell C and B in both the original setup and after the cells were turned, as can be seen in table 5.3. The exception for this is the change for the first experiment, when the behaviour of cell B was similar to that of cell A. The change in bias potential can be an indication of a change in the lithiated state of the electrodes during the experiment.

Table 5.3: The bias potential of the graphite cells before and after the temperature gradient was applied. The errors are 0.01 mV given to two standard deviations.

Temperature gradient applied at arrangement 1.						
External temperature gradient	Bias potential at constant temperature			Bias potential after the experiment		
	Cell A	Cell B	Cell C	Cell A	Cell B	Cell C
/ K	/ mV	/ mV	/ mV	/ mV	/ mV	/ mV
5	5.00	-0.44	0.14	-4.5	2.45	6.60
10 experiment 1	3.50	0.08	-3.20	4.14	-2.01	-9.61
15 experiment 1	3.20	-3.40	4.50	4.46	-6.00	-14.5
15 experiment 2	2.30	3.10	3.00	2.90	-0.50	-9.90
10 experiment 2	-1.50	-1.10	9.00	-0.80	-1.00	-15.00

The behaviour of the cells were unchanged after turning the cells around and thereby changing the sign of the bias potential. This means that the direction of the small electric field due to the bias potential is not significant for the behaviour of these cells. Because of this the electrode structure and the lithiated state are the most likely the factors determining how the thermoelectric potential

behaves. Evidence of thermal diffusion is not clearly shown. Just as for the LiCoO_2 cells, it took days to obtain a steady state value, which indicates that the Soret effects are present. Other contributions to the potential obstruct the contribution from the diffusion phenomena.

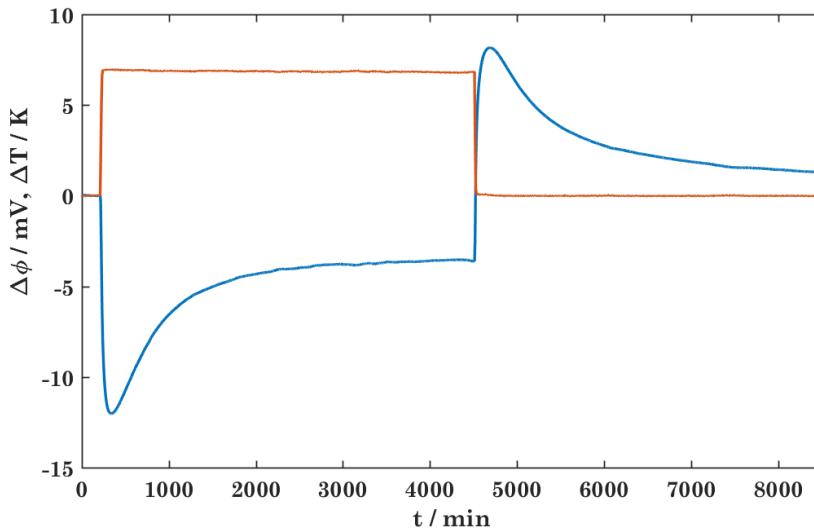


Figure 5.6: Plot of the internal temperature difference and the electric potential of graphite cell A with an external temperature difference of 15 K with arrangement 1.

It is evident from Figure C.20-C.22 that the behaviour of the cells are not similar to or as consistent the LiCoO_2 cells. Two types of behaviour have been observed; an initial step decrease to a minimum followed by a slow increase to a steady state plateau value or an initially step decrease that converges to a minimum value in the electric potential.

Initially cell B behaved similarly to cell A (see Figure C.12 in Appendix C), but during the course of the measurement series it changed to a behaviour similar to cell C. The change in the response of cell B is clearly shown in Figure C.27. The question is then; what is the cause of the discrepancies and how predictable will the individual behaviour of the cells be over time? The initial period behaviour is, however, similar to all cells. The steep decrease shown in the initial time period for all the cells can be interpreted as the initial thermoelectric potential. This time

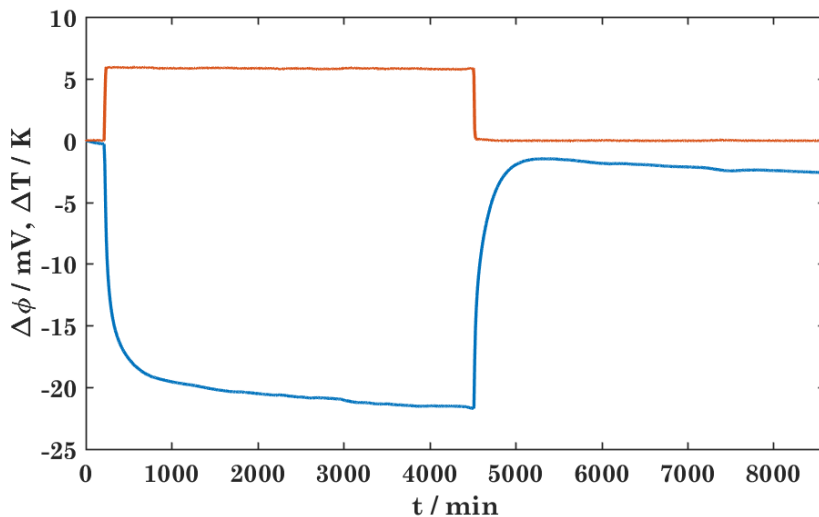


Figure 5.7: Plot of the internal temperature difference and the electric potential of graphite cell B with an external temperature difference of 15 K with arrangement 1.

period is of greatest importance for the thermal profile of Li-ion batteries. Charging typically last from minutes to an hour, during which the behaviour is similar for all the cells.

The measurements for cell B and cell C shows very high Seebeck coefficients, reaching as high as -6 mV/K (see Table 5.4). This is competitive with the highest Seebeck coefficients reported [6]. However, due to the changing bias potential, the uncertainty of these values is high. The Seebeck coefficient stated is the average between the value obtained from the response to the temperature gradient and the value from the relaxation curve. Because the difference between the two is relatively large, the uncertainty of the coefficient will also be large.

The lack of predictability of the values obtained and the large uncertainties will, however, be an obstacle for any practical application of these cells as thermoelectric cells. The bias potential of cell C changed considerably from before and after the temperature gradient was applied, resulting in increasingly larger uncertainties for the values measured. The sudden change in behaviour for cell B is another indication on the instability of these cells.

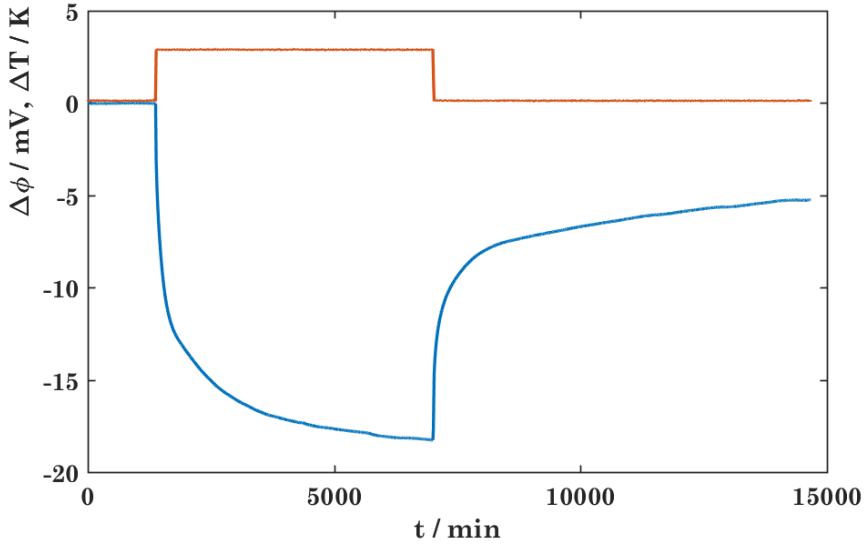


Figure 5.8: Plot of the internal temperature gradient and the electric potential of graphite cell C with an external temperature difference of 15K with arrangement 1.

As stated above, the initial response to the temperature gradient is of greatest importance for battery applications and in this time frame the cells behave more consistently. The values of the thermoelectric potential obtained from the potential measured at the time of the minimum point of cell A has been compared for the three cells in table 5.5. These values are, however, also vastly different for the different cells. Cell A and cell C have significantly different Peltier heats both initially and at steady state. Cell A has less than half the reversible heat effects on average than cell C at the initial time period and it is an order of magnitude smaller at steady state. Since both the initial and steady state values are different for the different cells, this must be related to the values of the terms relevant for both the initial and steady state expression, i.e. $S_{Li^+}^*$, $S_{Li(x,s)}$ and S_e^* .

If the transported entropy of the charge carrier in the electrode and the electrolyte is constant, only a change in $S_{Li(x,s)}$ can explain these discrepancies. The estimate of $S_{Li^+}^*$ from the $LiCoO_2$ cell was approximately 200 J/K mol. S_e^* for graphite was determined by Hansen *et al.* to be -2 J/K mol at around 550 °C [45]. If these values were valid for this cell, $S_{Li(x,s)}$ would be negative according to the data in Table 5.4 and Eq. 3.83. This is in violation of the second law of thermodynamics.

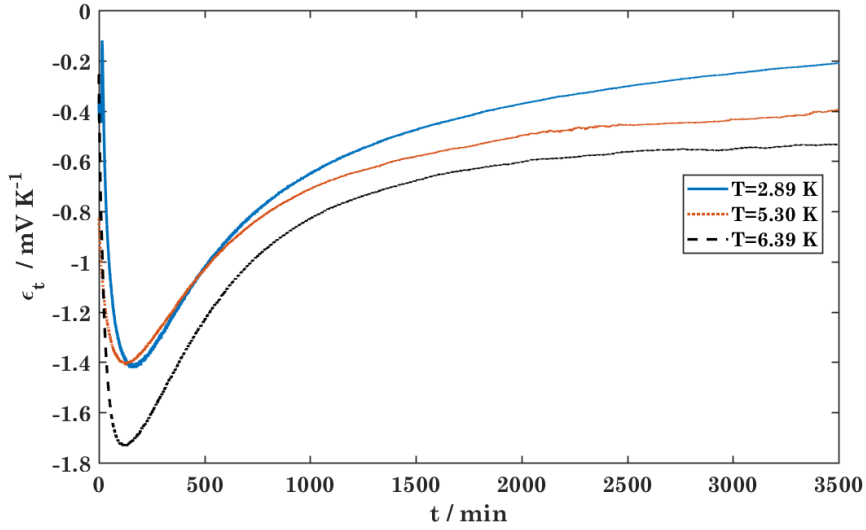


Figure 5.9: Plot of the thermoelectric potentials of the C_6 cell A for the 5, 10 and 15K external temperature difference measurement for arrangement 1.

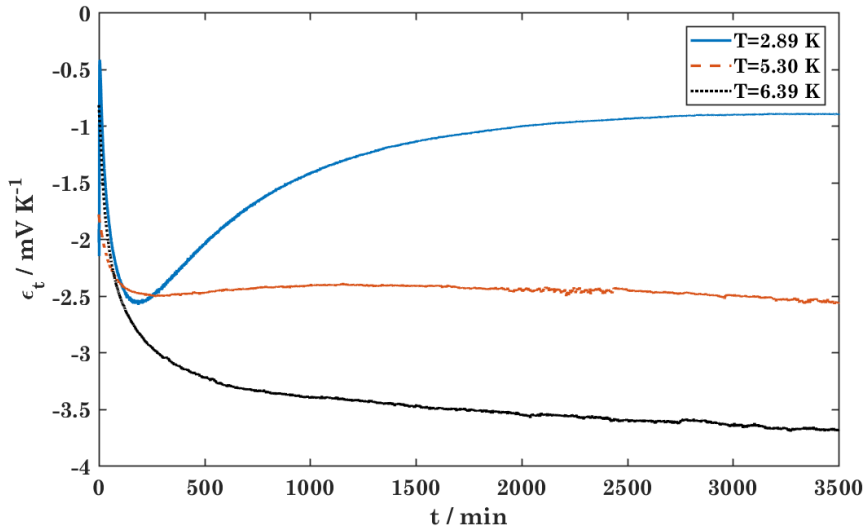


Figure 5.10: Plot of the thermoelectric potentials of the C_6 cell B for the 5, 10 and 15K external temperature difference measurement for arrangement 1.

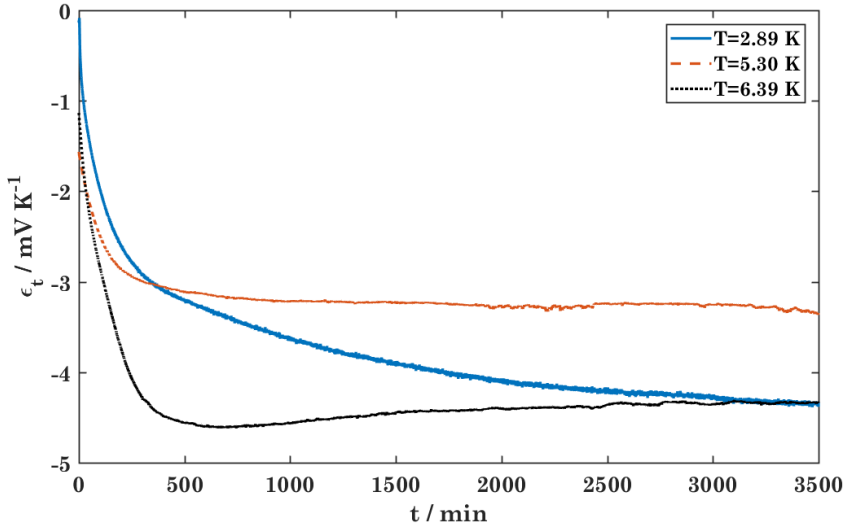


Figure 5.11: Plot of the thermoelectric potentials of the C_6 cell C for the 5, 10 and 15K external temperature difference measurement for arrangement 1. The bias potential changed during the measurement and this change is not accounted for in this figure.

Since this is impossible, S_e^* or $S_{Li^+}^*$ or both will have a different value.

If the value of S_e^* is different from the value measured by Hansen *et al.*, this could indicate changes in the structure of the electrode from the pristine condition prior to the measurements, possibly explained a change in the lithiated state. If the discrepancy is a result of a change in S_e^* , this would give a very large contribution to the Seebeck coefficients from the electrodes of up to -3mV/K for the material in question. This is incredibly high for a solid and thus it is highly unlikely that S_e^* alone contributes this.

This means that the estimate of $S_{Li^+}^*$ from the LiCoO_2 cell cannot be used here. It could also indicate that $S_{Li^+}^*$ is not constant for the different graphite cells or even for the same graphite cell. It is possible that $S_{Li^+}^*$ is associated with the electrode surface. If structural changes has occurred during the measurements, this could explain the change in the value of $S_{Li^+}^*$. If it is now assumed that $S_e^* = -2 \text{ J/K mol}$ and $S_{\text{Li}(x,s)} = 29 \text{ J/K mol}$ is valid for these cells, $S_{Li^+}^*$ values for the different measurements can be estimated from Eq. 3.83. These values are given in Table 5.6.

Table 5.4: The Seebeck coefficient at stationary state for the C₆ cells. *Since the cell changed behaviour after the first experiment, the first measurement is not included in the average. The errors are given to two standard deviations.

External temperature gradient / K	Seebeck coefficient, η_s		
	Cell A / mV K ⁻¹	Cell B / mV K ⁻¹	Cell C / mV K ⁻¹
5	-0.2 ± 0.2	-0.90 ± 0.05	-5.4 ± 0.3
10 - first measurement	-0.40 ± 0.03	-2.9 ± 0.12	-4.6 ± 0.2
15 - first measurement	-0.54 ± 0.03	-3.6 ± 0.2	-3.53 ± 0.12
15 - second measurement	-0.65 ± 0.03	-5.6 ± 0.2	-5.1 ± 1.2
10 - second measurement	-0.40 ± 0.03	-6.2 ± 0.3	-6.6 ± 6
Average	-0.4 ± 0.3	-4.6* ± 3.5	-5.0 ± 2.2
Peltier heat at electrode C ₆ /J K ⁻¹ mol ⁻¹	-12.7 ± 9.5	-132 ± 101	-144 ± 63

Table 5.5: Initial thermoelectric potential for the graphite cells. The values are obtained from the electric potential measured at the time of the minimum point of cell A. The errors are given to two standard deviations.

External temperature gradient / K	Initial thermoelectric potential, ϵ_0		
	Cell A / mV K ⁻¹	Cell B / mV K ⁻¹	Cell C / mV K ⁻¹
5	-2.00 ± 0.02	-2.54 ± 0.05	-3.65 ± 0.3
10 - first measurement	-1.96 ± 0.06	-2.37 ± 0.13	-3.77 ± 0.15
15 - first measurement	-1.39 ± 0.03	-2.97 ± 0.04	-3.79 ± 0.13
15 - second measurement	-1.73 ± 0.03	-2.6 ± 0.1	-3.0 ± 2.4
10 - second measurement	-1.34 ± 0.02	-4.3 ± 0.3	-3.7 ± 1.7
Average	-1.68 ± 0.62	-2.94 ± 1.52	-3.51 ± 0.71
Peltier heat at electrode C ₆ /kJ mol ⁻¹	-48.3 ± 17.9	-84.5 ± 43.7	-101 ± 20

It is impossible to isolate values for $S_{\text{Li}^+}^*$, S_e^* , $S_{\text{Li}(x,s)}$ and the contributions from heats of transfer from these measurements; all of the values are undetermined and the composition of the electrode is unknown.

Since the electrodes are pristine before the measurement, it is reasonable to assume that no solid electrolyte interphase (SEI) layer has developed. This could lead to diffusion of Li⁺ into the electrodes and possibly reactions between the electrolyte and the graphite. If this has occurred, structural changes from dissolved Li can explain the inconsistent behaviour. Since the stationary state thermoelectric

Table 5.6: Values of $S_{Li^+}^*$ calculated using $S_e^* = -2 \text{ J K}^{-1} \text{ mol}^{-1}$ and $S_{Li(x,s)} = 29 \text{ J K}^{-1} \text{ mol}^{-1}$. All errors are given to two standard deviations and are based on the standard deviation of the Seebeck coefficients of the cell. The uncertainty in the estimation of S_e^* and $S_{Li(x,s)}$ is not included. *Not included in the average.

External temperature gradient / K	Transported entropy of lithium ions, $S_{Li^+}^*$		
	Cell A / $\text{J K}^{-1} \text{ mol}^{-1}$	Cell B / $\text{J K}^{-1} \text{ mol}^{-1}$	Cell C / $\text{J K}^{-1} \text{ mol}^{-1}$
5	47 ± 2	$114^* \pm 5$	550 ± 30
10 - first measurement	66 ± 3	307 ± 12	470 ± 20
15 - first measurement	79 ± 3	370 ± 20	370 ± 12
15 - second measurement	90 ± 3	590 ± 20	520 ± 120
10 - second measurement	66 ± 2.4	625 ± 30	660 ± 580
Average	70 ± 32	470 ± 310	510 ± 210

potential also changes from measurement to measurement, this can also indicate structural changes in the electrodes. The system is not the same at the start and end of each experiment. Graphite electrode battery cells already have a well developed SEI layer after the first charge-discharge cycle [32]. This layer could also affect the Peltier heat. This and the inconsistent results means that the data obtained cannot be used to model the thermal profile of a Li-ion battery.

To obtain information regarding the Peltier heat of the C_6 electrode, further research should investigate electrodes already cycled in a battery and at known lithiated states. This would ensure that a stable SEI layer has formed prior to the measurements and will limit any structural changes that might have occurred with these cells. It will also ensure that the results are relevant to the electrodes in battery cells. The composition of the electrode would then be known and measurement on such a cell would give a more accurate picture of the thermal signature around these electrodes relevant to lithium-ion batteries in performance, and not in pristine condition.

5.3 Thermoelectric Potential of LiFePO_4 Pouch Cells

A plot of the temperature gradient inside LiFePO_4 cell A and the potential of the cell against time is shown in Figure 5.12 for the 5 K experiment. The plots for the 10, 12.5, 15 and 20 K experiment are shown in Figure C.33-C.36 in Appendix C.

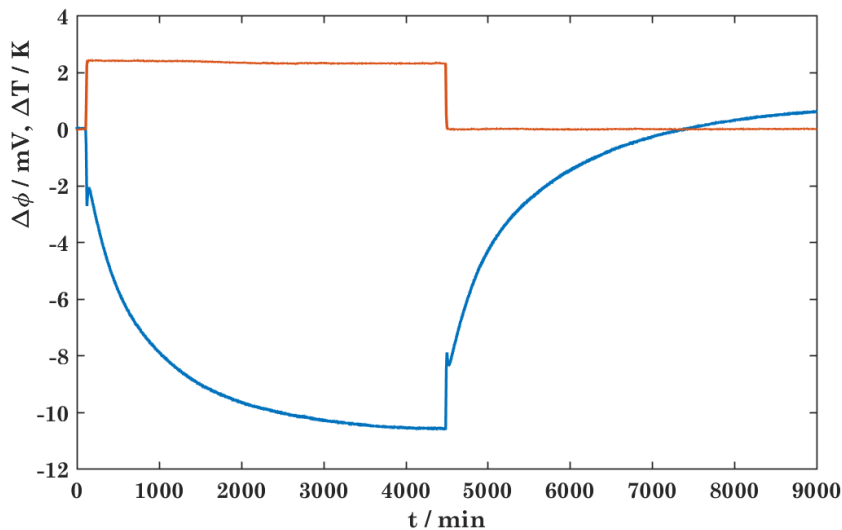


Figure 5.12: The temperature difference and electric potential of LiFePO_4 cell A for when the water bath was set to a 5 K temperature difference.

The same time-development as in LiCoO_2 cells are also present for these cells; the initial response is a decrease in the electric potential, followed by an increase to a local maximum and a decrease to a steady state plateau value. The initial response, however, seems to be more pronounced and have a smaller characteristic time (see Figure C.31) than in the LiCoO_2 cell. The thermoelectric potential at initial, intermediate and steady state (corresponding to the first minimum, maximum and final plateau value) are given in table 5.8. A plot of the measured electric potential over the temperature gradient in the cell is shown in Figure C.39. The high standard deviation is a result of the change in bias potential during the measurement of 0.5-2 mV.

Cell B had a high initial bias potential of around 20 mV. In addition it was unsta-

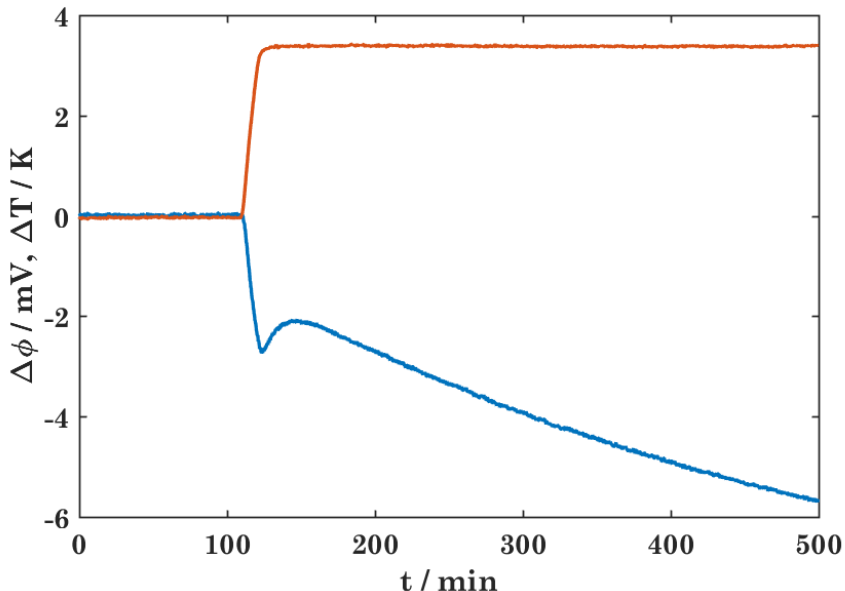


Figure 5.13: A zoom-in on the measurements at the initial time period of the temperature difference and electric potential of LiFePO_4 cell A for when the water bath was set to a 5 K temperature difference.

ble and broke after the first measurement. The same general trend was, however, repeated during the successful measurement of this cell. This is shown in Figure C.32 in Appendix C. No values could be extracted from this cell due to a change in bias potential of 4-5 mV during the measurement and the noise of the potential measurement. Cell A also showed a gradual change in bias potential during the measurements, although less than the graphite cells. The bias potential of the cell prior to and after the application of the temperature gradient is shown in Table 5.7.

The electric potential and temperature gradients from each measurement can be used to calculate the Seebeck coefficient and transported entropy, as for the LiCoO_2 cell. The results is shown in Table 5.8. An average value of -4.3 ± 0.6 mV/K was found for the Seebeck coefficient and 460 ± 60 J/K mol for the transported entropy of Li^+ . As mentioned for the LiCoO_2 section, the Seebeck coefficient is typically found by linear curve fitting of the results of $\Delta\phi$ against ΔT . More data points are available for this cell than for the LiCoO_2 cell. The result of a linear regression is shown in Figure 5.15. A value for the Seebeck coefficient of -3.7 ± 0.8 mV/K was

Table 5.7: The bias potential of the graphite cells before and after the temperature gradient was applied. The errors are given to two standard deviations.

Temperature gradient applied at arrangement 1.		
External temperature gradient	Bias potential at constant temperature / mV	Bias potential after the experiment
5	-2.09 ± 0.04	-1.52 ± 0.05
10	-1.4 ± 0.3	0.0 ± 0.3
12.5	0.2 ± 0.2	2.0 ± 0.3
15	1.7 ± 0.3	2.8 ± 0.6
20	2.7 ± 0.1	5.2 ± 0.1

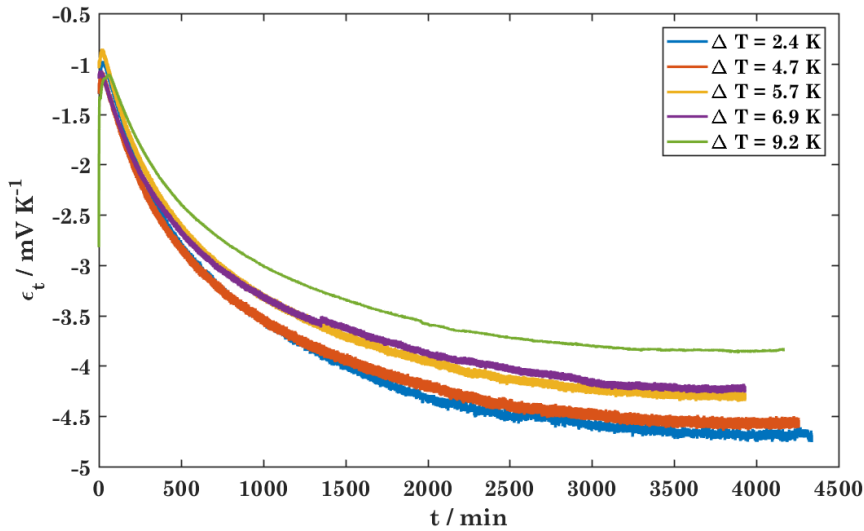


Figure 5.14: Plot of the electric potentials of the LiFePO_4 cell over the temperature differences within the cell (thermoelectric potential) for the 5, 10, 12.5, 15 and 20 K external water bath temperature difference measurement.

found from the fitted curve. This gives a transported entropy of $400 \pm 80 \text{ J/K mol}$ for Li^+ . The values found are not significantly different. This curve fitting contains a bias term of $-3.2 \pm 4.7 \text{ mV}$, which explains the discrepancy between these two methods. This bias term is not the same as the bias potential of the cell, which has already been subtracted. Ideally this term should therefore be 0, as there should be no thermoelectric potential at equilibrium conditions.

The values reported here are competitive with the high values reported by Bonetti

et al.. These high Seebeck coefficients can suggest that a possible application for the cells within energy harvesting.

Viswanathan *et al.* also reported the cell entropy of a Li_xFePO₄/Li_xC₆ cell with a 1M LiPF₆ EC/DMC 1:1 electrolyte [9]. At state of charge 0 (x=1 in Li_xFePO₄ and x=0 in Li_xC₆), the cell entropy change was -10 J/mol K. This gives a heat effect of 3 kJ/mol. The same method as for the LiCoO₂ cell can now be used to estimate the Peltier heat of C₆ in this cell. The results are shown in Table 5.8.

Table 5.8: Seebeck coefficients and electrode Peltier heats in LiFePO₄ at uniform electrolyte and at Soret equilibrium. The errors are given to two standard deviations. $\epsilon_{\infty,1}$ is found from the relaxation curves. The values of $S_{\text{Li}^+}^*$ are calculated using $S_e^* = 15 \text{ J K}^{-1} \text{ mol}^{-1}$ and $S_{\text{Li}(x,s)} = 29 \text{ J K}^{-1} \text{ mol}^{-1}$. The Peltier heat of C₆ is calculated from the entropy of the LiFePO₄/C₆ cell of -10 J/mol K (for x=1 in Li_xFePO₄ and x=0 in Li_xC₆) measured by Viswanathan *et al.* [9].

ΔT /K	ϵ_0 /mV K ⁻¹	$\epsilon_{\infty,1}$ /mV K ⁻¹	$\epsilon_{\infty,2}$ /mV K ⁻¹	$S_{\text{Li}^+}^*$ /J K ⁻¹ mol ⁻¹
2.4	-1.1 ± 0.2	-1.0 ± 0.2	-4.5 ± 0.2	480 ± 20
4.7	-1.1 ± 0.4	-0.8 ± 0.4	-4.6 ± 0.4	490 ± 40
5.7	-1.3 ± 0.4	-1.0 ± 0.4	-4.3 ± 0.4	460 ± 40
6.9	-1.4 ± 0.2	-0.9 ± 0.2	-4.2 ± 0.2	450 ± 20
9.2	-1.6 ± 0.4	-1.0 ± 0.4	-3.9 ± 0.4	420 ± 40
Average	-1.3 ± 0.4	-0.9 ± 0.2	-4.3 ± 0.6	460 ± 60
Single-electrode Peltier heat				
LiFePO ₄ /kJ mol ⁻¹	37 ± 9	26 ± 6	122 ± 12	-
C ₆ /kJ mol ⁻¹	-34 ± 9	-23 ± 6	-119 ± 12	-

The Peltier heats calculated for C₆ by Eq. 3.96 is not the same as that found for LiCoO₂. Indeed the expected Seebeck coefficient of C₆ according the Eq. 3.93 and Table 5.8 is -4.3 mV/K. One possible reason behind this discrepancy is that the LiCoO₂ cell showed slower diffusion phenomena than LiFePO₄. A possible explanation for this is discussed in the next section.

The stationary state Seebeck coefficient changes with the measurements. With the exception of the experiment with the internal temperature gradient of 4.7 K, the absolute value decreases for each consecutive measurement. Two explanations for this is suggested; the increase in the temperature gradient could decrease the

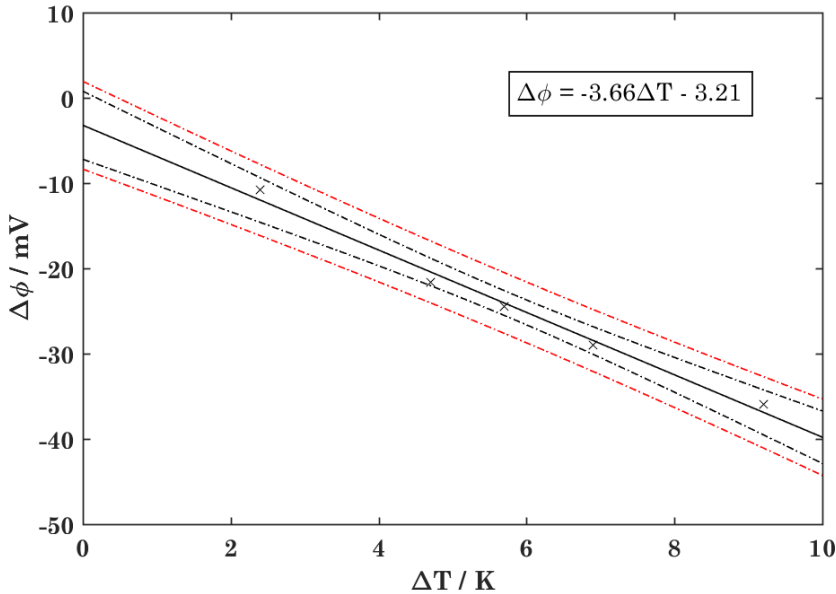


Figure 5.15: Plot of the electric potentials of the LiFePO_4 cell against the temperature with fitted curve and 95% confidence (black-dotted line) and prediction (red-dotted line) intervals.

value of the Seebeck coefficient or the change in the bias potential (as shown in Table 5.7) can either be the cause itself or indicate structural changes that can change the value for the transported entropy. The experiments should therefore be repeated to check the reproducibility of the data, to see whether the Seebeck coefficient is highly dependent on the temperature gradient or if there is a change in the electrode.

5.3.1 Diffusion Coefficients and Heats of Transfer

Because the local maximum in the electric potential occurs faster for these cells than for the LiCoO_2 cells, the integral complementary error function term from Equation 3.86 should be included in the curve fitting. Since the characteristic times of the two diffusion phenomena are unknown, one function containing these terms will be fitted in the beginning and another without them at a later time.

The curve obtained is given in below and the fit is shown in Figure C.37.

$$\epsilon_t \approx \begin{cases} \left(4.9 \cdot \frac{\exp(-0.0025 \cdot t)}{\sqrt{\pi}} + 4.9 \cdot \sqrt{0.0025 \cdot t} \cdot \operatorname{erfc}(\sqrt{0.0025 \cdot t}) \right. \\ \left. + 4 \cdot \sqrt{0.203 \cdot t} \cdot \operatorname{erfc}(\sqrt{0.203 \cdot t}) - 4 \cdot \frac{\exp(-0.203 \cdot t)}{\sqrt{\pi}} - 4.44 \right) & t < 300\text{min} \\ \left(2.2 \cdot \exp(-0.00004 \cdot t) - 3.1 \cdot \exp(-0.001522 \cdot t) - 4.44 \right) & t > 300\text{min} \end{cases}$$

The same curves could be used to describe the behaviour of cell A at the 5 and 10 K experiments. The curve at $t > 300$ has an R^2 -value of 0.9987. Just as for the LiCoO_2 cell, the coefficients are not in agreement with Tyrrell's theory. Again this is reasonable as the two phenomena both affect the electric potential at the same time and are coupled. The curve fitting will be related to the theory through the characteristic times, but it should be noted that there will be deviations from Tyrrell's theory by treating the two coupled phenomena individually. The diffusion coefficients obtained is shown in Table 5.9.

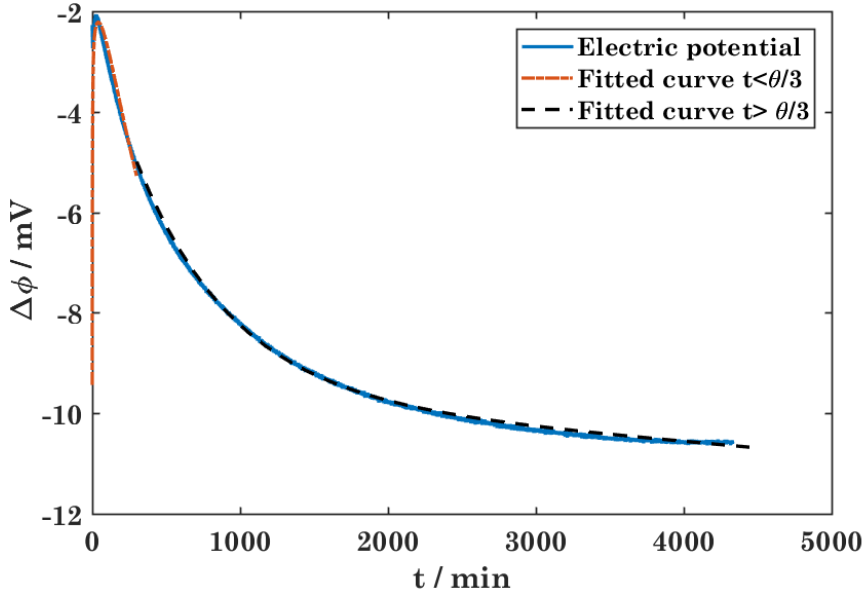


Figure 5.16: Shows the plot of the electric potential for the $\Delta T = 2.4$ K experiment and the fitted curves.

Estimates for $\left(t_1 - \frac{x_1}{x_3}t_3\right)q_1^*$, $\left(t_2 - \frac{x_2}{x_3}t_3\right)q_2^*$ and the corresponding Soret coefficients

Table 5.9: Heat of transfer and Soret coefficient data, characteristic times and corresponding diffusion coefficients obtained from the measurements of LiFePO₄ cells. The errors are given to two standard deviations. *Error could not be estimated from curve fitting. **Error could not be estimated using error propagation.

ΔT / K	$(t_1 - \frac{x_1}{x_3}t_3)q_1^*$ / kJ mol ⁻¹	$(t_2 - \frac{x_2}{x_3}t_3)q_2^*$ / kJ mol ⁻¹	$(t_1 - \frac{x_1}{x_3}t_3)s_{T,1}$ / K ⁻¹	$(t_2 - \frac{x_2}{x_3}t_3)s_{T,2}$ / K ⁻¹
2.4	-4.8 ± 8	98 ± 8	-0.003 ± 0.006	0.133 ± 0.011
4.7	-9.2 ± 16	107 ± 16	-0.007 ± 0.011	0.14 ± 0.02
5.7	-8.6 ± 16	101 ± 16	-0.006 ± 0.011	0.14 ± 0.02
6.9	-12.9 ± 8	95 ± 8	-0.009 ± 0.006	0.13 ± 0.011
9.2	-17.5 ± 12	76 ± 12	-0.012 ± 0.008	0.10 ± 0.016
Average	-11 ± 13	95 ± 20	-0.007 ± 0.009	0.13 ± 0.03
ΔT / K	θ_1 / min	θ_2 / min	D_1 / m ² s ⁻¹	D_2 / m ² s ⁻¹
-	12.3*	657 ± 2	4.4 · 10 ⁻¹⁰ **	8.21 · 10 ⁻¹² ± 0.03 · 10 ⁻¹²

were found from Equation 5.1, 5.2 and 3.59. The results are shown in Table 5.9. The values obtained for $(t_1 - \frac{x_1}{x_3}t_3)q_1^*$ and $(t_2 - \frac{x_2}{x_3}t_3)q_2^*$ for LiCoO₂ and LiFePO₄ should be the comparable, as these are values related to the electrolyte and the same electrolyte is used in both cells. The values obtained are, however, not the same. Despite being different, the values are of the same signs. For the second component the values are not significantly different. The deviation in the first diffusion process could be explained by the different characteristic times of the cells. Since there are several competing forces in the beginning of the experiment and the magnitude of the electric potential smaller, the relative error in the $\epsilon_{\infty,1}$ value estimated is likely larger than for $\epsilon_{\infty,2}$. This competition can explain the deviation. The LiFePO₄ cell responds slightly faster than the LiCoO₂ cells.

It is interesting to note that while the second diffusion process for the LiFePO₄ cell is comparable to the second diffusion process in the LiCoO₂ cell, the first is one order of magnitude faster. The LiFePO₄ cell was in pristine condition prior to the experiments. The LiCoO₂ cell had already been used for several experiments of the thermoelectric potential of shorter duration. Could the LiCoO₂ cell have been damaged in the prior experiment? If so, are the results reliable? Would the behaviour of a pristine LiCoO₂ cell be more consistent with that shown by LiFePO₄? Could the diffusion processes be related to the electrode surface, or could evaporation or crystallization of one component of the electrolyte explain this? Both the LiCoO₂ and LiFePO₄ measurements should be repeated by new cells to check the

reproducibility of these results.

5.4 Peltier Heats from Literature Data

Literature data on Peltier heats relevant to lithium ion batteries are scarce. Kuzminskii *et al.*, Hudak *et al.* and Black *et al.* are among the few contributing with this research [5, 16, 17]. The literature is characterized with short experiments with rapid changes in the temperature gradient applied. Initial thermoelectric potential measurements for aqueous-solution described by Agar included experimental set-ups for which prohibited diffusion phenomena [4]. This has not been considered in these studies. Experimental details are not comprehensive; cell dimensions are not given, thermal diffusivity is not considered and the sign convention is not consistent. In the experiments in this thesis, the system was allowed to obtain a steady state and the electric potential was recorded continuously. When measurements are done to obtain the initial thermoelectric potential and done within minutes, thermal diffusivity will be important to consider.

Kuzminskii *et al.* reported results of the same measurement with both positive and negative sign [5]. Hudak *et al.* and Black *et al.* both reported positive initial thermal powers [16, 17]. The results in this thesis indicates a large and positive $S_{\text{Li}^+}^*$ which, depending on the value of the contribution from the electrode, electrode surface and Soret effect, will give a negative Seebeck coefficient. The measurements are done on cathode materials. Local reversible cooling is reported for the LiCoO_2 cathode during charging [9], when it is acting as an anode. The sign convention used in this thesis is in agreement with this [25]. The Peltier heat of an anode material, for instance graphite, should not change with the change in the cathode material. If the sign convention used by Hudak *et al.* and Black *et al.* was valid, this would lead to a higher total reversible heat effect than reported in literature. When the results from Kuzminskii *et al.*, Hudak *et al.* and Black *et al.* is analyzed here, the same value will be used, but with a negative sign.

Hudak *et al.* investigated the response in *emf* when a temperature gradient was applied for around 3 minutes at a time to thermoelectric cells with Li_xTiS_2 or $\text{Li}_x\text{V}_2\text{O}_7$ electrodes and $\text{LiPF}_6/\text{EC}/\text{DMC}$ (dimethyl carbonate) electrolyte [16]. The temperature was monitored at the electrodes and the potential was measured after the temperature gradient had been set for one minute. Only the temperature of the hot electrode was changed. The temperature gradient was applied more rapidly than with the experimental set-up used for the measurements in this thesis. They reported the initial response for their system. The values measured by Hudak *et al.* can be analyzed using the theory in Chapter 3. They reported an initial ther-

moelectric potential with a value of 0.6-1.4 mV/K for the Li_xTiS_2 thermoelectric cell and 0.6-1.05 mV/K for $\text{Li}_x\text{V}_2\text{O}_2$ with various lithiated states $x=0-0.8$. These results are interpreted here as -0.6-1.4 and -0.6-1.05 mV/K respectively. Both cells had an electrolyte consisting of 1M LiPF_6 and 50:50 mixture of EC and DEC by volume [16]. This gives an initial Peltier heat for the electrode surroundings of 17.3-40.3 kJ/mol. Some deviation will be expected when comparing this to the cells investigated in this thesis, as the electrolyte used here is a 50:50 mixture of EC and DEC by mass. S_e^* for Li_xTiS_2 is in the range 0-2.5 J/K mol [46], while no value has been reported for $\text{Li}_x\text{V}_2\text{O}_2$.

Since no stationary state was reached, it is not possible to calculate $S_{\text{Li}^+}^*$ directly from the results of Hudak *et al.* (or Black *et al.*). The contribution from diffusion processes can be estimated, however, using values for $(t_1 - \frac{x_1}{x_3}t_3)q_1^*$ and $(t_2 - \frac{x_2}{x_3}t_3)q_2^*$ obtained from the LiCoO_2 measurements and LiFePO_4 measurements. The deviation between the electrolyte used in this thesis and the one used by Hudak *et al.* will be neglected in the estimation. The estimates are shown in Table 5.10.

Table 5.10: Values of η_s and $S_{\text{Li}^+}^*$ for the Li_xTiS_2 cell calculated using heat transfer data from the LiCoO_2 and LiFePO_4 measurements, $S_e^* = 2 \text{ J K}^{-1} \text{ mol}^{-1}$ and $S_{\text{Li}(x,s)} = 29 \text{ J K}^{-1} \text{ mol}^{-1}$.

x	LiCoO ₂		LiFePO ₄	
	η_s (Li_xTiS_2) / mV K ⁻¹	$S_{\text{Li}^+}^*$ (Li_xTiS_2) / J K ⁻¹ mol ⁻¹	η_s (Li_xTiS_2) / mV K ⁻¹	$S_{\text{Li}^+}^*$ (Li_xTiS_2) / J K ⁻¹ mol ⁻¹
0.0	-2.3 ± 2.6	250 ± 250	-3.3 ± 4	350 ± 390
0.2	-3.1 ± 2.7	330 ± 260	-3.9 ± 4	410 ± 390
0.4	-3.0 ± 2.6	310 ± 250	-4.4 ± 4	460 ± 390
0.6	-2.9 ± 2.6	310 ± 250	-3.8 ± 4	400 ± 390
0.8	-2.8 ± 2.6	300 ± 250	-3.8 ± 4	400 ± 390

The uncertainty reported for the results by Hudak and Amatucci combined with the uncertainty of the heat of transfer estimates means that no value can be estimated for the steady state Seebeck coefficient or for the transported entropy of Li^+ from these results. Making more accurate estimates on the value of $S_{\text{Li}^+}^*$ with the results by Hudak *et al.* is not possible without better estimates of the q^* 's of the system. At the time of the initial thermoelectric potential measurement, contributions from diffusion processes within the electrolyte already contributing to the electric potential. If the cells investigated by Hudak *et al.* have the same

time-dependent behaviour as the LiCoO_2 and LiFePO_4 cells investigated in this thesis, the number reported will be underestimated because of the competing contributions in the initial time period.

Neither Hudak *et al.* or Black *et al.* stated the characteristic times of the thermal diffusion processes of system. If the characteristic time of the system is close to that of the electrolyte in the LiFePO_4 cell, thermal diffusion may already be influencing the potential. If it is closer to the response of the LiCoO_2 cell, the initial response might not have been established. The electrolyte-wetted separator in Li-ion batteries has a low thermal conductivity [47]. This will give the cells a low thermal diffusivity (depending on the heat capacity of the specific system) and calls into question whether the temperature gradient has properly been established within the cell at the time of their measurements. If this is the case, a temperature gradient could also be present within the cell at the time between the measurements. Could the large change in bias potential observed by both Hudak *et al.* and Black *et al.* be a delayed thermal diffusion effect?

The same problem with thermal diffusivity and the response of the system is repeated in the literature. This is evident in the measurements by Kobayashi *et al.*, where thermal waves on the time-scale of seconds were used [18]. The value reported for thermoelectric coin cells by Kobayashi *et al.* cannot be considered the Seebeck coefficient, as the system would have no time to instil the temperature gradient.

Kuzminskii *et al.* investigated a similar set-up as Hudak *et al.* with a LiBF_4 in γ -butyrolactone electrolyte [5]. Different lithiated states of the electrode were investigated. The same theory can be used to study the cells in this thesis, with the simplification of a binary electrolyte instead of a ternary electrolyte. The temperature difference between the two electrodes was set to 60 K. Again only the initial thermoelectric potential was investigated. Values from -0.65 mV/K to -4.62 mV/K were reported. This gives an initial Peltier heat for the electrode surroundings of 19-133 kJ/mol. No uncertainties were given. The time at which this initial value was measured is not stated, neither is the method of temperature measurement.

The results by Kuzminskii *et al.* indicates that (if the Soret effect is neglected for a rapid charge-discharge cycle) the local heat effects around the Li_xTiS_2 electrode would change drastically during the charging process. The stationary state

expression is the same. The initial expression will in this case be:

$$\epsilon_0 = \frac{1}{F} \left(S_e^* - S_{\text{Li}^+}^* + S_{\text{Li}(x,s)} - t_1 \frac{q_1^*}{T} \right) \quad (5.3)$$

The different values measured by Kuzminskii *et al.* and Hudak *et al.* are given in Figure 5.17. The results reported by Hudak *et al.* and Kuzminskii *et al.* both

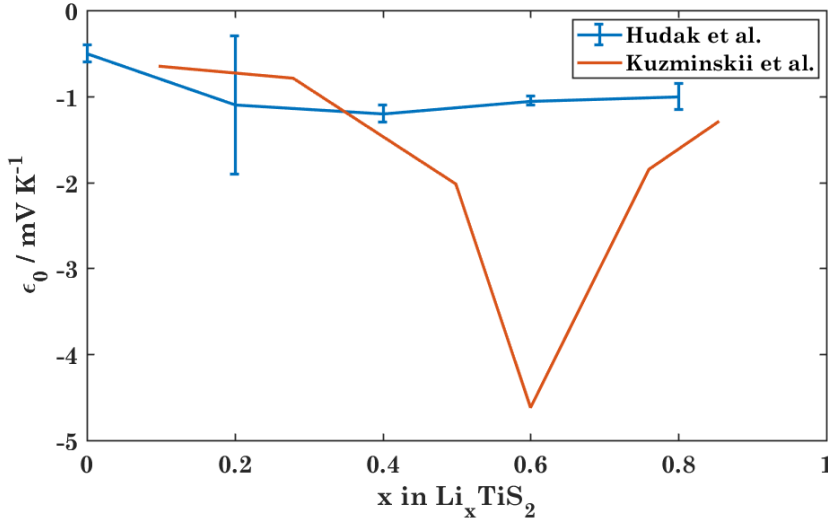


Figure 5.17: The values reported for the initial thermoelectric potential of Li_xTiS_2 thermocells with a LiBF_4/γ -butyrolactone (50:50 mol%) electrolyte by Kuzminskii *et al.* [5] and Li_xTiS_2 thermocells with LiPF_6 , EC/DMC (50:50 vol%) electrolyte by Hudak *et al.* [16]. The error bars are given to two standard deviations as given by Hudak *et al.*. No error estimation was given by Kuzminskii *et al.*. The values by Hudak *et al.* were reported with a positive sign, while Kuzminskii *et al.* reported the values with both positive and negative sign. The measurements are interpreted here to have a negative sign.

show a variation in the Peltier heat at the electrode for different states of charge. Further work should therefore include looking at cells at different lithiated states.

The discrepancy between the trends reported by Hudak *et al.* and Kuzminskii *et al.* can be a result of the different electrolyte used. However, it must be pointed out that the lack of experimental details and uncertainties from Kuzminskii *et al.* and the timing of the measurement by Hudak *et al.* makes comparisons between the two results difficult. The two systems will have different thermal diffusivities.

It is also very unclear whether Hudak and Amatucci had established a temperature gradient within the cell and therefore whether they reported the "correct" initial thermoelectric potential.

The difference in the values measured by Kuzminskii *et al.* for different lithiated states is too great to come solely from $S_{\text{Li}(x,s)}$, though it will contribute. Since the electrolyte concentration is the same, q^* will be the same and will therefore not be the source of the large difference. The contribution to the thermoelectric potential from S_e^* for Li_xTiS_2 is small (see Table C.1). This leaves $S_{\text{Li}^+}^*$. Is this then another indication that $S_{\text{Li}^+}^*$ is influenced by the composition of the electrode, and not just the composition of the electrolyte? These results indicate that the transition from the electrode to the electrolyte determines the value of $S_{\text{Li}^+}^*$.

Black *et al.* investigated a cell with two lithium metal electrodes in a 1M LiClO_4 and 1:1 EC/DEC electrolyte [17]. They also measured the thermoelectric potential of cells with one lithium metal electrode and a $\text{Li}_{3.5}\text{Fe}(\text{CN})_6$ electrode. The time-scales of the measurements used was the same as Hudak *et al.*. The Li cell was measured to have a Seebeck coefficient of 1.0 mV/K, which will be interpreted here as -1.0 mV/K. This gives a Peltier heat of 29 kJ/mol. It was pointed out by Black *et al.* that the Seebeck coefficient of this electrode. Viswanathan *et al.* measured the entropy change in electrodes using a lithium counter electrode, using the argument that the entropy change in the metal due to the cell reaction is negligible. The value reported by Black *et al.* clearly shows that though the entropy change is small, the local reversible heat effect around the electrode is not negligible. From the initial Peltier heat of Li, the initial Peltier heat of other cathodes and anodes can be estimated from the entropy changes reported by Viswanathan *et al.* with a Li-counter electrode using Eq. 3.96. The results are shown in Table 5.11.

Table 5.11: Initial Peltier heats and Seebeck coefficients for various electrodes calculated from the Peltier heat of the Li metal electrode reported by Black *et al.* and the entropy change reported by Viswanathan *et al.* for the electrode materials against a counter electrode of Li-metal [9, 17].

Electrode material	Entropy change $\text{J K}^{-1} \text{mol}^{-1}$	Peltier heat kJ mol^{-1}	Initial Seebeck coefficient mV K^{-1}
LiFePO_4	-36	40.0	-1.4
LiCoO_2	-40	40.7	-1.4
LiMnO_2	-20	34.7	-1.2
C_6	-60	-46.7	-1.6

The estimated initial Peltier heat and Seebeck coefficient for LiFePO_4 is in good agreement with the results from the LiFePO_4 cell in pristine condition. This gives further motivation to repeat the LiCoO_2 experiment with a pristine cell and to measure the thermoelectric potential of cells with LiMnO_2 electrodes. Viswanathan *et al.* reported the entropy change of the at different lithiated states. The same analysis can therefore also be performed on cells with different lithiated states.

5.5 Further Work

The results in this thesis show that contribution from thermal diffusion on these systems is significant. Future investigations on these cells as thermoelectric cells should therefore also allow the system to reach a steady state.

To gain a better understanding of the system, simulations can be used to determine the relative diffusion times of the components of the electrolyte. Estimates for t_2 and t_3 must be found to estimate q_1^* and q_2^* , which can be used to estimate q_3^* through Equation 3.29. Simulations to understand the electrolyte structure can contribute to insight into the concept of transported entropy of ions for non-aqueous solutions.

To increase the number of data points and improve the statistics, the experiment with LiCoO_2 and LiFePO_4 electrodes should be repeated with new cells.

Future studies might include different electrolytes and more electrode materials. Investigating the same cells at different states of charge of the electrodes will give a more accurate picture of the evolution of the Peltier heat at the electrode during the charging processes, as the Peltier heat is likely to change with both time and the lithiated state (seen in the results by Hudak *et al.* and Kuzminskii *et al.* [16, 5]) and the charging/discharging process involves a change in lithiated state over time. Investigating more Li-ion battery cathode materials such as LiMn_2O_4 and LiNiPO_4 can give more insight into how similar their behaviour are under the influence of a thermal gradient and expand on the knowledge of how $S_{\text{Li}^+}^*$ changes with different electrodes. As mentioned previously, already cycled graphite electrodes might be a possible way to investigate the graphite electrode to give results relevant to Li-ion batteries.

Reducing or increasing the number of carbonates in the electrolyte can give information on the thermal diffusion of multi-component systems. It can also be a way to obtain better estimates of heats of transfer. Studying the same electrode materials with different electrolytes will also give a better understanding of $S_{\text{Li}^+}^*$ for these systems.

Different pore sizes of the inert separator or different materials as separator might give better insight into the dependence on thermal diffusion, heat of transfer and the Seebeck coefficient on the pore size. Ion exchange membranes as electrolyte

and separator can give an interesting study where thermal diffusion is limited to the non-aqueous solution, excluding the salt flux.

Going beyond lithium-ions to electrode materials with sodium ions is also a possibility. In comparison to lithium, sodium resources are vast and a thermoelectric cell with sodium ions might be more sustainable.

Chapter 6

Conclusion

The thermoelectric potential of cells with a ternary electrolyte relevant to lithium-ion batteries consisting of lithium hexafluorophosphate (LiPF_6), ethylene carbonate and diethyl carbonate has been investigated for three different cells with lithium cobalt oxide (LiCoO_2), graphite (C_6) and lithium iron phosphate (LiFePO_4) electrodes using experimental measurements and the theory of non-equilibrium thermodynamics.

The time-development of the thermoelectric potential of LiCoO_2 indicated several diffusion phenomena of different characteristic times occurring during the measurement. It took several days to reach a steady state. Seebeck coefficients of -1.5 - 3.4 mV/K was obtained. Initial thermoelectric potentials of -2.5 - 3.5 mV/K was estimated. To further investigate the complex initial time-period, the experiment should be repeated using a more rapid method of thermostating the cell. The transported entropy of Li^+ in the cell was estimated to 200 ± 20 J/K mol. The Peltier heat of the electrode changed during the time-evolution of the measurement. An initial value of 84 ± 9 kJ/mol indicate large local reversible heat effects at the LiCoO_2 electrode in an during charging and discharging of a battery. A final value of 51 ± 6 kJ/mol was obtained. Estimates for the heat of transfer and Soret coefficients and diffusion coefficients for the electrolyte in the separator were also found.

The graphite thermoelectric cells showed both high and intermediate thermoelectric potentials. However, changes in the bias potentials and Seebeck coefficients indicated irreversible changes occurring inside the cells during the measurements, contributing to the potential. This inconsistency could indicate that structural changes occurred in the cell during and between the measurement. No common value for $S_{\text{Li}^+}^*$ could be obtained. This in combination with the lack of consistent behaviour of the cells means that the cells cannot be used in practical applications and the calculated Peltier heats cannot be used to determine the thermal profile of a lithium-ion battery. To obtain accurate results relevant to lithium ion batteries, the experiment should be repeated using cells with electrodes with well-established SEI layers.

The time-development of the thermoelectric potential of LiFePO_4 showed the same general behaviour as LiCoO_2 , but the first diffusion process was on a considerably faster time scale. High Seebeck coefficients of -3.9-4.7 mV/K was observed experimentally and a value of -3.7 ± 0.8 mV/K found from the regression line. Initial thermoelectric potentials of -1.0-1.2 mV/K was measured. The Peltier heat changed from 37 ± 9 to 26 ± 6 and reached a final value of 122 ± 12 kJ/mol. An average value of $S_{\text{Li}^+}^*$ was 460 ± 60 J/K mol from the experimental data and 400 ± 80 from the Seebeck coefficient found from the regression line. As for the LiCoO_2 cell, estimates for the heat of transfer, Soret coefficients and diffusion coefficients for the electrolyte in the separator were also found. Though these are values related to the electrolyte, the value for the first diffusion process are significantly different for the two cells. This discrepancy is explained by the higher uncertainty related to the estimation of the first diffusion process due to the opposing processes occurring at the same time.

It is possible that the large discrepancy between the LiCoO_2 and LiFePO_4 is due to the used condition of the LiCoO_2 and the pristine condition of the LiFePO_4 cells. The measurements should therefore be repeated to investigate this and to check the reproducibility of the results.

Local heat effects have not previously been included in thermal modeling of these batteries. The results given in this thesis indicates that local heat effects should be included in a description of the cells. The Peltier heats found at both the LiCoO_2 and LiFePO_4 indicates large local heat effects occur around the electrodes in lithium ion batteries, and consequently also at the anode materials. This gives further motivation to continue investigating Peltier heats for these materials.

Hudak *et al.*, Kuzminskii *et al.* and Black *et al.* investigated the Seebeck effect in cells relevant to lithium-ion batteries and the possibility of using these cells as thermoelectric cells. In agreement with the results in this thesis, these studies indicates large local reversible heat effects around the electrode surfaces. The systems were not allowed to reach a Soret equilibrium. The results in this thesis shows clearly that the effects from thermal diffusion is substantial for these systems. Future studies should therefore allow the system to reach a steady state.

As the Peltier heat change with time it is clear that the charging time of Li-ion batteries is of importance for the local heating at the electrodes. The results by

Hudak *et al.* and Kuzminskii *et al.* strongly indicate that the Peltier heat is dependent on the lithiated state of the electrodes. To get a more accurate temperature profile in a battery during a charge-discharge cycle, the Peltier heat at different lithiated states should be investigated.

The differences in the Seebeck coefficient between the cells, and therefore also the values for $S_{\text{Li}^+}^*$ estimated, suggest that the transported entropy of the ion involved in the reversible electrode reaction could be a property associated with the electrode surface. This gives new insight into the concept of the transported entropy which should be explored further.

References

- [1] Frank Richter, Astrid Gunnarshaug, Odne Stokke Burheim, Preben J. S. Vie, and Signe Kjelstrup. Single Electrode Entropy Change for LiCoO₂ Electrodes. *ECS Transactions*, 80(10):219–238, 2017.
- [2] John B. Goodenough and Kyu-Sung Park. The Li-Ion Rechargeable Battery: A Perspective. *Journal of the American Chemical Society*, 135(4):1167–1176, 2013. PMID: 23294028.
- [3] Huaqiang Liu, Zhongbao Wei, Weidong He, and Jiyun Zhao. Thermal Issues About Li-ion Batteries and Recent Progress in Battery Thermal Management Systems: A Review. *Energy Conversion and Management*, 150(Supplement C):304 – 330, 2017.
- [4] J. N. Agar. *Thermogalvanic Cells*. Interscience, New York, 1963.
- [5] Y.V. Kuzminskii, V.A. Zasukha, and G.Y. Kuzminskaya. Thermoelectric Effects in Electrochemical Systems. Nonconventional Thermogalvanic Cells. *Journal of Power Sources*, 52(2):231 – 242, 1994.
- [6] M. Bonetti, S. Nakamae, M. Roger, and P. Guenoun. Huge Seebeck Coefficients in Nonaqueous Electrolytes. *The Journal of Chemical Physics*, 134(11):114513, 2011.
- [7] Frank Richter, Preben J.S. Vie, Signe Kjelstrup, and Odne Stokke Burheim. Measurements of Ageing and Thermal Conductivity in a Secondary NMC-hard Carbon Li-ion Battery and the Impact on Internal Temperature Profiles. *Electrochimica Acta*, 250(Supplement C):228 – 237, 2017.
- [8] J. David Bazak, Sergey A. Krachkovskiy, and Gillian R. Goward. Multi-Temperature in Situ Magnetic Resonance Imaging of Polarization and Salt Precipitation in Lithium-Ion Battery Electrolytes. *The Journal of Physical Chemistry C*, 121(38):20704–20713, 2017.
- [9] Vilayanur V. Viswanathan, Daiwon Choi, Donghai Wang, Wu Xu, Silas Towne, Ralph E. Williford, Ji-Guang Zhang, Jun Liu, and Zhenguo Yang. Effect of Entropy Change of Lithium Intercalation in Cathodes and Anodes on Li-ion Battery Thermal Management. *Journal of Power Sources*, 195(11):3720 – 3729, 2010.

- [10] O. S. Burheim, M. A. Onsrud, J. G. Pharoah, F. Vullum-Bruer, and P. J. S. Vie. Thermal Conductivity, Heat Sources and Temperature Profiles of Li-Ion Batteries. *ECS Transactions*, 58(48):145–171, 2014.
- [11] Q. Xu, S. Kjelstrup, and B. Hafskjold. Estimation of Single Electrode Heats. *Electrochimica Acta*, 43(18):2597 – 2603, 1998.
- [12] S.R. de Groot and P. Mazur. *Non-equilibrium Thermodynamics*. Dover Books on Physics. Dover Publications, 1984.
- [13] Signe Kjelstrup and Dick Bedeaux. *Non-Equilibrium Thermodynamics of Heterogeneous Systems*. World Scientific Publishing Co. Pte. Ltd., 2008.
- [14] Preben J.S. Vie and Signe Kjelstrup. Thermal Conductivities from Temperature Profiles in the Polymer Electrolyte Fuel Cell. *Electrochimica Acta*, 49(7):1069 – 1077, 2004.
- [15] S.R. De Groot. Théorie Phénoménologique De L'effet Soret. *Physica*, 9(7):699 – 708, 1942.
- [16] Nicholas S. Hudak and Glenn G. Amatucci. Energy Harvesting and Storage with Lithium-Ion Thermogalvanic Cells. *Journal of The Electrochemical Society*, 158(5):A572–A579, 2011.
- [17] Jeffrey J. Black, Jason B. Harper, and Leigh Aldous. Temperature effect upon the thermoelectrochemical potential generated between lithium metal and lithium ion intercalation electrodes in symmetric and asymmetric battery arrangements. *Electrochemistry Communications*, 86:153 – 156, 2018.
- [18] Wataru Kobayashi, Akemi Kinoshita, and Yutaka Moritomo. Seebeck effect in a battery-type thermocell. *Applied Physics Letters*, 107(7):073906, 2015.
- [19] J. N. Agar and W. G. Breck. Thermal Diffusion in Non-Isothermal Cells: Part 1.-Theoretical Relations and Experiments on Solutions of Thallous Salts. *Transactions of the Faraday Society*, 53:p. 67, 1957.
- [20] Soon-Ki Jeong, Minoru Inaba, Yasutoshi Iriyama, Takeshi Abe, and Zempachi Ogumi. Surface Film Formation on a Graphite Negative Electrode in Lithium-Ion Batteries: {AFM} Study on the Effects of Co-Solvents in Ethylene Carbonate-Based Solutions. *Electrochimica Acta*, 47(12):1975 – 1982, 2002.
- [21] Andreas Bursvik. *Soret Effect in Li-Ion Batteries*. Project Report, NTNU, 2017.

- [22] Kevin L. Gering. Prediction of Electrolyte Conductivity: Results from a Generalized Molecular Model Based on Ion Solvation and a Chemical Physics Framework. *Electrochimica Acta*, 225:175 – 189, 2017.
- [23] Ken A. Dill and Sarina Bromberg. *Molecular Driving Forces: Statistical Thermodynamics in Biology, Chemistry, Physics, and Nanoscience*. Garland Science, 2011.
- [24] A. Grimstvedt, S. K. Ratkje, and T. Førland. Theory of Thermocells: Transported Entropies, and Heat of Transfer in Sulfate Mixtures. *Journal of The Electrochemical Society*, Vol. 141(No. 5), May 1994.
- [25] K. S. Førland, T. Førland, and S. Kjelstrup. *Irreversible Thermodynamics: Theory and Applications*. Tapir, 2001.
- [26] J. N. Agar, C. Y. Mou, and Jeong Long Lin. Single-ion heat of transport in electrolyte solutions: a hydrodynamic theory. *The Journal of Physical Chemistry*, 93(5):2079–2082, March 1989.
- [27] Carl H. Hamann, Andrew Hamnett, and Wolf Vielstich. *Electrochemistry*. Wiley-VCH, 2nd edition edition, 2007.
- [28] J. Newman and K. Thomas-Alyea. *Electrochemical Systems*. Wiley, 3rd edition edition, 2004.
- [29] B.E. Conway. Two-Dimensional and Quasi-Two-Dimensional Isotherms for Li Intercalation and upd Processes at Surfaces. *Electrochimica Acta*, 38(9):1249 – 1258, 1993.
- [30] J. R. Dahn, W. R. McKinnon, J. J. Murray, R. R. Haering, R. S. McMillan, and A. H. Rivers-Bowerman. Entropy of the Intercalation Compound $\text{Li}_x\text{Mo}_6\text{Se}_8$ From Calorimetry of Electrochemical Cells. *Physical Review B*, 32:3316–3318, Sep 1985.
- [31] Karen E. Thomas and John Newman. Heats of Mixing and of Entropy in Porous Insertion Electrodes. *Journal of Power Sources*, 119–121:844 – 849, 2003. Selected papers presented at the 11th International Meeting on Lithium Batteries.
- [32] Seong Jin An, Jianlin Li, Claus Daniel, Debasish Mohanty, Shrikant Nagpure, and David L. Wood. The State of Understanding of the Lithium-Ion-Battery Graphite Solid Electrolyte Interphase (SEI) and its Relationship to Formation Cycling. *Carbon*, 105(Supplement C):52 – 76, 2016.

- [33] Pallavi Verma, Pascal Maire, and Petr Novák. A Review of the Features and Analyses of the Solid Electrolyte Interphase in Li-ion Batteries. *Electrochimica Acta*, 55(22):6332 – 6341, 2010.
- [34] B. G. Silbernagel and M. S. Whittingham. An NMR study of the alkali metal intercalation phase Li_xTiS_2 : Relation to structure, thermodynamics, and ionicity. *The Journal of Chemical Physics*, 64(9):3670–3673, 1976.
- [35] Marit Takla Børset. *Energy Dissipation and Recovery in the Context of Silicon Production : Exergy Analysis and Thermoelectricity*. PhD thesis, NTNU, 2015.
- [36] James A. Bierlein. A Phenomenological Theory of the Soret Diffusion. *The Journal of Chemical Physics*, 23(1):10–14, 1955.
- [37] H. J. V. Tyrrell. *Diffusion and Heat Flow in Liquids*. Butterworths, London, 1961.
- [38] A. Latz and J. Zausch. Thermodynamic consistent transport theory of li-ion batteries. *Journal of Power Sources*, 196(6):3296 – 3302, 2011.
- [39] John Newman. Thermoelectric effects in electrochemical systems. *Industrial & engineering chemistry research*, 34(10):3208–3216, 1995.
- [40] Henrik Lundgren, Mårten Behm, and Göran Lindbergh. Electrochemical characterization and temperature dependency of mass-transport properties of lipf6 in ec:dec. *Journal of The Electrochemical Society*, 162(3):A413–A420, 2015.
- [41] Sathiyaraj Kandhasamy, Luca Calandrino, Odne Stokke Burheim, Asbjørn Solheim, Signe Kjelstrup, and Geir Martin Haarberg. Influence of Electrode Gas Flow Rate and Solid Oxide Ratio in Electrolyte on the Seebeck Coefficient of Molten Carbonate Thermocell. *Journal of The Electrochemical Society*, 164(8):H5271–H5276, 2017.
- [42] Andrey Gunawan, Chao-Han Lin, Daniel A. Buttry, Vladimiro Mujica, Robert A. Taylor, Ravi S. Prasher, and Patrick E. Phelan. Liquid Thermoelectrics: Review of Recent and Limited New Data of Thermogalvanic Cell Experiments. *Nanoscale and Microscale Thermophysical Engineering*, 17(4):304–323, 2013.
- [43] Kikuko Hayamizu. Temperature Dependence of Self-Diffusion Coefficients of Ions and Solvents in Ethylene Carbonate, Propylene Carbonate, and Diethyl Carbonate Single Solutions and Ethylene Carbonate + Diethyl Carbonate Binary Solutions of LiPF_6 Studied by NMR. *Journal of Chemical & Engineering Data*, 57:2012–2017, 06 2012.

- [44] Yanbo Liu, Zhijun Cai, Lei Tan, and Lei Li. Ion exchange membranes as electrolyte for high performance li-ion batteries. *Energy & Environmental Science*, 5(10):9007–9013, September 2012.
- [45] Ellen Marie Hansen, Espen Egner, and Signe Kjelstrup. Peltier Effects in Electrode Carbon. *Metallurgical and Materials Transactions B*, 29(1):69–76, Feb 1998.
- [46] A. Honders, J.M. der Kinderen, A.H. van Heeren, J.H.W. de Wit, and G.H.J. Broers. The Thermodynamic and Thermoelectric Properties of Li_xTiS_2 and Li_xCoO_2 . *Solid State Ionics*, 14(3):205 – 216, 1984.
- [47] Frank Richter, Signe Kjelstrup, Preben J.S. Vie, and Odne S. Burheim. Thermal Conductivity and Internal Temperature Profiles of Li-ion Secondary Batteries. *Journal of Power Sources*, 359:592 – 600, 2017.
- [48] Gordon Aylward and Tristan Findlay. *SI Chemical Data*. Wiley, 6th edition.
- [49] T. Motohashi, T. Ono, Y. Sugimoto, Y. Masubuchi, S. Kikkawa, R. Kanno, M. Karppinen, and H. Yamauchi. Electronic Phase Diagram of the Layered Cobalt Oxide System Li_xCoO_2 ($0.0 \leq x \leq 1.0$). *Physical Review B*, 80:165114, Oct 2009.
- [50] Janina Molenda, Andrzej Kulka, Anna Milewska, Wojciech Zajac, and Konrad Świerczek. Structural, Transport and Electrochemical Properties of LiFePO_4 Substituted in Lithium and Iron Sublattices (Al, Zr, W, Mn, Co and Ni). *Materials*, 6(5):1656–1687, 2013.
- [51] Yousef Saad. *Iterative Methods for Sparse Linear Systems*. SIAM, 2003.
- [52] Edward Armand Guggenheim. *Mixtures: The Theory of the Equilibrium Properties of Some Simple Classes of Mixtures Solutions and Alloys*. Clarendon Press, 1952.
- [53] Taichi Abe and Toshiyuki Koyama. Thermodynamic Modeling of the LiCoO_2 – CoO_2 Pseudo-Binary System. *Calphad*, 35(2):209 – 218, 2011.
- [54] H. J. Orman and P. J. Wiseman. Cobalt(III) Lithium Oxide, CoLiO_2 : Structure Refinement by Powder Neutron Diffraction. *Acta Crystallographica Section C*, 40(1):12–14, Jan 1984.
- [55] Tianran Zhang, Daixin Li, Zhanliang Tao, and Jun Chen. Understanding Electrode Materials of Rechargeable Lithium Batteries via DFT Calculations. *Chinese Materials Research Society*, 23:256–272, 06 2013.

Chapter 7

List of Symbols and Abbreviations

Table 1 - Greek symbols

Symbol	Dimension	Explanation
γ_i	-	Activity coefficient of component i
Δ_{ij}	-	Difference from i to j
ϵ	V K^{-1}	Thermoelectric power
η_s	V K^{-1}	Seebeck coefficient
θ	min^{-1}	Characteristic time
κ	$\text{J s}^{-1} \text{K}^{-1} \text{m}^{-2}$	Thermal conductivity
λ	$\text{J s}^{-1} \text{K}^{-1} \text{m}^{-2}$	Stationary state thermal conductivity
μ_i	J mol^{-1}	chemical potential of component i
π	J mol^{-1}	Peltier coefficient, Peltier heat
$\prod_{i=1}^n$	-	Product of elements 1 to n
ρ	kg m^{-3}	Density
σ	$\text{J s}^{-1} \text{K}^{-1} \text{m}^{-3}$	Entropy production
$\sum_{i=1}^n$	-	Sum of elements 1 to n
τ_i	$\text{J K}^{-1} \text{mol}^{-1}$	Thomson coefficient of component i
τ	K	Temperature difference
ϕ	V	Electric potential

Table 2 - Latin symbols

Symbol	Dimension	Explanation
c_i	mol dm^{-3}	concentration of component i
D_i	$\text{m}^2 \text{s}^{-1}$	Diffusion coefficient of component i
D'_i	$\text{m}^2 \text{s}^{-1}$	Thermal diffusion coefficient of component i
e	C	unit charge of a proton
F	C mol^{-1}	Faraday's constant
h	m	Diffusion path length
J_q	$\text{J m}^2 \text{s}^{-1}$	Total heat flux
J'_q	$\text{J m}^2 \text{s}^{-1}$	Measurable heat flux
J_i	$\text{mol m}^2 \text{s}^{-1}$	Mass flux of component i
j	A m^{-2}	Current density
L_{ii}	-	Main coefficient
L_{ij}	-	Coupling constant between i and j
l_{ij}	-	Phenomenological coefficient for coupling of fluxes
n	-	Number of electrons involved in electrode reaction
p	Pa	Pressure
Q^{rev}	J mol^{-1}	Total reversible heat effect
q^*	J mol^{-1}	Measurable heat of transfer
R	$\text{J K}^{-1} \text{mol}^{-1}$	Gas constant
S	$\text{J K}^{-1} \text{mol}^{-1}$	Entropy
S^*	$\text{J K}^{-1} \text{mol}^{-1}$	Transported entropy
s_i	$\text{J K}^{-1} \text{mol}^{-1}$	Partial specific entropy of component i
s_T	-	Soret coefficient
T	K	Temperature
t	s	Time
t_i	-	Transference coefficient for component i
v	$\text{m}^3 \text{mol}^{-1}$	specific volume
W	-	Multiplicity
X_j	-	General symbol for driving force
x_i	-	Molar fraction of component i
x	-	Amount of Li in electrode
x	m	Dimension
z_i	-	Number of charges on component i

Table 3 - Abbreviations

Abbreviation	Explanation
DEC	Diethyl carbonate
DMC	Dimethyl carbonate
EC	Ethyl carbonate
SEI	Solid electrolyte interphase
PET	Polyester polyethylene terephthalate
PE	Polyethylene
<i>emf</i>	electromotive force

Appendix A

Statistics

The standard deviation of a sample s given by:

$$s = \sqrt{\frac{\sum_{i=1}^N (x_i - \bar{x})^2}{N - 1}} \quad (\text{A.1})$$

Where x_1, x_2, \dots, x_N are the individual values making up the sample and \bar{x} is the mean.

If the variables of a function $f(x, y, \dots)$ are assumed to be independent, the standard deviation of the function can be approximated using Gauss' error propagation:

$$s_{f(x,y,\dots)} = \sqrt{\left(\frac{\partial f}{\partial x}\right)^2 \cdot s_x^2 + \left(\frac{\partial f}{\partial y}\right)^2 \cdot s_y^2 + \dots} \quad (\text{A.2})$$

where s_x is the standard deviation of the variable x .

Stirling's approximation is given by [23]:

$$\ln n! = n \ln n - n \quad (\text{A.3})$$

Appendix B

Thermal Profile from Fourier's Law

The cell dimensions and thermal conductivity data used to determine the the temperature gradient present inside the cell is given in Table B.1.

Table B.1: Thickness and thermal conductivity of cell materials as measured by Richter et Al. [7].

Part of the cell	Thickness /10 ⁻³ m	Thermal conductivity /WK ⁻¹ m ⁻¹
Al current collector	0.014	237 [48]
Cu end plates and current collectors	2.000	401 [48]
Cell house wall	0.132	0.25 [1]
C ₆ electrode	0.030	1.11 [47]
LiCoO ₂ electrode (LCO)	0.030	1.03 [47]
LiFePO ₄ electrode (LCO)	0.030	0.32 [47]
Electrolyte-soaked separator	1.787	0.19 [47]

According to Fourier's law, which can be assumed valid for the cell at stationary state, the measurable heat flux through the copper plates and the cell is given by:

$$J'_q = \frac{T_h - T_c}{2 \frac{x_{Cu}}{\lambda_{Cu}} + 2 \frac{x_{PCH}}{\lambda_{PCH}} + 2 \frac{x_{Al}}{\lambda_{Al}} + 2 \frac{x_{LCO}}{\lambda_{LCO}} + \frac{x_{separator}}{\lambda_{separator}}} \quad (\text{B.1})$$

Where T_h and T_c is the hot and cold temperature measured by the thermocouples outside the copper plates. By using this equation, an internal temperature gradient of 89% of the external gradient was predicted. The temperature profile in this case is shown in Figure B.1.

However, the calibration measurement used indicated that only 71% of the external temperature gradient is present in the cell. When an air gap resistance is added between the copper plates and the cell housing, the measurable heat flux is then found from the following equation:

$$J'_q = \frac{T_h - T_c}{2 \frac{1}{h_{air}} + 2 \frac{x_{Cu}}{\lambda_{Cu}} + 2 \frac{x_{PCH}}{\lambda_{PCH}} + 2 \frac{x_{Al}}{\lambda_{Al}} + 2 \frac{x_{LCO}}{\lambda_{LCO}} + \frac{x_{separator}}{\lambda_{separator}}} \quad (\text{B.2})$$

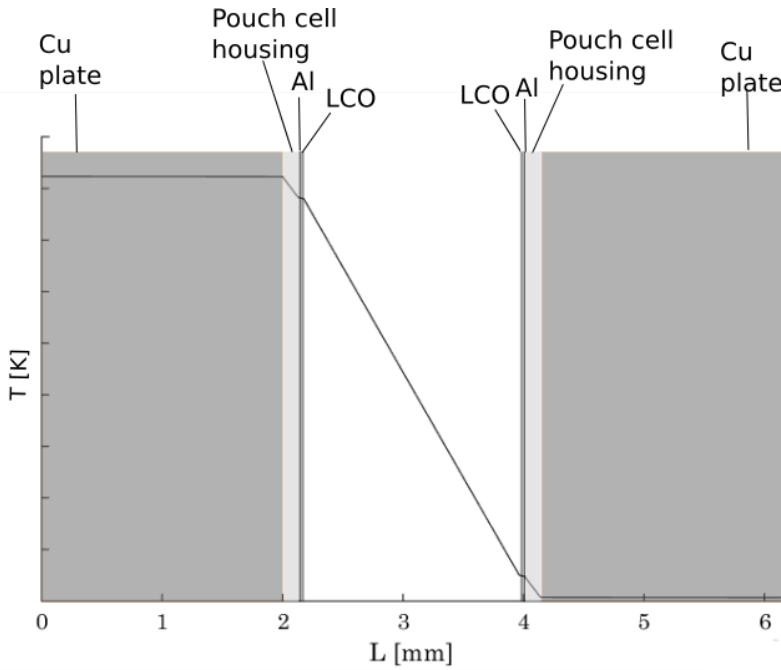


Figure B.1: The theoretical thermal profile of the LiCoO_2 symmetric cell including the cell dimensions, calculated using Fourier's law and thermal conductivity data. Heat losses to the surroundings is not taken into account in this calculation.

Where h_{air} is the heat transfer coefficient between the copper plates and the cell housing. The heat transfer coefficient of the air gap can be found from J'_q . However, J'_q must be found using the heat transfer coefficient. By using experimental temperature measurements, the heat transfer coefficient and J'_q was calculated iteratively. The result is shown below.

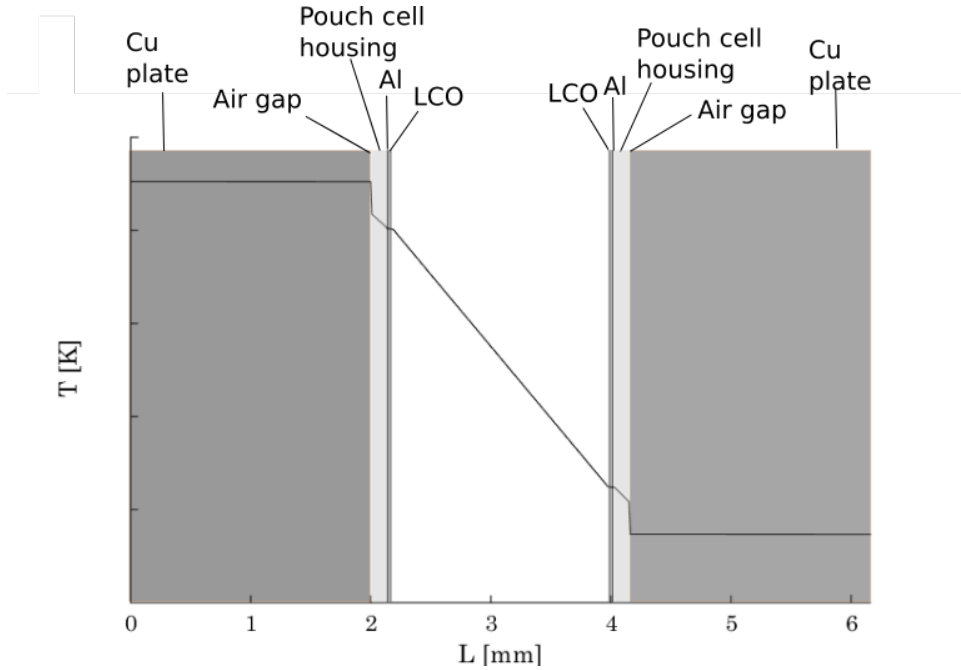


Figure B.2: The stationary state temperature profile measured by thermocouples inside a pouch cell. The loss due to air gap resistance is calculated using an iteratively estimated heat transfer coefficient. In this graph it is assumed thermostatted electrodes, that approximately the same air gap resistance is present on both sides of the cell and that the heat conduction between the cell materials is follow Fourier's law.

Appendix C

Thermoelectric Potential Data

The plots of the measured electric potential and temperature gradients from the thermoelectric potential measurements of the LiCoO_2 , C_6 and LiFePO_4 cells are given in this appendix. The values used in the treatment of the data is found in Table C.1.

Table C.1: Table of transported entropies of charge carriers in electrodes and standard entropy of compounds found in literature. *At x in $\text{Li}_x\text{CoO}_2 > 0.94$ **At $300\text{-}550\text{C}^\circ$ ***At $150\text{-}250\text{C}^\circ$.

Electrode material	$S_{e^-}^*$ / $\text{J K}^{-1} \text{mol}^{-1}$
Lithium Cobalt Oxide, LiCoO_2	10* [49]
Graphite, C_6	-2** [45]
Lithium Iron Phosphate, LiFePO_4	15*** [50]
Lithium Titanium disulfide, $\text{Li}_{0.13}\text{TiS}_2$	2.5 [46]
Lithium Titanium disulfide, $\text{Li}_{0.26}\text{TiS}_2$	2.4 [46]
Lithium Titanium disulfide, $\text{Li}_{0.61}\text{TiS}_2$	0.4 [46]
Lithium Titanium disulfide, $\text{Li}_{0.80}\text{TiS}_2$	0 [46]
Compound	S^0 / $\text{J K}^{-1} \text{mol}^{-1}$
Lithium, Li	29 [48]

C.1 LiCoO₂ Measurements

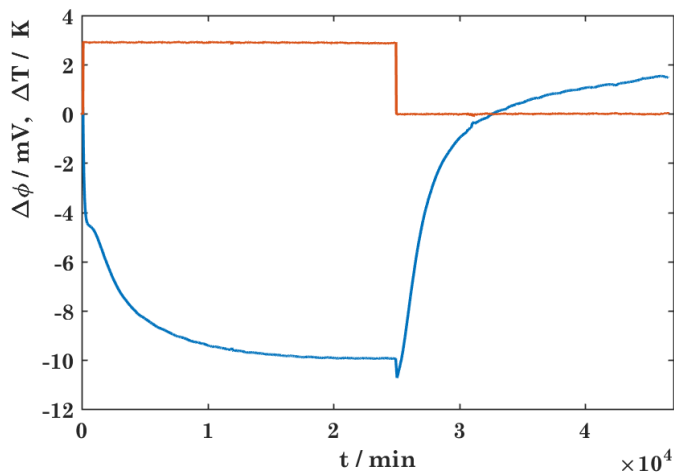


Figure C.1: The internal temperature difference and electric potential of LiCoO₂ cell A when the water bath temperature difference was set to 5 K.

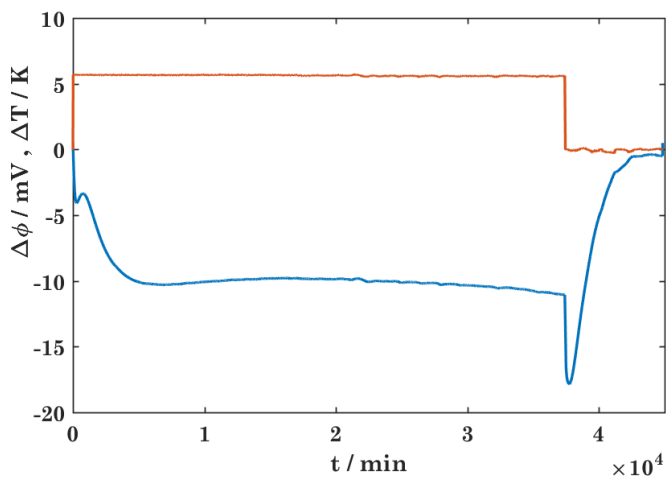


Figure C.2: The plot shows the internal temperature difference and electric potential of LiCoO₂ cell A when the water bath temperature difference was set to 10 K.

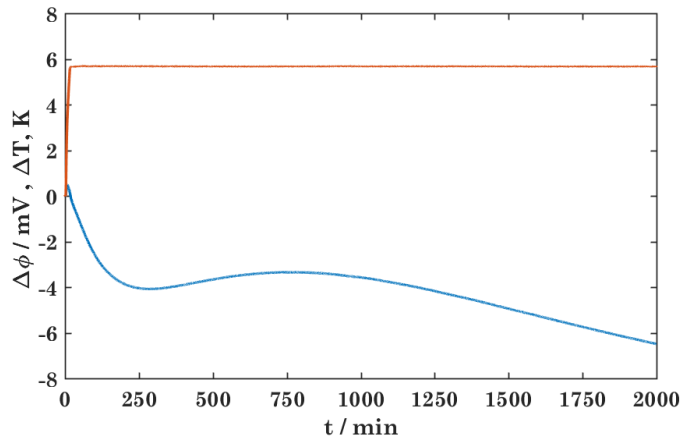


Figure C.3: A zoom-in on the measurements at the initial time-period of the LiCoO_2 Cell A when the water bath temperature difference was set to 10 K.

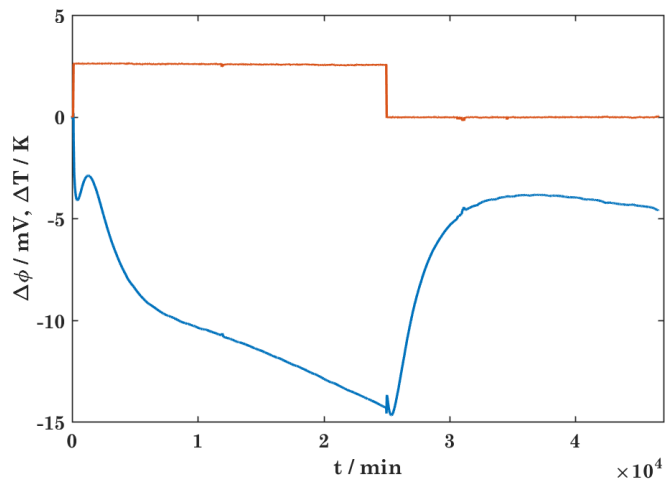


Figure C.4: The plot shows the internal temperature difference and electric potential of LiCoO_2 cell B when the water bath temperature difference was set to 5 K.

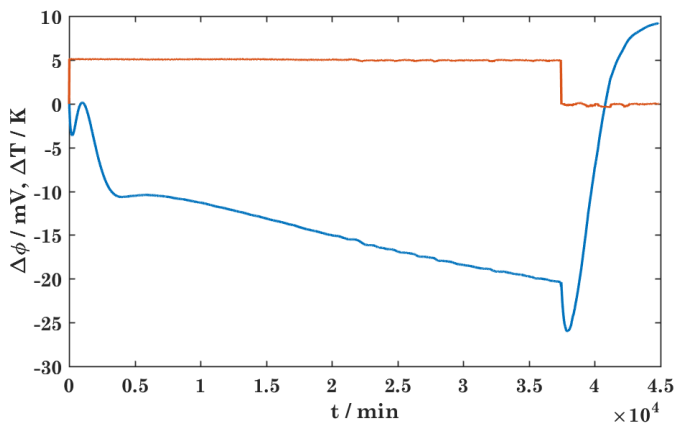


Figure C.5: The plot shows the internal temperature difference and electric potential of LiCoO_2 cell B when the water bath temperature difference was set to 10 K.

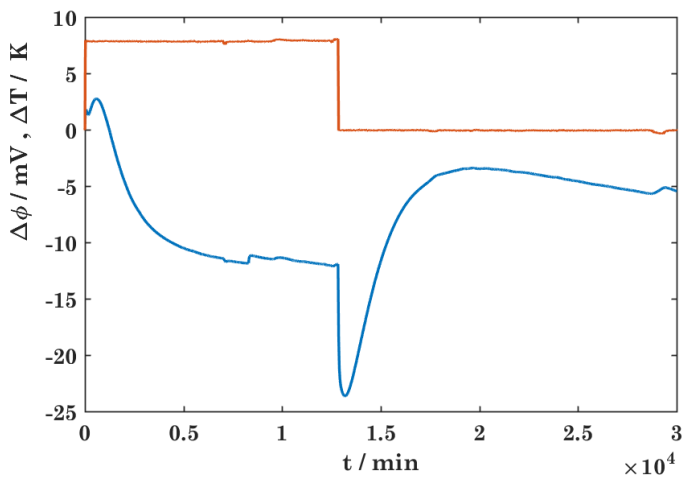


Figure C.6: The internal temperature difference and electric potential of LiCoO_2 cell A when the water bath temperature gradient was set to 15 K.

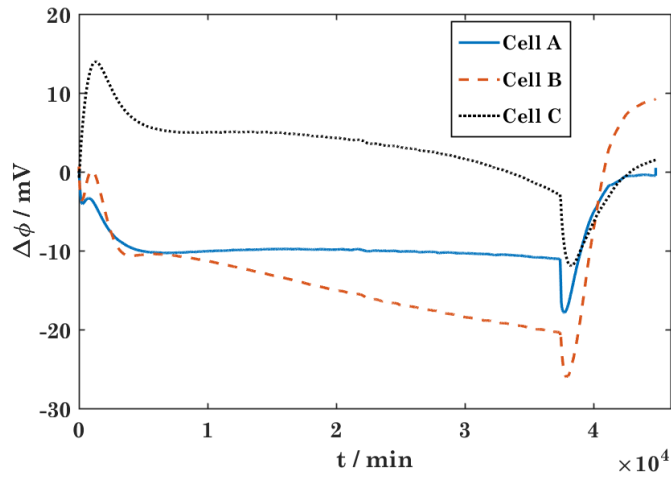


Figure C.7: The electric potential measurement of LiCoO_2 cell A, B and C when the water bath temperature difference was set to 10 K.

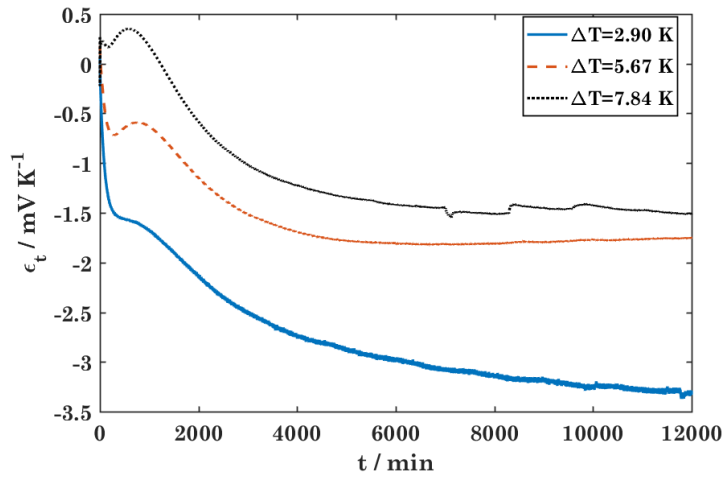


Figure C.8: The thermoelectric potential of LiCoO_2 cell A.

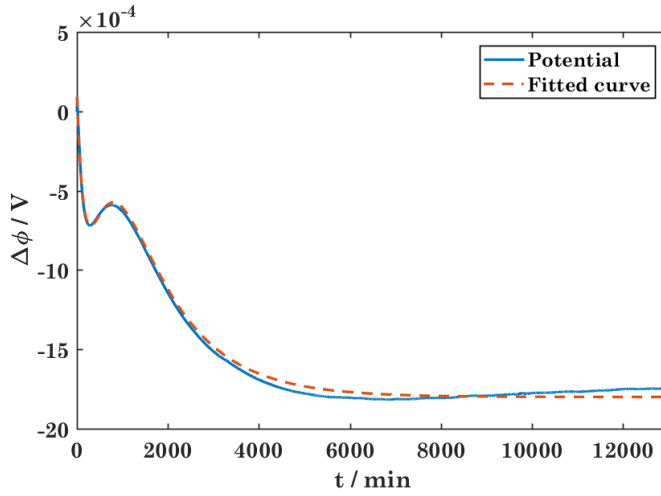


Figure C.9: Shows the plot of the electric potential measurement at an internal temperature difference of 5.7 K and the fitted curve.

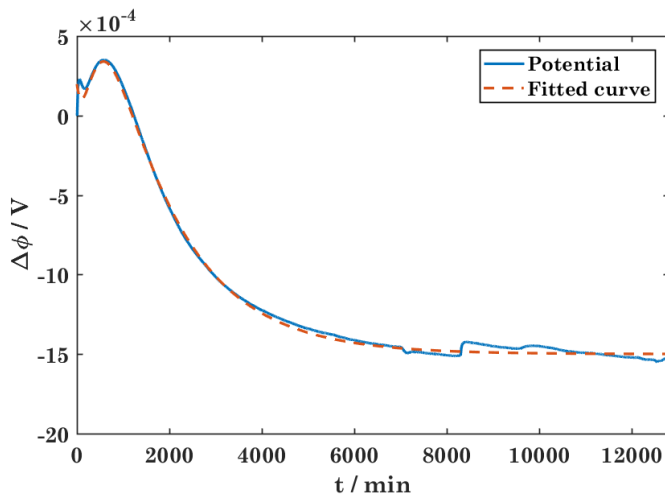


Figure C.10: Shows the plot of the electric potential measurement at an internal temperature difference of 7.8 K and the fitted curve.

C.2 C_6 Measurements

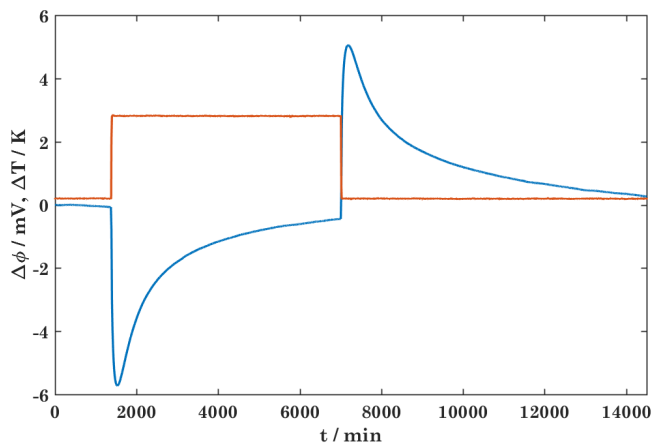


Figure C.11: The temperature difference and electric potential of C_6 cell A when the water bath temperature difference was set to 5 K.

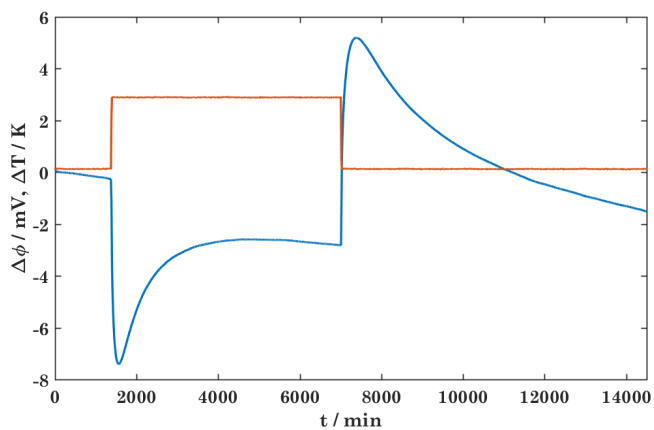


Figure C.12: The temperature difference and electric potential of C_6 cell B when the water bath temperature difference was set to 5 K.

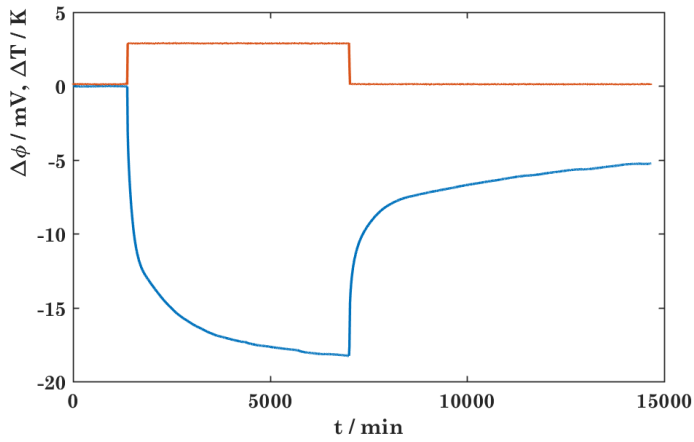


Figure C.13: The temperature difference and electric potential of C_6 cell C when the water bath temperature difference was set to 5 K.

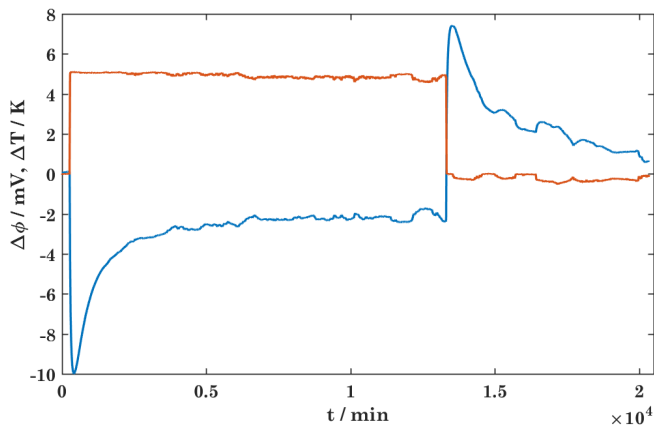


Figure C.14: The temperature difference and electric potential of C_6 cell A of the first experiment when the water bath temperature difference was set to 10 K. The thermostating was disturbed during the measurement.

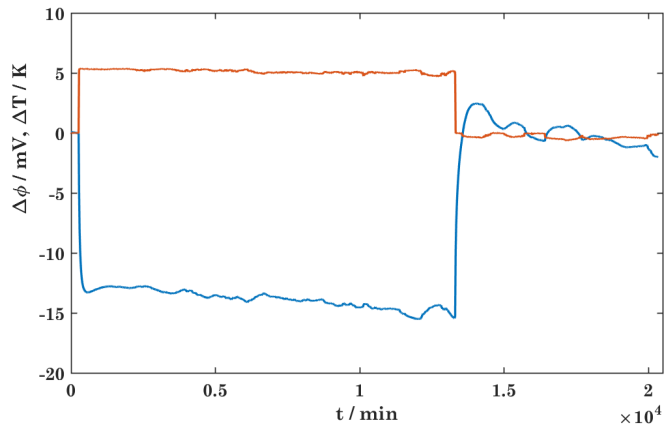


Figure C.15: The temperature difference and electric potential of C_6 cell B of the first experiment when the water bath temperature difference was set to 10 K. The thermostating was disturbed during the measurement.

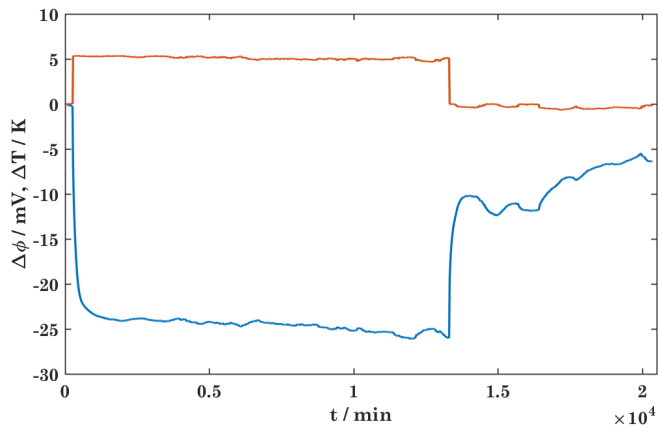


Figure C.16: The temperature gradient and electric potential of C_6 cell C of the first experiment when the water bath temperature gradient was set to 10 K. The thermostating was disturbed during the measurement.

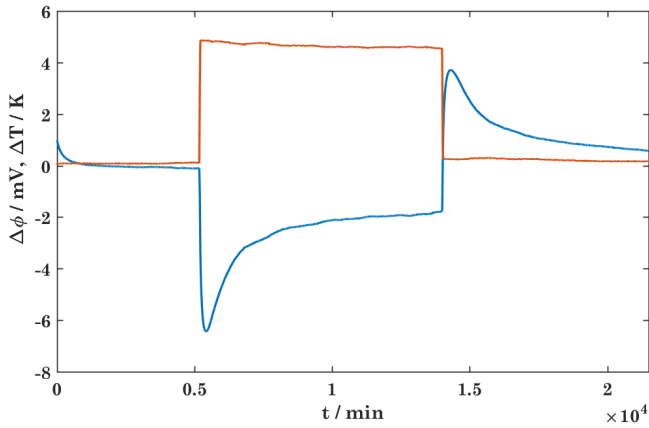


Figure C.17: The temperature difference and potential of C_6 cell A of the second experiment when the water bath temperature difference was set to 10 K.

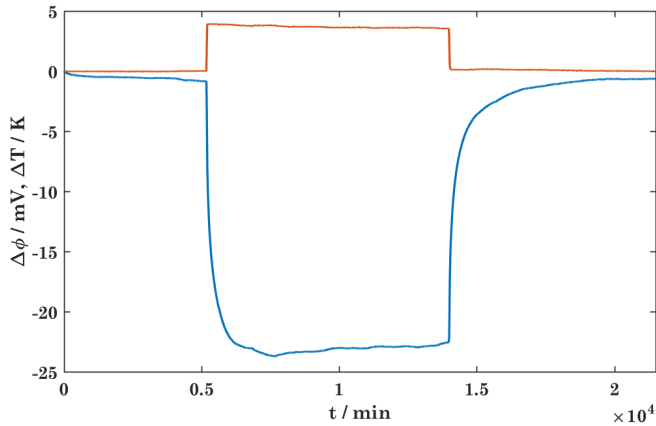


Figure C.18: The temperature difference and electric potential of C_6 cell B of the second experiment when the water bath temperature gradient was set to 10 K.

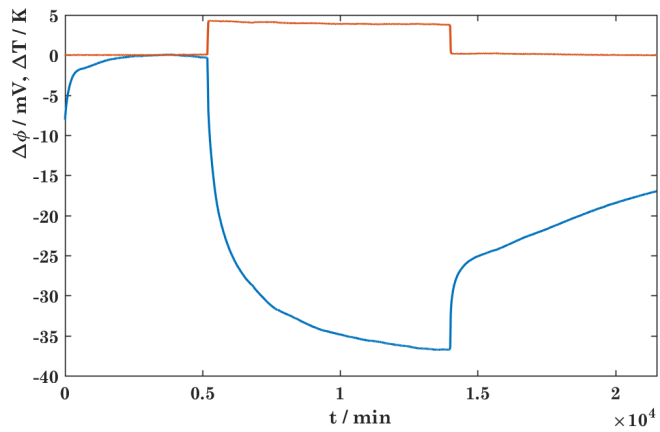


Figure C.19: The temperature difference and electric potential of C_6 cell C of the second experiment when the water bath temperature difference was set to 10 K.

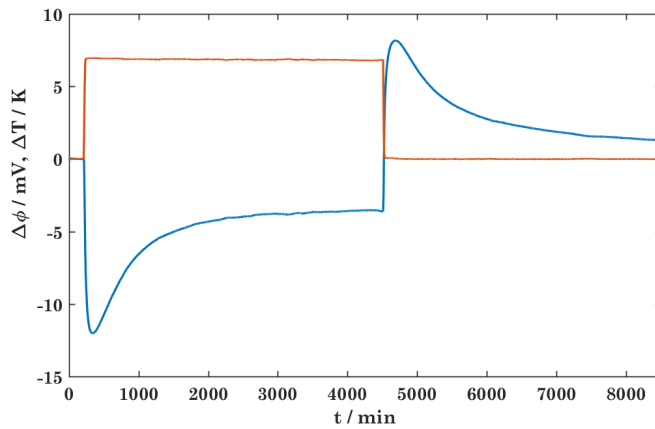


Figure C.20: The temperature difference and potential of C_6 cell A of the first experiment when the water bath temperature difference was set to 15 K.

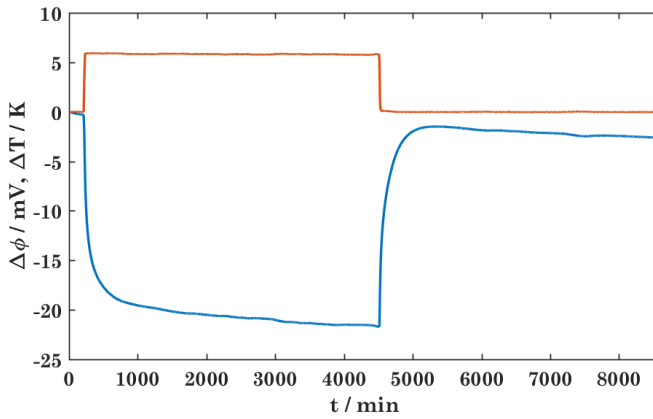


Figure C.21: The temperature difference and electric potential of C_6 cell B of the first experiment when the water bath temperature difference was set to 15 K.

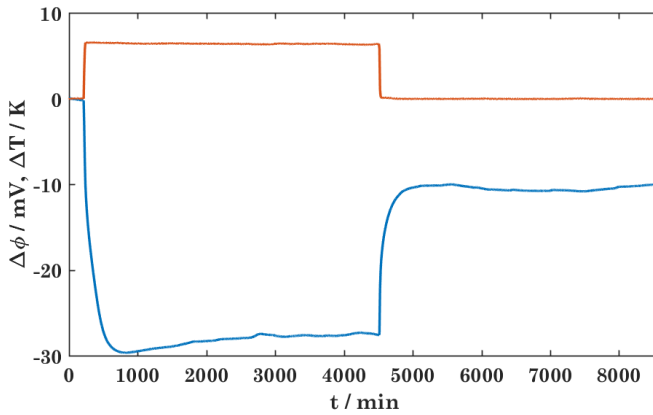


Figure C.22: The temperature difference and electric potential of C_6 cell C of the first experiment when the water bath temperature difference was set to 15 K.

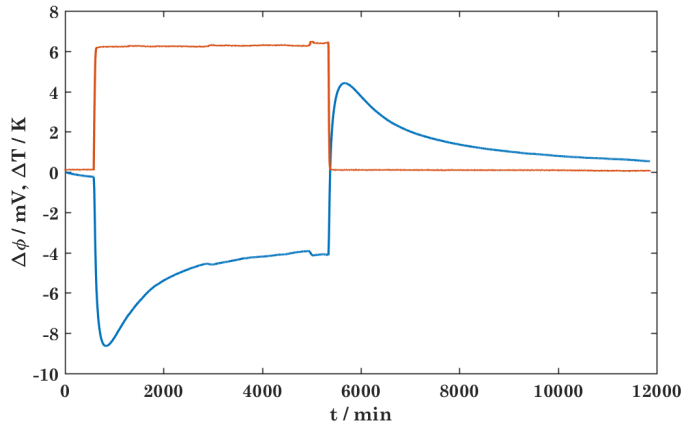


Figure C.23: The temperature difference and electric potential of C_6 cell A of the second experiment when the water bath temperature difference was set to 15 K.

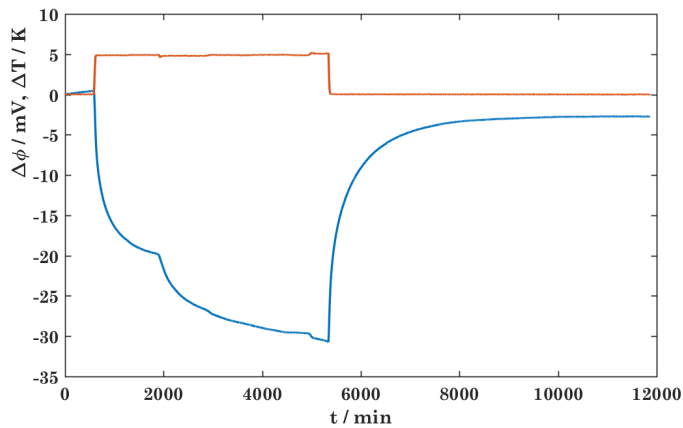


Figure C.24: The temperature difference and electric potential of C_6 cell B of the second experiment when the water bath temperature difference was set to 15 K.

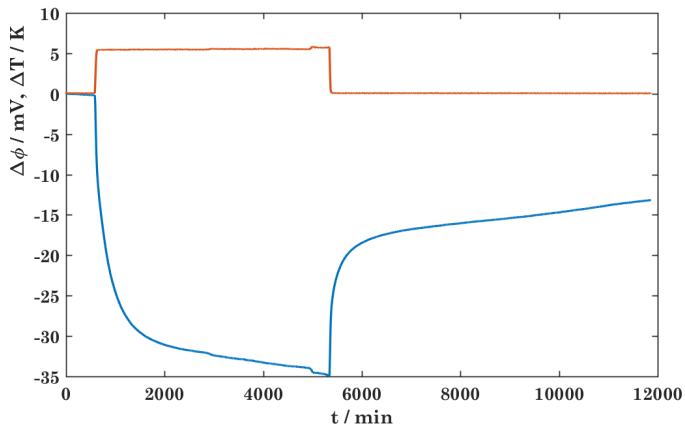


Figure C.25: The temperature difference and electric potential of C₆ cell B of the second experiment when the water bath temperature difference was set to 15 K.

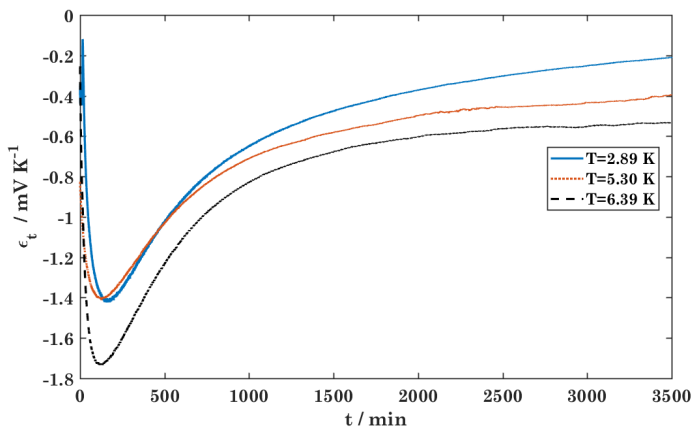


Figure C.26: Plot of the thermoelectric potential of C₆ cell A for when the water bath was set to a 5, 10 and 15K temperature difference for arrangement 1. The bias potential changed during the measurement and this change is not accounted for in this figure.

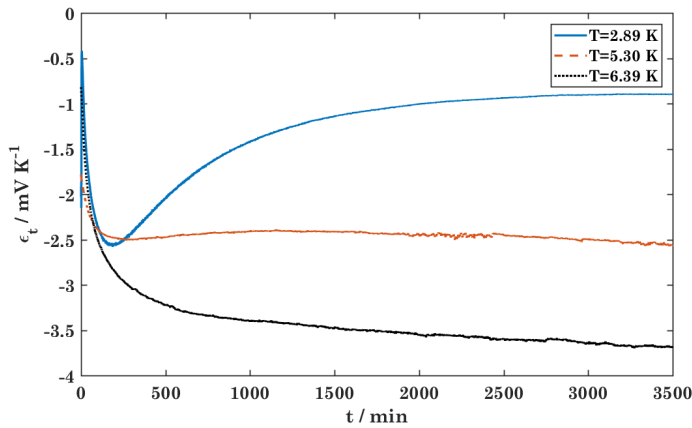


Figure C.27: Plot of the thermoelectric potential of C_6 cell B for when the water bath was set to a 5, 10 and 15K temperature difference for arrangement 1. The bias potential changed during the measurement and this change is not accounted for in this figure.

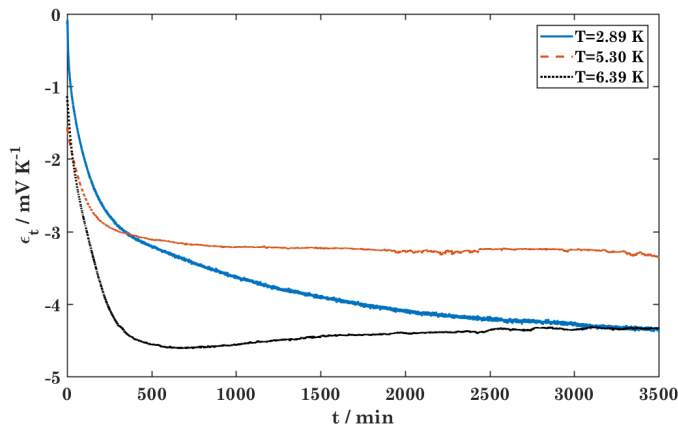


Figure C.28: Plot of the thermoelectric potential of C_6 cell C for when the water bath was set to a 5, 10 and 15K temperature difference for arrangement 1. The bias potential changed during the measurement and this change is not accounted for in this figure.

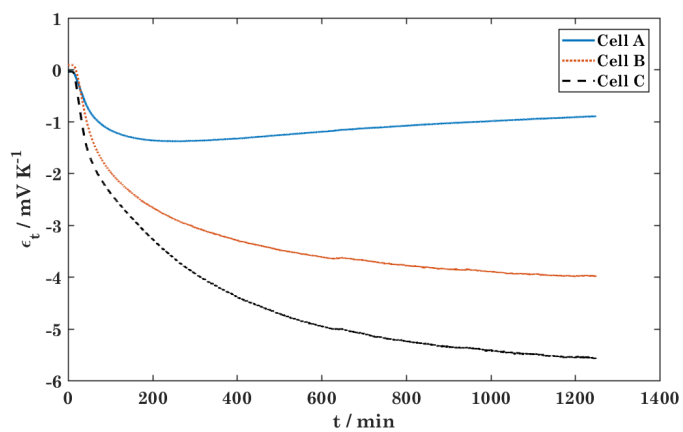


Figure C.29: Plot of the thermoelectric potential of C_6 cell A, B and C for when the water bath was 15K temperature difference for arrangement 2. The bias potential changed during the measurement and this change is not accounted for in this figure.

C.3 LiFePO_4 Measurements

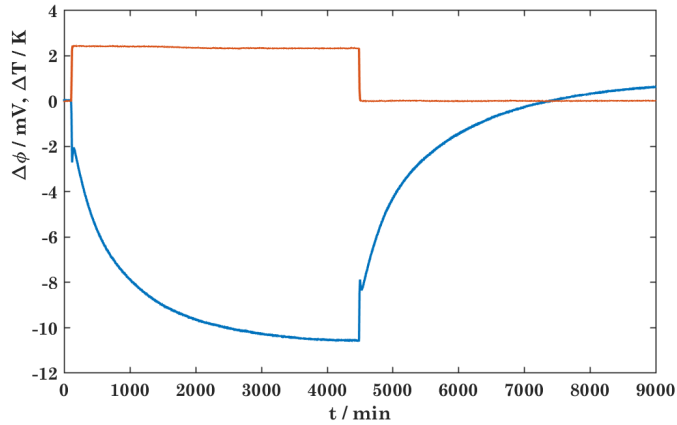


Figure C.30: The temperature gradient and electric potential of LiFePO_4 cell A for when the water bath was set to a 5 K temperature difference.

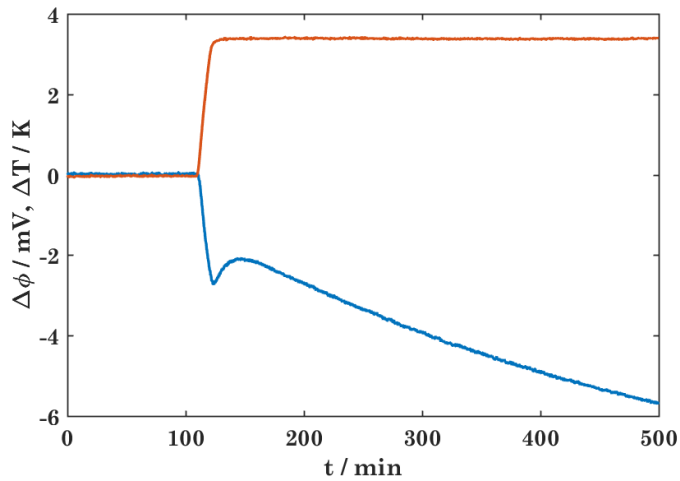


Figure C.31: A zoom-in on the measurements at the initial time period of the temperature difference and electric potential of LiFePO_4 cell A for when the water bath was set to a 5 K temperature difference.

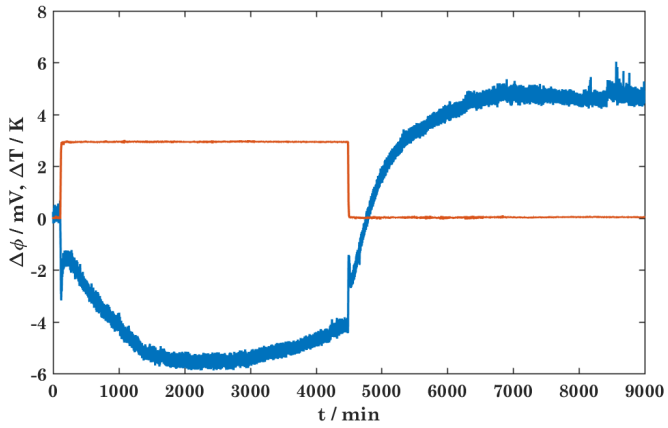


Figure C.32: The temperature gradient and electric potential of LiFePO₄ cell B for when the water bath was set to a 5 K temperature difference.

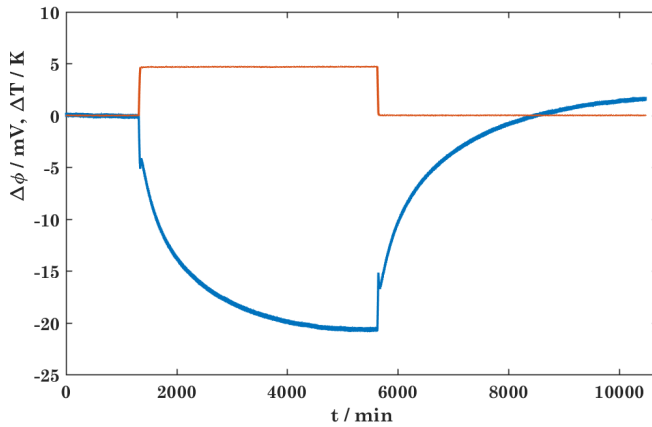


Figure C.33: The temperature difference and electric potential of LiFePO₄ cell A for when the water bath was set to a 10 K temperature difference.

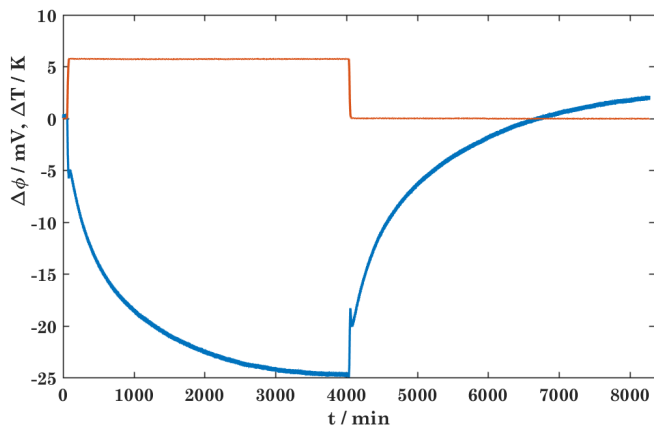


Figure C.34: The temperature difference and electric potential of LiFePO_4 cell A for when the water bath was set to a 12.5 K temperature difference.

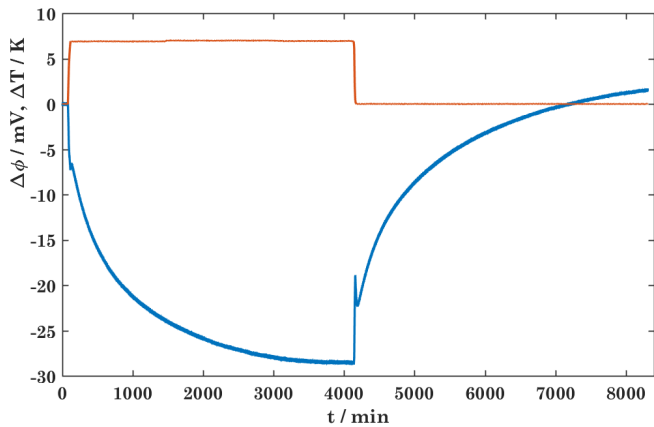


Figure C.35: The temperature difference and electric potential of LiFePO_4 cell A for when the water bath was set to a 15 K temperature difference.

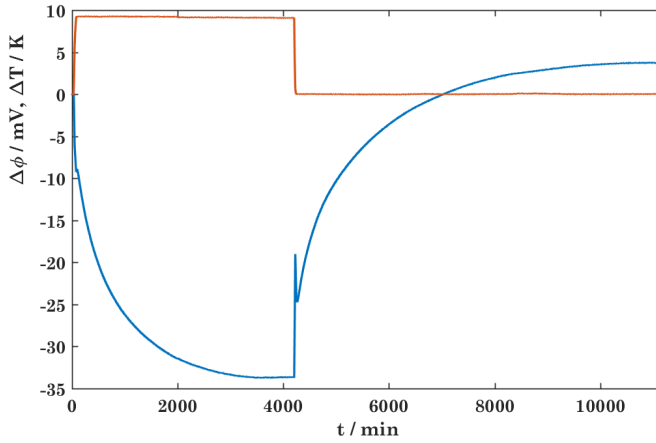


Figure C.36: The temperature difference and electric potential of LiFePO_4 cell A for when the water bath was set to a 20 K temperature difference.

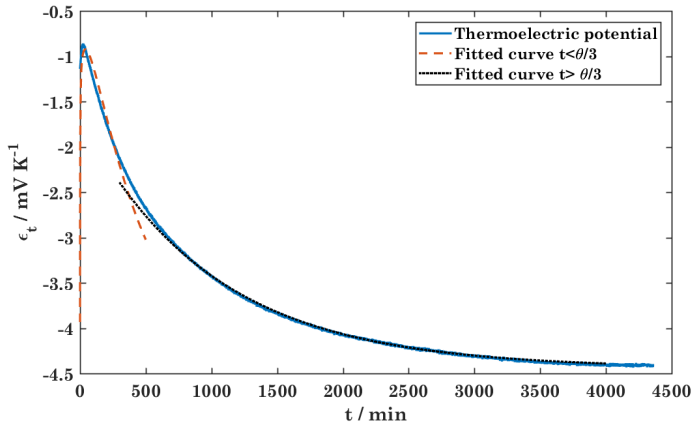


Figure C.37: Shows the plot of the thermoelectric potential for the $\Delta T = 2.4$ K experiment and the fitted curves.

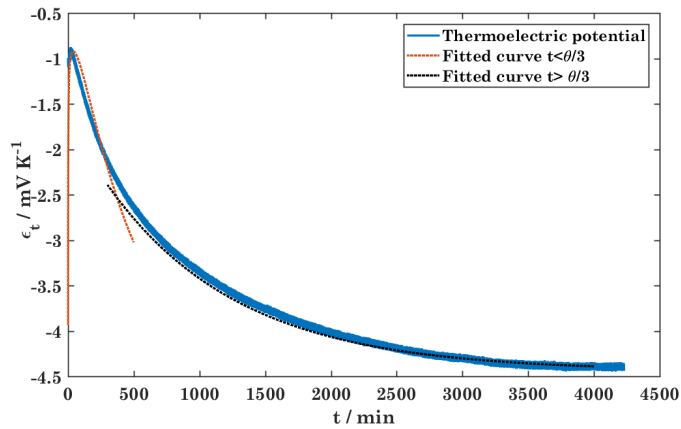


Figure C.38: Shows the plot of the thermoelectric potential for the $\Delta T = 4.7$ K experiment and the fitted curves.

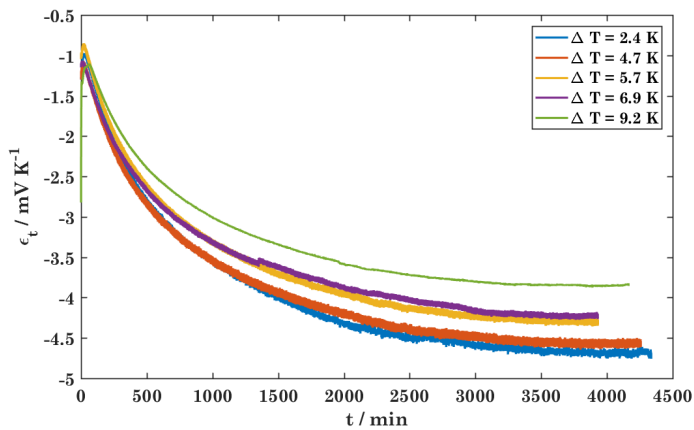


Figure C.39: Plot of the electric potentials of the LiFePO_4 cell over the temperature difference within the cell (thermoelectric potential) for the 5, 10, 12.5, 15 and 20 K external water bath temperature difference measurement.

Appendix D

Time Evolution of Multi-Component Diffusion

The time development of thermal diffusion phenomena of binary mixtures have been addressed by de Groot, Bierlein and Tyrrell [15, 36, 37]. However, a similar theory for thermal diffusion in ternary mixtures has not been developed. The derivation of the time evolution of the concentration gradients must first be found, as it appears in the expression for the electric potential (see Equation 3.33). The change in composition of a ternary solution with time is derived here.

Gibbs-Duhems equation applies:

$$d\mu_3 = -\frac{x_1}{x_3}d\mu_1 - \frac{x_2}{x_3}d\mu_2 \quad (\text{D.1})$$

The mass flux of component 1 and 2 for a ternary mixture is then given as:

$$\begin{aligned} J_1 &= -\frac{l_{1q}}{T^2} \frac{\partial T}{\partial x} - \left(\frac{l_{11}}{T} - \frac{x_1}{x_3} \frac{l_{13}}{T} \right) \frac{\partial \mu_{1,T}}{\partial x} - \left(\frac{l_{12}}{T} - \frac{x_2}{x_3} \frac{l_{23}}{T} \right) \frac{\partial \mu_{2,T}}{\partial x} \\ &= -\frac{l_{1q}}{T^2} \frac{\partial T}{\partial x} - \left(\frac{l_{11}}{T} - \frac{x_1}{1-x_1-x_2} \frac{l_{13}}{T} \right) \frac{\partial \mu_{1,T}}{\partial x} - \left(\frac{l_{12}}{T} - \frac{x_2}{1-x_1-x_2} \frac{l_{23}}{T} \right) \frac{\partial \mu_{2,T}}{\partial x} \end{aligned} \quad (\text{D.2})$$

$$\begin{aligned} J_2 &= -\frac{l_{2q}}{T^2} \frac{\partial T}{\partial x} - \left(\frac{l_{21}}{T} - \frac{x_1}{x_3} \frac{l_{23}}{T} \right) \frac{\partial \mu_{1,T}}{\partial x} - \left(\frac{l_{22}}{T} - \frac{x_2}{x_3} \frac{l_{23}}{T} \right) \frac{\partial \mu_{2,T}}{\partial x} \\ &= -\frac{l_{2q}}{T^2} \frac{\partial T}{\partial x} - \left(\frac{l_{21}}{T} - \frac{x_1}{1-x_1-x_2} \frac{l_{23}}{T} \right) \frac{\partial \mu_{1,T}}{\partial x} - \left(\frac{l_{22}}{T} - \frac{x_2}{1-x_1-x_2} \frac{l_{23}}{T} \right) \frac{\partial \mu_{2,T}}{\partial x} \end{aligned} \quad (\text{D.3})$$

This shows that the problem is given in a one-dimensional case. The flux equations can be rewritten using the approximation

$$\frac{\partial \mu_{i,T}}{\partial x} \approx \frac{RT}{x_i} \frac{\partial x_i}{\partial x} \quad (\text{D.4})$$

The following diffusion coefficients can then be defined:

$$\begin{aligned}
 D_i &= - \left[\frac{J_i}{(\partial c_i / \partial x)} \right]_{d\mu_{j \neq i}=0} = \frac{l_{ii} x_i}{R} \\
 D'_i &= - \left[\frac{J_i}{c_i (\partial T / \partial x)} \right]_{dc_i=0} = \frac{l_{ii} q}{c_i T^2} \\
 D_{ij} &= - \left[\frac{J_i}{(\partial c_j / \partial x)} \right]_{(\partial c_{i \neq j} / \partial x)=0} = \frac{l_{ij} x_j}{R}
 \end{aligned} \tag{D.5}$$

For electrolyte solutions this expression must be adapted for salts to account for the number of ions (see Eq. 3.31). This approximation will from now on be assumed valid. The mass flux equations can now be expressed as:

$$\begin{aligned}
 J_1 &= - \frac{D'_1}{c_1} \frac{\partial T}{\partial x} - \left(D_1 - \frac{x_1}{1-x_1-x_2} D_{1,3} \right) \frac{\partial x_1}{\partial x} - \left(D_{1,2} - \frac{x_2}{1-x_1-x_2} D_{2,3} \right) \frac{\partial x_2}{\partial x} \\
 &= - \frac{D'_1}{c_1} \frac{\partial T}{\partial x} - \frac{1}{\rho} \left(D_1 - \frac{c_1}{c_{\text{tot}} - c_1 - c_2} D_{1,3} \right) \frac{\partial c_1}{\partial x} - \frac{1}{\rho} \left(D_{1,2} - \frac{c_2}{c_{\text{tot}} - c_1 - c_2} D_{2,3} \right) \frac{\partial c_2}{\partial x}
 \end{aligned} \tag{D.6}$$

$$\begin{aligned}
 J_2 &= - \frac{D'_2}{c_2} \frac{\partial T}{\partial x} - \left(D_{2,1} - \frac{x_1}{1-x_1-x_2} D_{1,3} \right) \frac{\partial x_1}{\partial x} - \left(D_2 - \frac{x_2}{1-x_1-x_2} D_{2,3} \right) \frac{\partial x_2}{\partial x} \\
 &= - \frac{D'_1}{c_1} \frac{\partial T}{\partial x} - \frac{1}{\rho} \left(D_{2,1} - \frac{c_1}{c_{\text{tot}} - c_1 - c_2} D_{1,3} \right) \frac{\partial c_1}{\partial x} - \frac{1}{\rho} \left(D_2 - \frac{c_2}{c_{\text{tot}} - c_1 - c_2} D_{2,3} \right) \frac{\partial c_2}{\partial x}
 \end{aligned} \tag{D.7}$$

From now on the derivation will follow the assumptions made in Bierlein's similar derivation for the time dependence of binary solutions [36]; the temperature gradient and diffusion coefficients are assumed to be a constant. This is not strictly true. As seen in section 3.1, the temperature gradient will not be entirely constant for this system. However it is reasonable to assume that the deviation from a linear temperature profile is small and thus the assumption will be used for this derivation. The diffusion coefficients will vary both with the temperature and the composition. However for small changes in temperature and composition this variation is negligible. Thus the following will only be valid for small temperature gradients and small changes in composition.

The change in concentration with time is related to the flux equations:

$$\frac{\partial J_i}{\partial x} = - \frac{\partial c_i}{\partial t} \tag{D.8}$$

This gives the following changes to composition with time gives the following set of equations:

$$\begin{aligned} \frac{\partial c_1}{\partial t} = & - \left(\frac{D'_1 \tau}{c_1^2 h} \right) \frac{\partial c_1}{\partial x} + \left(\frac{D_1 - D_{1,3}/(c_{\text{tot}} - c_1 - c_2)}{\rho} \right) \frac{\partial^2 c_1}{\partial x^2} - \left(\frac{D_{1,3}}{\rho} \frac{1}{c_1} \right) \frac{\partial^2 c_1}{\partial x^2} \\ & - \left(\frac{D_{1,3} c_2}{\rho c_1^2} \right) \frac{\partial c_2}{\partial x} \frac{\partial c_1}{\partial x} + \left(\frac{D_{1,2} - D_{2,3}/(c_{\text{tot}} - c_1 - c_2)}{\rho} \right) \frac{\partial^2 c_2}{\partial x^2} - \left(\frac{D_{2,3} c_2}{c_1^2} \right) \frac{\partial c_1}{\partial x} \frac{\partial c_2}{\partial x} \\ & - \left(\frac{D_{2,3}}{c_2} \right) \frac{\partial^2 c_2}{\partial x^2} \end{aligned} \quad (\text{D.9})$$

$$\begin{aligned} \frac{\partial c_2}{\partial t} = & - \left(\frac{D'_2 \tau}{c_2^2 h} \right) \frac{\partial c_2}{\partial x} + \left(\frac{D_{2,1} - D_{1,3}/(c_{\text{tot}} - c_1 - c_2)}{\rho} \right) \frac{\partial^2 c_1}{\partial x^2} - \left(\frac{D_{1,3}}{\rho} \frac{1}{c_1} \right) \frac{\partial^2 c_1}{\partial x^2} \\ & - \left(\frac{D_{1,3} c_1}{\rho c_2^2} \right) \frac{\partial c_2}{\partial x} \frac{\partial c_1}{\partial x} + \left(\frac{D_2 - D_{2,3}/(c_{\text{tot}} - c_1 - c_2)}{\rho} \right) \frac{\partial^2 c_2}{\partial x^2} - \left(\frac{D_{2,3} c_2}{c_1^2} \right) \frac{\partial c_1}{\partial x} \frac{\partial c_2}{\partial x} \\ & - \left(\frac{D_{2,3}}{c_2} \right) \frac{\partial^2 c_2}{\partial x^2} \end{aligned} \quad (\text{D.10})$$

Where τ is the temperature difference over the cell and h is the diffusion path length. The initial conditions are:

$$\lim_{t \rightarrow 0} c_1 = c_{1,0} \quad (\text{D.11})$$

$$\lim_{t \rightarrow 0} c_2 = c_{2,0} \quad (\text{D.12})$$

At the electrodes there is no mass flux. Therefore the boundary conditions given at the electrode interfaces:

$$\lim_{x \rightarrow 0} \frac{\partial c_1}{\partial t} = \lim_{x \rightarrow h} \frac{\partial c_1}{\partial t} = 0 \quad (\text{D.13})$$

$$\lim_{x \rightarrow 0} \frac{\partial c_2}{\partial t} = \lim_{x \rightarrow h} \frac{\partial c_2}{\partial t} = 0 \quad (\text{D.14})$$

These are homogeneous Neumann boundary conditions [51], where the boundary is given for the electrode surfaces. It is reasonable to assume that the cross terms with $\frac{\partial c_1}{\partial x} \frac{\partial c_2}{\partial x}$ will be small. D_i can be assumed to be the dominating term for the diffusion terms, as $D_i \gg D_{ij}$ because in most cases $l_{ii} \gg l_{ij}$. It can be seen from the definition of D_{ij} that when the approximation $l_{ij} \approx 0$ is made, the problem reduces to two independent partial differential equations, i.e. there is no coupling between the mass fluxes. The change in composition of one component with time is then independent of the other, and hence the approximation done in Section 5.1.1 is valid. The derivation then follow the steps of Bierlein's work, simply done for

two independent equations [36].

$$\Delta x_1 = -\frac{D'_1}{D_1} \Delta T x_{1,0} (1 - x_{1,0}) \left[1 - \frac{8}{\pi^2} \exp(-t/\theta_1) \right] \quad (\text{D.15})$$

$$\Delta x_2 = -\frac{D'_2}{D_2} \Delta T x_{2,0} (1 - x_{2,0}) \left[1 - \frac{8}{\pi^2} \exp(-t/\theta_2) \right] \quad (\text{D.16})$$

where $x_{i,0}$ is the composition expressed with molar fractions at time 0. This can then be inserted into equation 3.33 for the electric potential:

$$\begin{aligned} \Delta\phi(t) = & -\frac{\pi}{TF} \Delta T + \frac{t_1 RT}{F x_1} \frac{D'_1}{D_1} \Delta T x_{1,0} (1 - x_{1,0}) \left[1 - \frac{8}{\pi^2} \exp(-t/\theta_1) \right] \\ & + \frac{t_2 RT}{F x_2} \frac{D'_2}{D_2} \Delta T x_{2,0} (1 - x_{2,0}) \left[1 - \frac{8}{\pi^2} \exp(-t/\theta_2) \right] \end{aligned} \quad (\text{D.17})$$

Appendix E

Entropy of Intercalation

The lattice model is a theoretical model used in statistical mechanics to treat a simple system using statistics. The molecules in the system is treated as a hard sphere and are distributed on a lattice [23]. Each sphere can only occupy one lattice point. A lattice point may or may not be occupied. The “crude treatment” of lattices for use in lattice models described by Guggenheim will be used in this section [52]. In this treatment all interaction between the atoms are neglected and a completely random distribution is used, meaning that there is no long or short range order. Each distribution of molecules in the lattice is considered equally probable, and thermodynamic properties can be found using the multiplicity of the different compositions of the lattice [23, 52].

The entropy of the LiCoO_2 , LiFePO_4 and C_6 electrodes will depend on the amount of intercalated lithium. In other words, it will depend on the state of charge of the electrodes. In literature the electrode material is referred to as the host lattice [29, 30]. Since the entropy is a state function, the entropy of the electrode is only dependent on the amount of intercalated Li and (if diffusion between layers and channels is not possible) position in the lattice and not on the order of intercalation. Therefore it does not matter for the value of the entropy of the Li atoms is added to the host lattice one by one or if the total amount of Li is added at once, if at the end the lattice is the same, the result is the same. Therefore it can be regarded as the result of two lattices; one Li lattice and one host lattice, in which the total entropy of calculated for the combined structure. However, for the purposes of this thesis, only the entropy of Li intercalated in the electrode is sought, and not the entropy of the electrode as a whole. This will be interpreted as the Li lattice.

In LiCoO_2 , C_6 and other intercalation electrodes lithium is inserted into two-dimensional layers. In the literature, the multiplicity of the system is treated for the whole lattice, not layer by layer. This means that the intercalation is treated as if totally independent on the number of Li atoms already present in the different layers. In addition the entire lattice of Li is regarded as one system and the multiplicity is thereby defined by this.

The entropy of the electrodes is given by Boltzmann's law [23]:

$$S = k_B \ln W \quad (\text{E.1})$$

where W is the multiplicity of the system given by:

$$W = \frac{M!}{m_{\text{Li}}! (M - m_{\text{Li}})!} \quad (\text{E.2})$$

where M is the number of lattice sites that can be occupied by Li, m_{Li} is the number of lattice sites occupied by Li in the lattice and $(M - m_{\text{Li}})$ is the number of unoccupied sites. The change in entropy can then be written as:

$$\Delta S = k_b \ln \frac{M!}{m_{\text{Li}}! (M - m_{\text{Li}})!} = k_b \ln \frac{(M \cdot 1)!}{(Mx)! (M(1-x))!} \quad (\text{E.3})$$

where x is the number of Li atoms per CoO_2 unit, i.e. the fraction of the sites M occupied. Using Stirling's approximation [23]:

$$\begin{aligned} \Delta S &= k_b ((M \ln(M) - M) - (Mx \ln(Mx) - Mx) - (M(1-x) \ln(M(1-x)) - M(1-x))) \\ &= k_b \left(M \ln \left(\frac{M}{M(1-x)} \right) - Mx \ln \left(\frac{Mx}{M(1-x)} \right) \right) = k_b M (-(1-x) \ln(1-x) - x \ln x) \end{aligned} \quad (\text{E.4})$$

This is similar to the expression of the molar entropy of mixing found by Guggenheim [52]. It can also be regarded as the entropic contribution in the Langmuir model. The difference is that this expression is given for the number of lattice sites available to Li, M , and x in the above expression is not the mole fraction but, as mentioned above, the x in Li_xCoO_2 . This equation shows that the entropy of an ideal system is greatest when half the number of lattice points are occupied.

The model mentioned above is the one currently used in literature. Only the total number of lattice points and amount of Li in the lattice must be known, making it easy to implement. However, when looking from a mesoscopic point of view, there will not be an equal distribution on the number of Li atoms present in each layer. The number of Li atoms in a layer may be independent on the number present on the neighboring layers. The layers will in that case be separate systems and must be treated thereafter. Each layer must be treated individually and the multiplicity of the lattice as a whole is given as the product of the multiplicity of the individual layers.

$$W = \prod_{i=1}^K W_i \quad (\text{E.5})$$

where K is the total number of intercalation layers in the electrode.

In this case the logarithm of the multiplicity is given by:

$$\ln W = \sum_{i=1}^K (N - n_i) \ln \left(\frac{N}{N - n_i} \right) + n_i \ln \left(\frac{N}{n_i} \right) \quad (\text{E.6})$$

where n_i is the number of Li atoms on layer i and N is the number of sites in each layer. The change entropy is then given by:

$$\Delta S = k_b \ln W = k_b \left(\sum_{i=1}^K (N - n_i) \ln \left(\frac{N}{N - n_i} \right) + n_i \ln \left(\frac{N}{n_i} \right) \right) \quad (\text{E.7})$$

A special case is obtained when it is assumed that each layer contains the same number of Li atoms, i.e. $W_1 = W_2 = \dots = W_K$. This approximation becomes valid when $N \rightarrow \infty$, $K \rightarrow \infty$ and n_i is large, i.e. as the macroscopic area is approached. The change entropy is then given by:

$$\Delta S = k_b K \left(\left(N - \frac{m_{\text{Li}}}{K} \right) \ln \frac{N}{N - \frac{m_{\text{Li}}}{K}} + \frac{m_{\text{Li}}}{K} \ln \left(\frac{N}{\frac{m_{\text{Li}}}{K}} \right) \right) \quad (\text{E.8})$$

The total number of sites ($K \cdot N$) is the same as M . $m_{\text{Li}}/K \cdot N$ is then equal to x . This can then be rewritten to:

$$\Delta S = k_b \cdot K \cdot N \left((1 - x) \ln \frac{1}{(1 - x)} + x \ln \frac{1}{x} \right) \quad (\text{E.9})$$

which is exactly equal to the ideal case. This shows that when the multiplicities of the layers are equal, which will be a valid approximation with random distribution in the macroscopic area, the ideal model is valid.

This model is not as simple as in literature, but it can be argued that it is a more realistic model, especially when looking at the mesoscopic range. The number of layers in the electrode and the size (i.e. the number of lattice points) of the layers must be found in addition to the number of Li atoms to calculate the multiplicity and thus the entropy. This makes it much harder to implement, as this is normally not known and difficult to obtain for a macroscopic system. How large must a system be for the ideal model to be valid for intercalation electrodes? A hypothetical system will be used to make comparison between the two models, to see how large a system is needed before the ideal model is valid.

These models are general for simple lattices. For lithium-based electrodes, some host-lattices contains separate sublattices where only one will be filled initially [53]. The same model can then be used, by treating each layer within those sublattices as individual systems. Each electrode material must therefore be looked at to determine the complexity of the host-lattice before implementing this model.

E.1 Li_xCoO_2 electrode

Li_xCoO_2 consists of a host lattice of CoO_6 octahedral unit cells in one layer, giving the total stoichiometry CoO_2 , with oxygen on the edge of the layer and Li atoms intercalated between the oxygen edges of two layers. The Li-intercalation has been referred to as "quasi-two-dimensional", as Li is intercalated between layers of CoO_2 [29]. When the number of layers goes to infinity, there will be for each CoO_2 one free site in the lattice to be occupied by a Li atom. The Cobalt oxide electrode structure will change with the state of charge, as will the interlayer distance [54]. LiCoO_2 consists of CoO_6 octahedral unit cells in one layer, with oxygen on the edge of the layer, with Li atoms intercalated between the oxygen edges of two layers.

Thomas et al. observed that the pattern of the reaction of entropy they measured at open circuit conditions in a $\text{Li-Li}_x\text{CoO}_2$ cell follows what would be expected when lithium is solvated into a lattice in which all the lithium sites are equivalent [31]. The same behaviour was observed for Dahn et al. for the $\text{Li}_x\text{Mo}_6\text{Se}_8$ electrode. This means that the Li intercalated is distributed randomly on the available sites. This is not an unreasonable, as Li can diffuse within the lattice sites [55]. This, in addition to the lattice structure of the host material, are good arguments for why a simple lattice model can be used to predict the entropy of lithium in the electrode. Dahn et al. observed that theoretical studies on intercalation compounds usually are based on lattice models and that often these models only consider the changes of Li entropy and not the changes of the entropy of the host lattice. However in this thesis this is not a problem as $S_{\text{Li}(\text{CoO}_2)}$ is what is wanted and not $S_{\text{Li}_x\text{CoO}_2}$.

The host lattice CoO_2 can have several structures, and the structure of the material depends on the amount of Li intercalated and the temperature. Most importantly is the structure observed at $x > 0.4$, which has the structure O3. This structure can be either ordered or disordered. At certain temperatures and degrees of intercalation, this structure can behave as though the host lattice has two separate sublattices. Then only one sublattice will be filled at a time and Li-diffusion will not

happen between the two lattices. The structure is then separated into two systems which must be treated separately. At higher temperatures or higher x -values, the structure changes to a disordered structure where the entire host lattice act as one system. This must be taken into consideration before calculating the entropy of the electrode. If the ordered system is present at $x=0.5$, one lattice will be completely filled while the other is empty, giving a multiplicity of 1 for both sublattices. The same model can however be used if this is taken into consideration.

E.2 Methodology

The matlab code used to generate a lattice of Li atoms and calculate the multiplicity using both an ideal model and a layer-by-layer model is given in Appendix E.4. This matlab code generated a random lattice containing the numbers 0 (unoccupied lattice site) and 1 (occupied lattice site). The size of the lattice was given from input parameters. The program then generated matrices with a Li content from 0 to 100% by insertion at random lattice points. The logarithm of the multiplicity of each of these randomly generated matrices was then computed for each lattice for the layer-by-layer model. This multiplicity was then compared to the ideal model multiplicity (only dependent on the total Li content in the matrix) and plotted against the number of Li atoms intercalated into the lattice.

E.3 Results and Discussion

A Matlab function was made to compare the models described in section E. The Matlab code can be found in section E.4. An example of a randomly generated lattice is shown in Figure E.1. The logarithm of the total multiplicity of the lattice was calculated using both methods. This was done for a content from 0 to a completely filled lattice. The results are shown in Figure E.2 to E.6 below and in Appendix E.

The results from lattice model calculations are given in the figures below. As seen in equation E.9, the layer-by-layer model and the ideal model will be identical when it is assumed that the multiplicity of the individual layers are identical. This occurs in the limit when the number of layers, the number of lattice points on each layer and the amount of lithium intercalated is large. The question is then when the system can be treated using the ideal model. Because the calculations used involves lattices created with random insertion of Li, one calculation will for a small number of lattice sites be inaccurate. This random generation means that

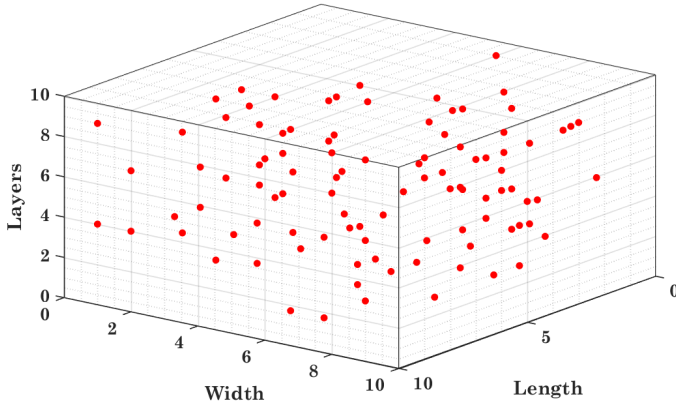


Figure E.1: A three dimensional figure displaying a randomly generated lattice with 100 atoms distributed over a lattice with 10 layers, a width of 10 sites and a length of 10 sites.

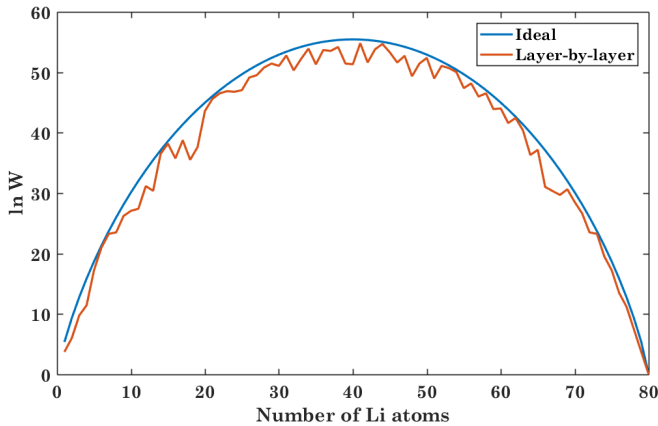


Figure E.2: One calculation of $\ln W$ for the ideal model and layer-by-layer model with randomly generated lattices with a total of 80 lattice points distributed over 5 layers.

the total multiplicity may be different for the different lattice as a Li atom can be inserted into any layer. Therefore the multiplicity of the individual layers will vary from lattice to lattice. This is also likely to occur in a real system if a complete random insertion is the case (which depends on the interaction between the Li atoms).

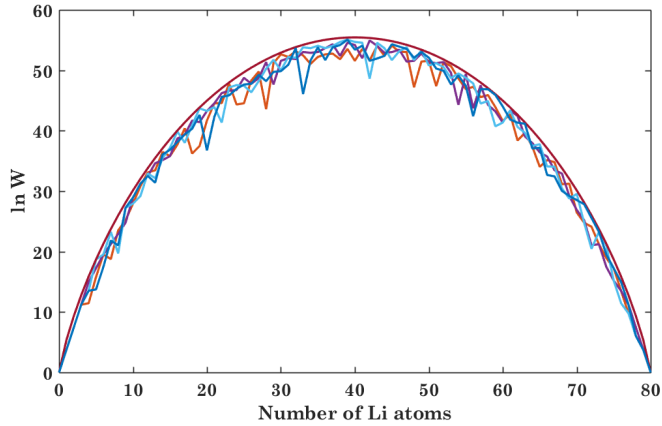


Figure E.3: Calculations of $\ln W$ for the ideal model and layer-by-layer model with randomly generated lattices with a total of 80 lattice points distributed over 5 layers.

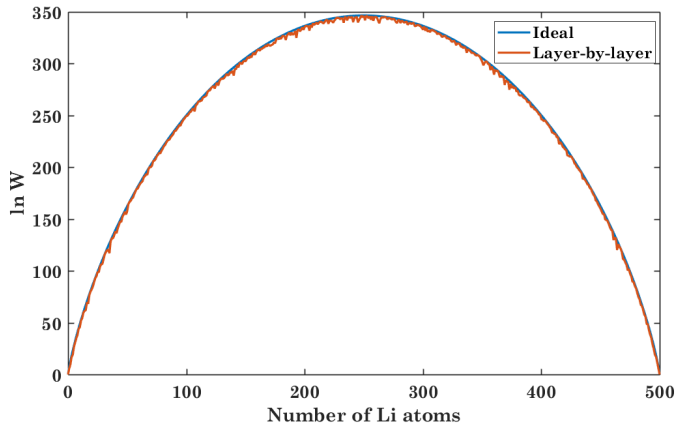


Figure E.4: One calculation of $\ln W$ for the ideal model and layer-by-layer model with a total of 500 lattice points distributed over 5 layers.

In Figure E.3 layer-by-layer model calculations were made on several randomly generated lattices of the same size and compared to the ideal model. What can generally be seen is that the different randomly generated lattices will not have an equal entropy. This fits the discussion above on the lattices generated by the code. Another interesting aspect is that the ideal model seem to overestimate the

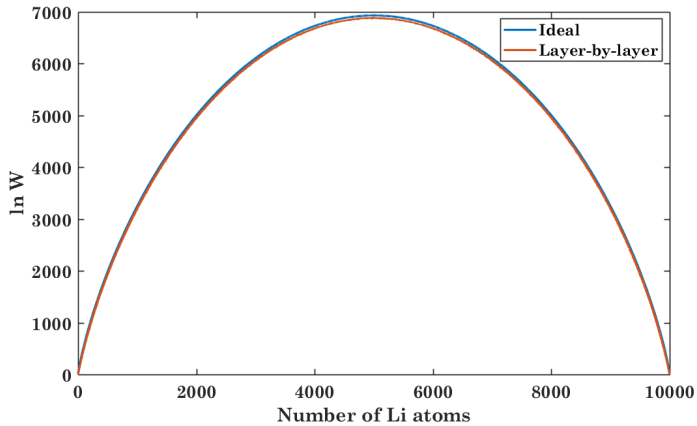


Figure E.5: Calculation of $\ln W$ for the ideal model and layer-by-layer model with a total of 10000 lattice points distributed over 100 layers.

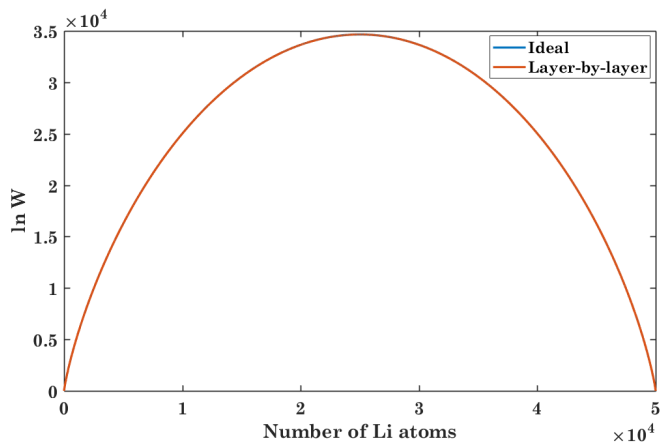


Figure E.6: Calculation of $\ln W$ for the ideal model and layer-by-layer model with a total of 50000 lattice points distributed over 5 layers.

entropy compared to the layer-by-layer model. This overestimation stems from the very principle difference of the two models. When the first Li atom is inserted into the lattice, the multiplicity in the ideal model will be calculated for the entire lattice, while for the layer-by-layer model only one layer will have an increase in multiplicity and the other empty layers will still have a multiplicity of 1. This effect will be present as long as some layers are more filled than others, which gives the

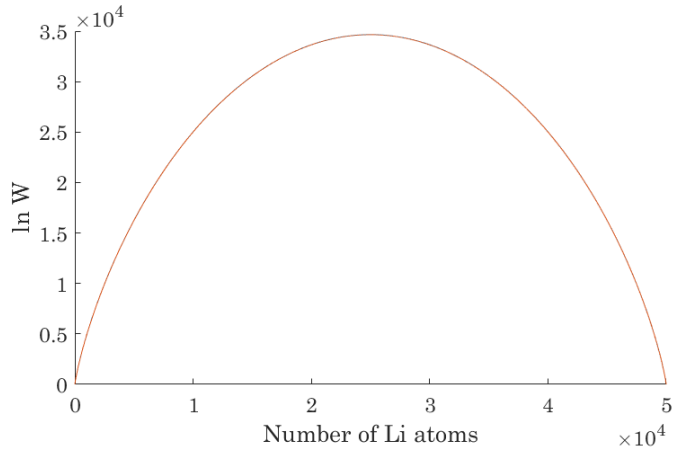


Figure E.7: Calculation of $\ln W$ for the ideal model and layer-by-layer model with a total of 50000 lattice points distributed over 10 layers.

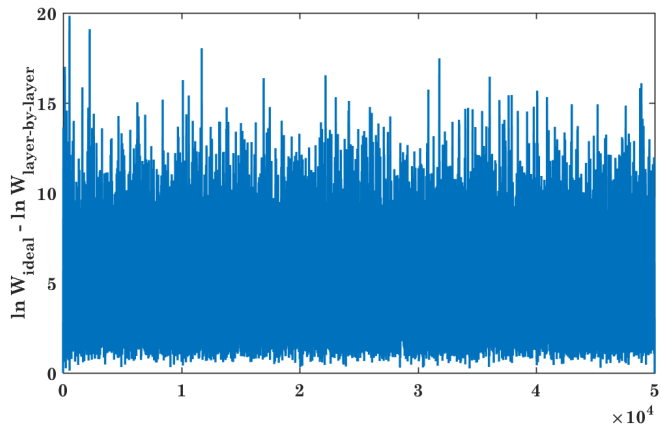


Figure E.8: Calculation of the difference between $\ln W_{ideal}$ and $\ln W_{layer-by-layer}$ for a total of 50000 lattice points distributed over 10 layers.

following relation:

$$W_{layer-by-layer} \leq W_{ideal}$$

This relation can also be verified by looking at Figure E.8 in Appendix E, where the difference between $\ln W_{ideal}$ and $\ln W_{layer-by-layer}$ is computed. It can be seen that except at 0 and complete filling, there is a difference between the two models, in which the ideal model always has the greater value.

Despite the difference between the two models is still present in the calculations with a high number of lattice sites (i.e. from 50000 lattice sites), the relative difference becomes smaller and smaller as the number of sites increases. This can easily be seen by comparing Figure E.2 and E.6. Thereby it can be concluded that the difference between the two models when 50000 lattice sites is reached (which cannot be seen in Figure E.6 and Figure E.7, but is still present according to Figure E.8) is negligible. For lattices of greater sizes than this, the ideal model can be used for calculations.

Figure E.9 shows a randomly generated lattice where one sublattice is completely filled while the other is only partly filled and the particles inside is distributed randomly.

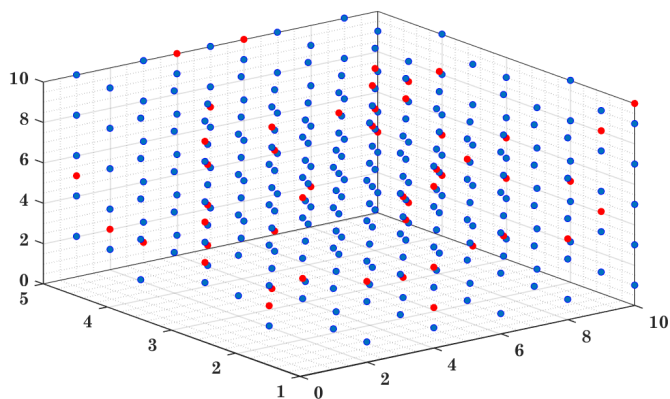


Figure E.9: A three dimensional figure displaying a randomly generated lattice consisting of two sublattices filled with 300 atoms distributed over a lattice with 10 layers, a width of 5 sites and a length of 10 sites.

From Figure E.10 it is evident that the ideal model is a good approximation for systems with sublattices as well, as long as the ideal model is used on the two subsystems individually and not on the entire host lattice.

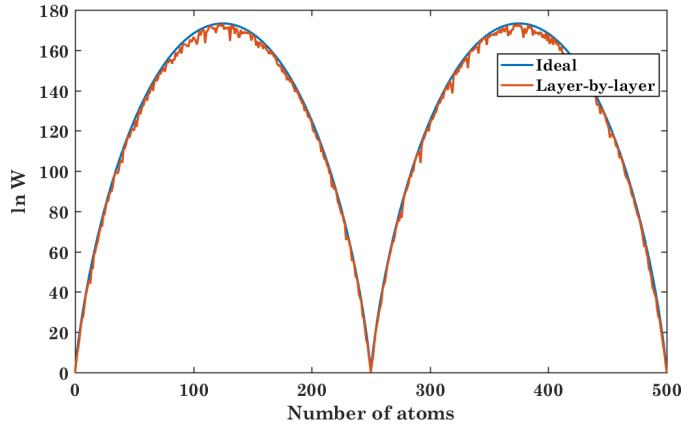


Figure E.10: Calculation of $\ln W$ for the ideal model and layer-by-layer model with a total of 5000 lattice points distributed over 10 layers and two sublattices.

E.4 Matlab Codes Lattice Model Calculations

```
function lnW_meso = entropy2(K,L,W)
%K=number of layers
%L=length of the sides of each layer
%M = number of Li atoms
N=L*W;
O=K*N;      % total number of sites
lnW_ideal=zeros(O,1);
lnW_meso=zeros(O,1);

for M=0:O      %Changes the number of Li atoms from 1 to the
maximum number
Lattice=zeros(K,L,W);      %Defining the matrices
i=0;

if M==0
lnW_meso(1,1)=0;
lnW_ideal(1,1)=0;
else

%Putting Li atoms into the lattice
```

```

while i <M
l=randi(K);
k=randi(L);
m=randi(W);
if Lattice(l,k,m)==0
Lattice(l,k,m)=1;
i=i+1;
end
end

lnW=zeros(K,1);
m=zeros(K,1);
%counter
%calculating the multiplicities
for i=1:K
for j=1:L
for k=1:W
if Lattice(i,j,k)==1
m(i)=m(i)+1;
end
end
end
if m(i)>0 && m(i) <N
lnW(i,1)=(N-m(i))*log(N/(N-m(i))) + m(i)*log(N/m(i));
else
lnW(i,1)=0;
end
end

%Total multiplicity calculations

if M <0
lnW_ideal(M+1,1) = M*log(O/M)+(O-M)*log(O/(O-M));
else
lnW_ideal(M+1,1)=0;
end
lnW_meso(M+1,1)=sum(lnW,1);

```

```
end
end
x=0:0;
plot(x,lnW_ideal); hold on
plot(x,lnW_meso);

legend('Ideal', 'Layer-by-layer')
end
```